TRAUMATIC BRAIN INJURY: NOVEL TARGETS FOR POTENTIAL THERAPIES

By

PRZEMYSLAW SWIATKOWSKI

A dissertation submitted to the

School of Graduate Studies

Rutgers, The State University of New Jersey

In partial fulfillment of the requirements

For the degree of

Doctor of Philosophy

Graduate Program in Cellular and Molecular Pharmacology

Written under the direction of

Bonnie L. Firestein

And approved by

_____

_____

_____

_____

_____

New Brunswick, New Jersey

January 2018

ABSTRACT OF THE DISSERTATION

TRAUMATIC BRAIN INJURY: NOVEL TARGETS FOR POTENTIAL THERAPIES

By PRZEMYSLAW SWIATKOWSKI

Dissertation Director:

Bonnie L. Firestein

Traumatic brain injury (TBI) induces severe neurological damage leading to significant deficits in learning and memory and poor quality of life. It is a pathology that involves a variety of molecular and physiological responses, and in order to find an effective treatment these responses need to be addressed in a comprehensive manner. This study involves several approaches that aim to investigate specific proteins, molecular pathways, as well as cellular responses to brain injury. Cytosolic PSD-95 interactor (cypin), a guanine deaminase, regulates dendritic spine reemergence and promotes neuronal survival in an *in vitro* N-methyl-D-aspartate (NMDA) induced injury model of TBI. In this study, we identify novel small molecule activators, H9 and G5, and an inhibitor, B9, of cypin and show neuroprotective potential of cypin activators *in vitro* and *in vivo* in mice subjected to controlled cortical impact (CCI) injury. Hippocampal neurons pretreated with H9 or G5 display preserved physiology and survival after injury, phenotypes that are lost in cultures pretreated with B9 or when cypin is knocked down. Secondly, we expanded our scope and focused on the role of the PI3K/Akt/mTORC1 pathway in brain injury. We show

that exposure to sublethal levels of NMDA does not alter phosphorylation of Akt, S6, and GSK3β at two and twenty-four hours following injury. Electrophysiological recordings show that NMDA-induced injury causes a significant decrease in spontaneous excitatory postsynaptic currents at both two and twenty-four hours, and this phenotype can be prevented by inhibiting mTORC1 or GSK3β, but not Akt. Additionally, inhibition of mTORC1 or GSK3β promotes neuronal survival following NMDA-induced injury. Thus, NMDA-induced excitotoxicity involves a mechanism that requires the permissive activity of mTORC1 and GSK3β, demonstrating the importance of these kinases in the neuronal response to injury. Finally, we investigated the role of microglia, the resident immune cells in the central nervous system, in brain injury using a combination of two-photon imaging, electrophysiology, and genetic tools. We show that ATP-induced outward current in microglia, which has been implicated in microglial chemotaxis in response to injury, is largely dependent on P2Y12R activation and mediated by G-proteins. Similarly, P2Y12R-coupled outward current is also evoked in response to laser-induced single neuron injury. Taken together, we progress our understanding of the complexity of brain injury using a multidimensional approach and propose new therapeutic targets for further investigation.

TABLE OF CONTENTS

LIST OF FIGURES

Chapter 1: Introduction

1.1 Traumatic Brain Injury

Traumatic brain injury (TBI) affects approximately 1.7 billion people each year and is the leading cause of death in people under 45 years of age in the United States.[1,2] The leading causes of TBI in the United States are vehicular accidents, falls, sport related injuries, and blast injury in military personnel.[2,3] TBI is primarily caused by deformations of the brain tissue due to mechanical trauma, followed by rapid release of neurotransmitters and subsequent excitotoxicity, all of which lead to various cognitive dysfunctions.[4-7] Although TBI has a strong presence in our society, there is no reliable cure of treatment, and the effect of TBI on most of the fundamental biological mechanisms, such as learning and memory, are still largely unknown.[6,7]

Traumatic brain injury consists of two major injury paradigms: primary injury and secondary injury. The primary injury is caused by trauma to the brain, leading to mechanical deformation of the delicate nervous tissue.[6,7] Any trauma to the head can cause tearing and stretching of neurons, which causes release of neurotransmitters and ions otherwise tightly regulated.[6,7] The rapid release of neurotransmitters, such as glutamate, and ions, such a potassium, leads to overactivation of neighboring neurons and subsequent excitotoxicity.[3-7] Glutamate is the most common neurotransmitter, and among many other ionotropic and metabotropic receptors, glutamate activates N-methyl-D-aspartate receptors (NMDA).[5] NMDA receptors are naturally permeable to calcium ions, and when overactivated, they cause accumulation of intracellular calcium, which then leads to

activation of various intracellular cascades, some of which are apoptotic and effectively cause cell injury or death.[4] Ionic imbalance caused by the release of intracellular potassium and sodium from injured neurons depolarizes neighboring neurons, leading to release of the magnesium block of NMDA receptors, further contributing to their overactivation and excitotoxic damage.[3-7] TBI and activation of NMDA receptors also cause activation of the resident immune cells of the brain, microglia. In a healthy brain, microglia scout the tissue for cellular debris and abnormalities; however, following TBI, microglia can become pro- or anti-inflammatory, which can be either detrimental or beneficial.[4-8] Existing treatment therapies employ NMDA antagonists to limit excitotoxic damage and aid in recovery of cellular health and cognitive health of affected individuals. Unfortunately, many of the clinical trials failed, due to the importance of normal NMDA function in human brain. In fact, a recent study shows the importance of NMDA activation shortly after injury, rather than its inhibition, for recovery of long-term potentiation (LTP) and cognitive function in mice subjected to TBI.[9] Although not yet widely accepted in the scientific community, this study points to a novel role of NMDA receptors in TBI that should be addressed in the future. In addition to neurotransmitter receptor dysfunction, TBI also causes decreased proteasomal activity, which then causes imbalance of synaptic receptor composition and dysfunction of long-term potentiation (LTP), a process critical for learning and memory.[9-11] Both primary and the secondary injury lead to a number of behavioral dysfunctions, most of which are still poorly characterized.[8-9] Therefore, it is of great interest and importance to elucidate the mechanisms governing changes in cognitive functions following TBI in order to identify reliable therapeutic targets.

1.2 Experimental models of TBI

Traumatic brain injury in humans is classified based on type and severity of the injury. Closed TBI is generally associated with dynamic loading, a rapid acceleration/deceleration of the brain, which can be classified into impulsive or impact loading.[12] Impulsive loading takes place when the head is set to motion or stop impulsively, while impact loading occurs when the head comes into forcible contact with a blunt object. Closed TBI can also be caused by static loading as well as prolonged exposure to a heavy weight, although this type of TBI is rare. Penetrating brain injury is most common among the armed forces and occurs due to missile wounds.[12,13] Severity of this injury depends on the location of impact, mass, shape, and velocity of the missile, all of which contribute to large clinical variability of diagnosis, proposed treatment, and outcome.

Controlled cortical impact (CCI) is a mechanical model of TBI first developed in the late 1980s, and is currently the gold standard technique to study the biomechanics of TBI.[12-14] What makes CCI so desirable is the precise and customizable impounder shape and size, impact depth, highly controlled velocity, and location of impact, all of which allow for precise injury, relatively low degree of variability from specimen to specimen, and most importantly induce some of the response mechanisms that resemble those of human TBI.[13,14] Some of the phenotypes observed following CCI include, but are not limited to, disrupted cellular and axonal morphology, alterations in cerebral blood flow, disruption of the blood brain barrier, subdural and intraparenchymal hematoma, edema, and inflammation. As all models of human disease, CCI has its limitations and downfalls. Most notably, CCI induces a significant cortical contusion, whereas not all human TBI seen in the clinic present with cortical contusions. Additionally, CCI requires a craniotomy

to be performed, which has been shown to induce glia response potentially inducing non-desirable effects in sham control groups and masking effects induced by injury in CCI groups.[12-14]

Secondary injury is classified as delayed, indirect injury mechanism following the primary mechanical trauma. This type of injury is most commonly associated with rapid release of glutamate from injured neurons, leading to overactivation of glutamatergic receptors on neighboring neurons, effectively leading to intracellular damage and apoptosis, glia activation and subsequent inflammation further exacerbating the injury.[7,12] NMDA-induced injury is among the most common *in vitro* models of secondary injury.[5-7] Several studies have shown that activation of synaptic or extrasynaptic NR2B-containing NMDA receptors, but not NR2A-containing NMDA receptors, leads to neuronal injury and apoptosis. This is attributed to higher permeability of NR2B-containing NMDA receptors to calcium, the ubiquitous secondary messenger involved in a broad variety of functions, especially neuronal death.[5-7] NR2B activation leads, therefore, to large Ca^{2+} influx, massive activation of proteases and phospholipases causing cell death.[3-7] Primary and subsequent secondary injury mechanisms have long lasting and devastating neurobehavioral effects which affect the quality of life of affected individuals, and urge scientific investigation and innovation.

1.3 Changes to LTP after TBI

Long-term potentiation (LTP) is a hippocampal dependent process of strengthening synaptic connections between neurons critical for formation of long-term memories.

Induction of LTP is dependent upon activation of NMDA and α-amino-3-hydroxyl-5-methyl-4-isoxazole-propionate (AMPA) receptors, and downstream signaling effectors, CaMKII, PKC, and PKMz, leading to an increase in activation and synaptic localization of AMPA receptors, while the maintenance phase of LTP is dependent upon protein expression and proper function of the proteasome. Traumatic brain injury impairs learning and memory through disruption of proper hippocampal function.[5,6] A number of studies conducted on humans report persistent atrophy of the hippocampus, which contributes to impaired cognitive abilities.[1,3] TBI and subsequent excitotoxic damage cause accumulation of calcium and activation of calcium-dependent pathways important for LTP. Several studies found TBI to cause activation of CaMKI, II, and IV, as well as extracellular receptor kinase 1/2 (ERK1/2) and PKC, which persists up to 24h after injury.[2,3,33] PKA activation and cAMP levels are decreased up to 3 days following injury.[1] In addition to decreased AMPA- and NMDA-mediated currents after TBI, all of the above contribute to deregulation of gene expression and protein synthesis required for the maintenance of LTP.

1.4 Cypin and brain injury

Cytosolic PSD-95 interactor (cypin) is a 50 kDa protein and has been described by the Firestein laboratory for its regulatory function on dendritogenesis and PSD-95 binding ability.[15,16] Cypin consists of a GDA (guanine deaminase) domain, a CRMP (collapsin response mediator protein) homology domain, and a PSD-95 binding domain. Through its carboxyl terminus, cypin binds PSD-95 and decreases its localization at the postsynapse.[15,16] This decrease in PSD-95 localization might effectively lead to a decrease

in AMPA and NMDA receptor localization at the postsynaptic site, leading to physiological and behavioral impairments in healthy organisms, but also neuroprotection after injury. A recently published study from the Firestein laboratory shows that postsynaptic density-95 (PSD-95) and cytosolic PSD-95 interactor (cypin) have opposite effects on morphological changes to neurons subjected to sublethal NMDA receptor activation.[17] Cypin plays a promoting role in dendritic branching, where overexpression increases the number of dendrites, while knockdown results in fewer dendrites.[17] This phenotype might have functional consequences as shown in Chapter 2. Additionally, cypin was found to bind snapin via the carboxyl-terminal coiled-coil domain (H2) of snapin and the CRMP homology domain of cypin, and this binding has a regulatory effect on dendritic branching by modulating cypin-promoted microtubule assembly since snapin competes with tubulin for binding to cypin.[38] Snapin is a SNAP-25/23 interacting protein that induces an increase in synaptotagmin binding to the SNARE complex, effectively leading to an increase in vesicle release.[39] It is possible, therefore, that cypin plays a regulatory effect when bound to snapin, although it is unclear whether this effect is positive or negative. Finally, cypin has a zinc-dependent GDA activity, which deaminates guanine to xanthine, making cypin the major guanine deaminase in the brain.[18] Published data from our laboratory show that overexpression of cypin is neuroprotective in an NMDA-induced injury model of traumatic brain injury, an effect that may be caused by increased uric acid levels.[17]

To identify compounds that modulate cypin's enzymatic activity (GDA), we screened a library of small molecule probes. Modulation of cypin activity via the use of drugs creates a tremendous therapeutic potential since many diseases respond differently

to uric acid levels. For example, patients with autism display increased levels of uric acid and may benefit from a decrease in cypin activity, while patients with Parkinson's disease exhibit diminished levels of uric acid and could benefit from increased GDA activity.[19] The discovery of these drugs enables us to carefully manipulate cypin *in vivo* without affecting its protein levels, and effectively creates tailored therapies for different individuals.

1.5 PSD-95 in TBI

PSD-95 (postsynaptic density protein 95) is a membrane-associated guanylate kinase (MAGUK), a scaffolding protein abundant at the postsynaptic density (PSD) of excitatory glutamatergic synapses.[20] PSD-95 forms vertical filaments and orthogonal horizontal elements deep inside the PSD, and is essential for the anchoring of AMPA and NMDA receptors at the postsynaptic site.[21] Knockdown of PSD-95 in rat hippocampal neurons has been shown to disrupt PSD structure and cause loss of AMPA and NMDA receptors at the postsynaptic site.[21] Following mild controlled cortical impact (CCI) model of TBI PSD-95 expression was found to decrease at 7 days post injury in the ipsilateral hippocampus, which correlated with the onset of behavioral deficits.[23] In an *in vivo* cerebral ischemia-reperfusion model of brain injury, overexpression of PDZ1 domain of PSD-95 disturbed the interaction between glutamate ionotropic receptor kainite type subunit 2 (GRIK2) and PSD-95 suppressing the assembly of GRIK2.PSD-95.MLK3 and effectively inhibiting the c-Jun N-terminal kinase (JNK) activation, resulting in neuroprotection against oxygen-glucose deprivation.[24] Additionally, TBI has been shown to induce

activation of PRK-like ER kinase (PERK) and subsequent phosphorylation of PSD-95 leading to a decrease in its expression and cognitive impairments.[25] Taken together, these reports show the importance of PSD-95 expression and modulation following brain injury.

1.6 Microglia in brain injury

Microglia are highly motile cells of the brain. During neuronal injury, microglia are attracted and recruited to the sites of injury by the factors released from the damaged neurons, such as ATP.[26-28] An accumulating body of evidence shows involvement of ATP-induced activation of purinergic receptors in microglial chemotaxis towards the site of brain injury.[26,29,30] A number of studies have also shown coupling of purinergic receptors to a currently unidentified potassium channel.[29-32] Interestingly, inhibition of the potassium current resulted in no microglial chemotaxis towards the source of ATP.[32] Although microglial chemotaxis to the site of brain insult is a dynamic field, purinergic signaling coupling to the potassium channel is poorly documented.[33] It is therefore of pivotal importance to progress our understanding of purinergic coupling to potassium channels, and effectively microglial function following brain injury. P2Y12 receptor function has been indicated to be critical for microglia chemotaxis, and inhibiting its function in microglial cell cultures promotes neuronal survival post oxygen-glucose deprivation (OGD).[34] However, recent findings using epithelial cells and cultured microglia point towards another purinergic receptor, P2Y6, as a potential regulator of microglial chemotaxis, which may open another gateway for microglia modulation under pathological conditions.[35,36]

Chapter 2: Cypin overexpression and activation using small molecule compounds prevents neuronal death and loss of function following NMDA-induced injury

2.1 Introduction

Traumatic brain injury (TBI) has seen an increased incidence over the last several decades due to escalating military conflicts and the frequent use of small explosives in terror attacks.[40,41] TBI is currently the leading cause of death for people under the age of 45 in the US and is associated with disability, early-onset dementias, cognitive disorders, mental illness, and epilepsy.[40-42] As a result, research into the mechanisms of TBI in the brain has intensified in recent years, focusing on *in vitro*, rodent, and large mammal models alike. To date, the molecular mechanisms guiding spine loss and recovery following traumatic brain injury have been poorly investigated. Therefore, the objective of this study was to investigate whether and how postsynaptic proteins guide dendritic reconstruction and rebuild neural circuits following controlled cortical impact (CCI), a model of TBI. Published data show that postsynaptic density-95 (PSD-95) and cytosolic PSD-95 interactor (cypin) have opposite effects on morphological changes to neurons subjected to sublethal N-methyl-D-aspartate receptor activation.[43] Cypin, a guanine deaminase that converts guanine to xanthine, also promotes cell survival of hippocampal neurons in an NMDA-induced injury model when cypin was overexpressed, a phenotype that was lost with cypin knockdown.[43] In this study, we describe, for the first time the effect of modulation of cypin with small molecules on single cell electrophysiology, further describing cypin's potential neuroprotective function, and we show induction of cypin and

PSD-95 expression following CCI. Furthermore, we screened a number of small molecules to identify activators or inhibitors of cypin and found that compounds that increase the guanine deaminase activity of cypin promote neuronal survival and function in NMDA-induced injury *in vitro*.

2.2 Results

2.2.1 The role of cypin in neuronal electrophysiology

We previously showed that overexpression of cypin alters neuronal circuit synchrony (Ana R. Rodriguez, doctoral dissertation). However, the effects of cypin on synaptic neurotransmission are still largely unknown. Here, we transduced rat primary hippocampal neurons at day *in vitro* 7 (DIV7) with lentivirus for GST or cypin knockdown (Figure 2.1), or for GFP or cypin overexpression (Figure 2.2) and recorded miniature excitatory postsynaptic currents (mEPSCs) at DIV14. Interestingly, cypin knockdown increased the amplitude of mEPSCs with no change to frequency, while neurons overexpressing cypin displayed increased frequency of mEPSCs with no change to amplitude. Both cypin overexpression and knockdown shifted the cumulative probability curves for amplitude to the right (Figures 2.1C, 2.2C). These data suggest that cypin plays both pre- and postsynaptic roles in the neuron and might be a target for modulation following injury.

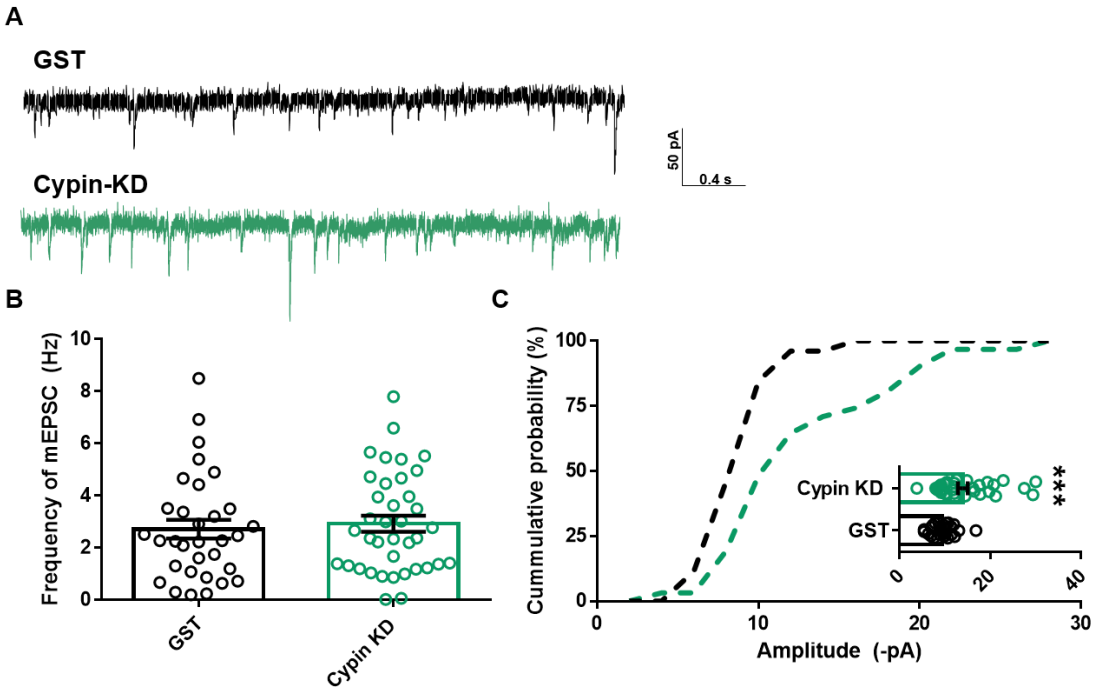

Figure 2.1. Knockdown of cypin increases amplitude of mEPSCs. *A.* Representative traces of mEPSCs. *B.* Knockdown of cypin has no effect on frequency of mEPSCs when compared to GFP control. *C.* Knockdown of cypin increases amplitude of mEPSCs when compared to GFP control and causes a right shift of the cumulative probability curve (***p<0.005). Statistics calculated by one-way ANOVA followed by Tukey's multiple comparisons test (n = 17 for GFP, 21 for cypin knockdown).

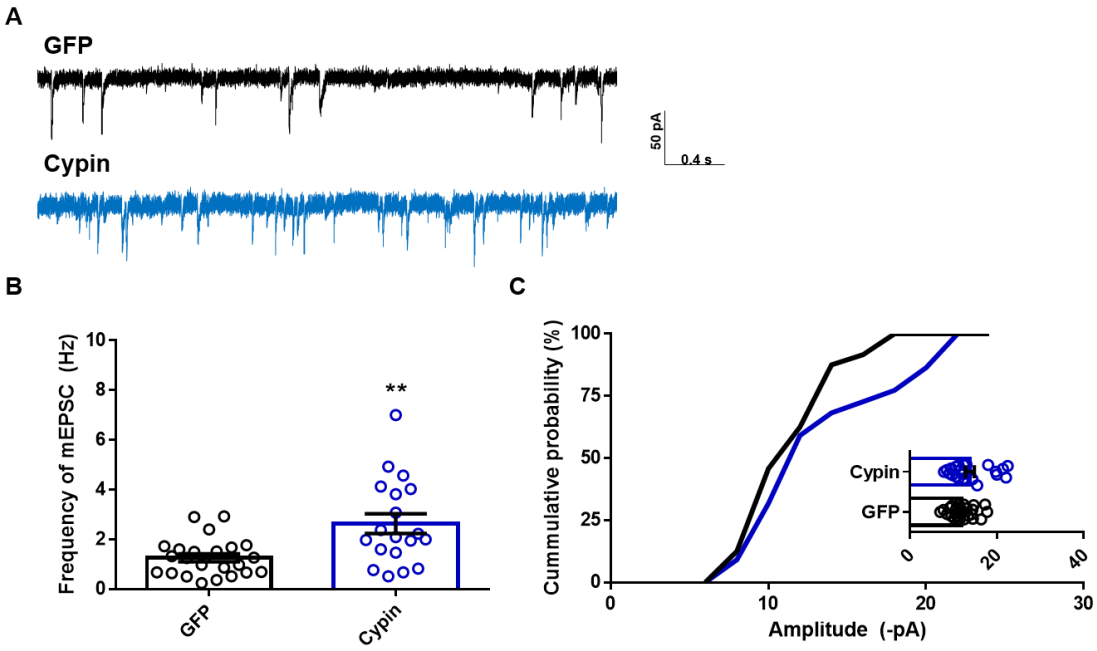

Figure 2.2. Overexpresion of cypin results in increased frequency of mEPSCs. *A.* Representative traces of mEPSCs. *B.* Overexpression of cypin increases the frequency of mEPCs (**p<0.01). *C.* The amplitude of sEPSCs remains unchanged after overexpression, with a slight right shift of the cumulative probability curve. Statistics calculated by one-way ANOVA followed by Tukey's multiple comparisons test (n = 26 for GFP, 22 for cypin).

Next, we were interested in investigating cypin's function on neuronal network communication. While mEPSCs reflect activity at a single synapse, independently of action potentials, we were curious as to how cypin overexpression or knockdown affects neuronal communication where action potentials are not blocked. We transduced neurons with lentiviral vectors for GFP (control), cypin, or cypinΔPDZ at DIV14 and recorded spontaneous excitatory postsynaptic currents (sEPSCs) at DIV21. Overexpression of cypin

resulted in no changes to frequency or amplitude of sEPSCs, while PDZ-lacking cypin mutant decreased frequency of sEPSCs (Figure 2.3). These data suggest compensatory mechanisms that tune overall network activity to adjust for increase in frequency seen at the synapse (mEPSC) following cypin overexpression.

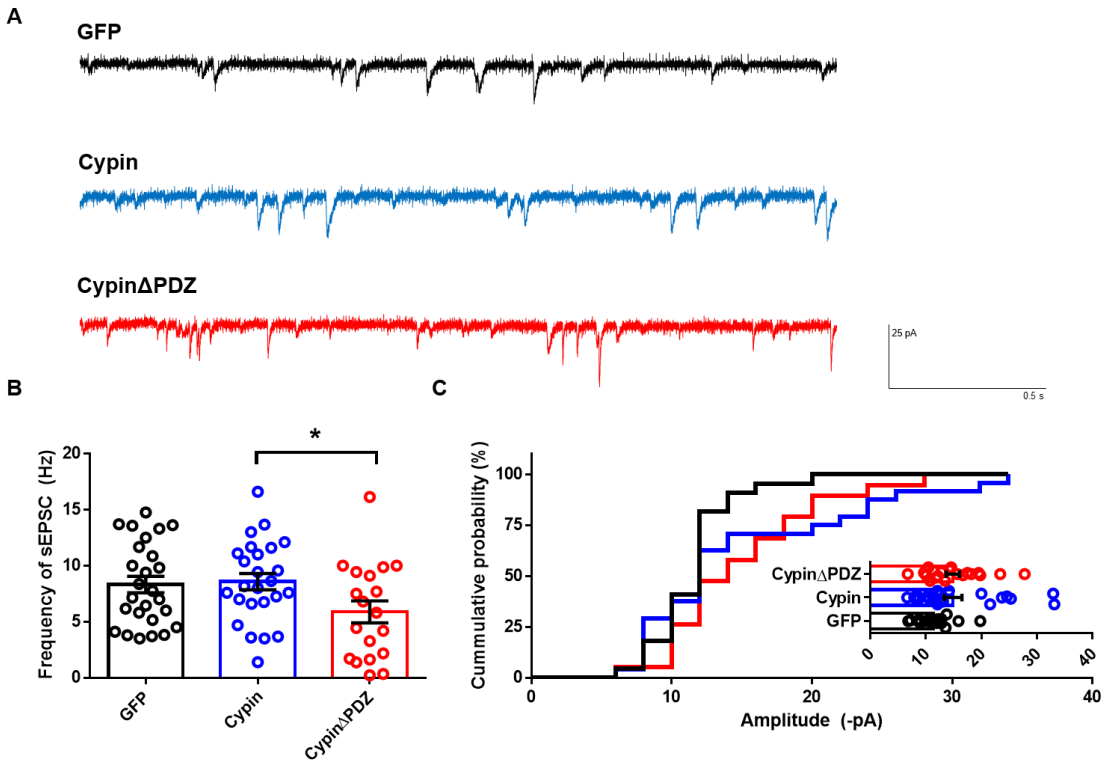

Figure 2.3. Overexpression cypinΔPDZ but not cypin results in decreased frequency of sEPSCs. *A.* Representative traces of sEPSCs. *B.* Overexpression of cypin does not change the frequency of sEPCs; however, overexpression of cypinΔPDZ decreases the frequency of sEPSCs when compared to cypin (*p<0.05). *C.* The amplitude of sEPSCs remains unchanged after overexpression. Statistics calculated by one-way ANOVA followed by Tukey's multiple comparisons test (*n* = 26 for control, 25 for cypin and 19 for cypinΔPDZ).

Additionally, we measured bursting events, which are indicative of synchronized network depolarization.[44,45] Overexpression of cypin decreased the frequency of bursting events but increased their duration, suggesting increased synchrony of neuronal network activity (Figure 2.4). Interestingly, neurons expressing a mutant of cypin that does not bind to PSD-95, cypinΔPDZ, displayed even lower levels of bursting frequency when compared to GFP control or cypin, and increased burst duration suggesting that cypin plays an important function in network regulation and this effect is even greater when cypin is not in a complex with PSD-95 (Figure 2.4).

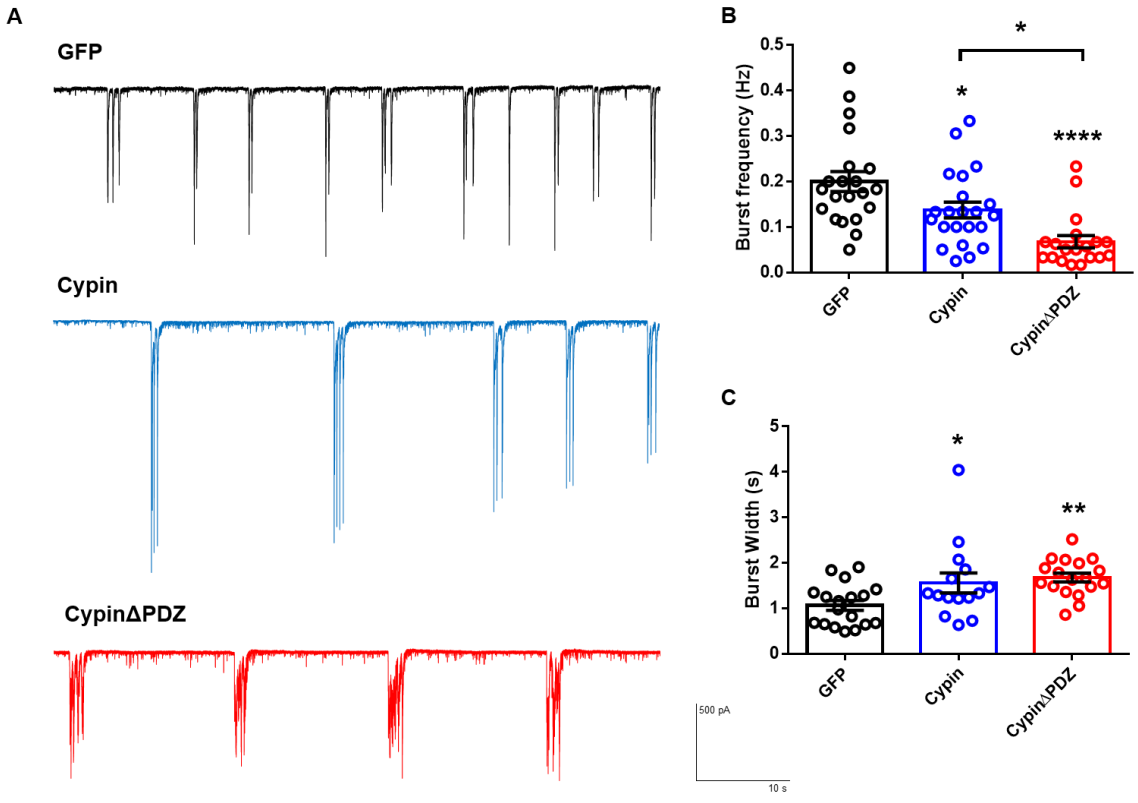

Figure 2.4. Overexpresion of cypin or cypinΔPDZ results in decreased bursting frequency but increased duration. *A.* Representative traces of sEPSCs and bursting

events. *B.* Overexpression of cypin or cypinΔPDZ decreases the frequency of bursting events when compared to GFP control (*p<0.05, ****p<0.001). *C.* Burst width increases with overexpression of cypin or cypinΔPDZ. Statistics calculated by one-way ANOVA followed by Tukey's multiple comparisons test (*n* = 29 for control, 25 for cypin and 19 for cypinΔPDZ).

2.2.2 Analysis of cypin and PSD-95 expression in mice brain post CCI

The controlled cortical impact (CCI) rodent model of TBI has been shown to differentially elevate protein levels depending on the severity of impact.[46-48] In this study, we analyzed cortical and hippocampal brain tissue at 2 hours, 1, 7, and 14 days after mild injury, or at 1, 7, and 14 days following moderate injury for changes to cypin and PSD-95 protein levels. We observed an increase in cypin levels at 1 day post injury in ipsilateral and contralateral cortex, with no significant changes to cypin expression in the hippocampus (Figures 2.5D-E, 2.6). There were no significant changes to PSD-95 following mild injury, while moderate injury led to an increase in PSD-95 at 1 day in the contralateral hippocampus (Figures 2.8A-C). Time points earlier than 1 day were not included in analysis of brain tissue subjected to moderate CCI since this type of injury often results in acute subdural hematoma and cypin is present in the blood, confounding results. These data indicate that in mild injury, cypin expression is induced during the early stages of injury in the cortex, suggesting that cypin may play a role in recovery mechanisms. Interestingly, we found no elevation of cypin expression following moderate injury, suggesting that either moderate

CCI does not induce cypin expression or that any potential induction is transient and occurs at time points not analyzed in this study.

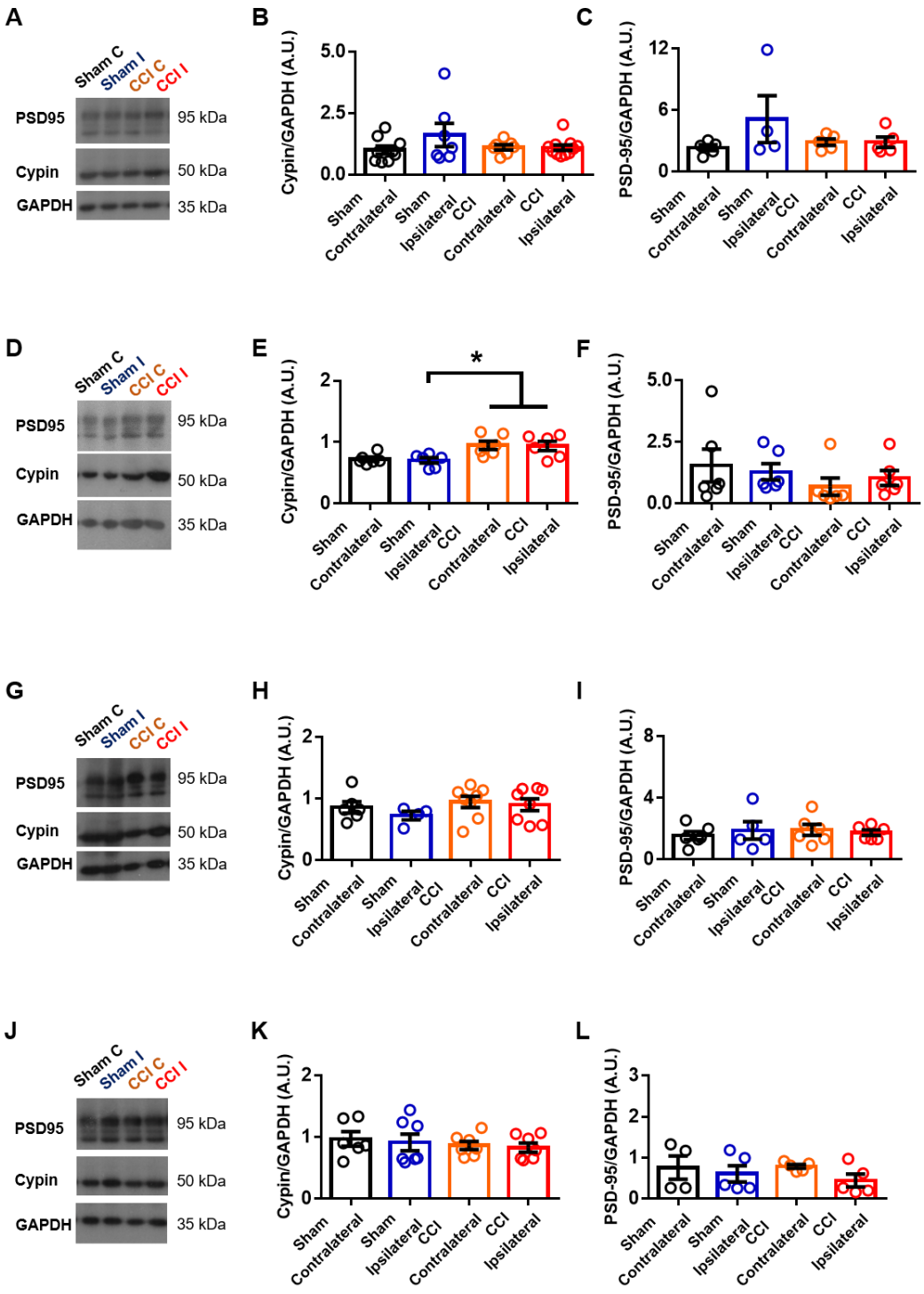

Figure 2.5. Cypin and PSD-95 expression in mouse cortex following mild CCI. *A,D,G,J.* Representative Western blot bands for PSD-95, cypin, and GAPDH in mouse cortex at 2hrs, 1, 7, and 14 days post mild CCI. *B,C,E,F,H,I,K,L.* Quantitative analysis of band intensity normalized to GAPDH shows elevated cypin protein levels at 1 day post injury in ipsilateral and contralateral hemispheres. Western blot bands are representative from at least five replicates of the experiment. *$p<0.05$ determined by one-way ANOVA followed by Tukey-Kramer multiple comparisons test. Error bars indicate ± SEM.

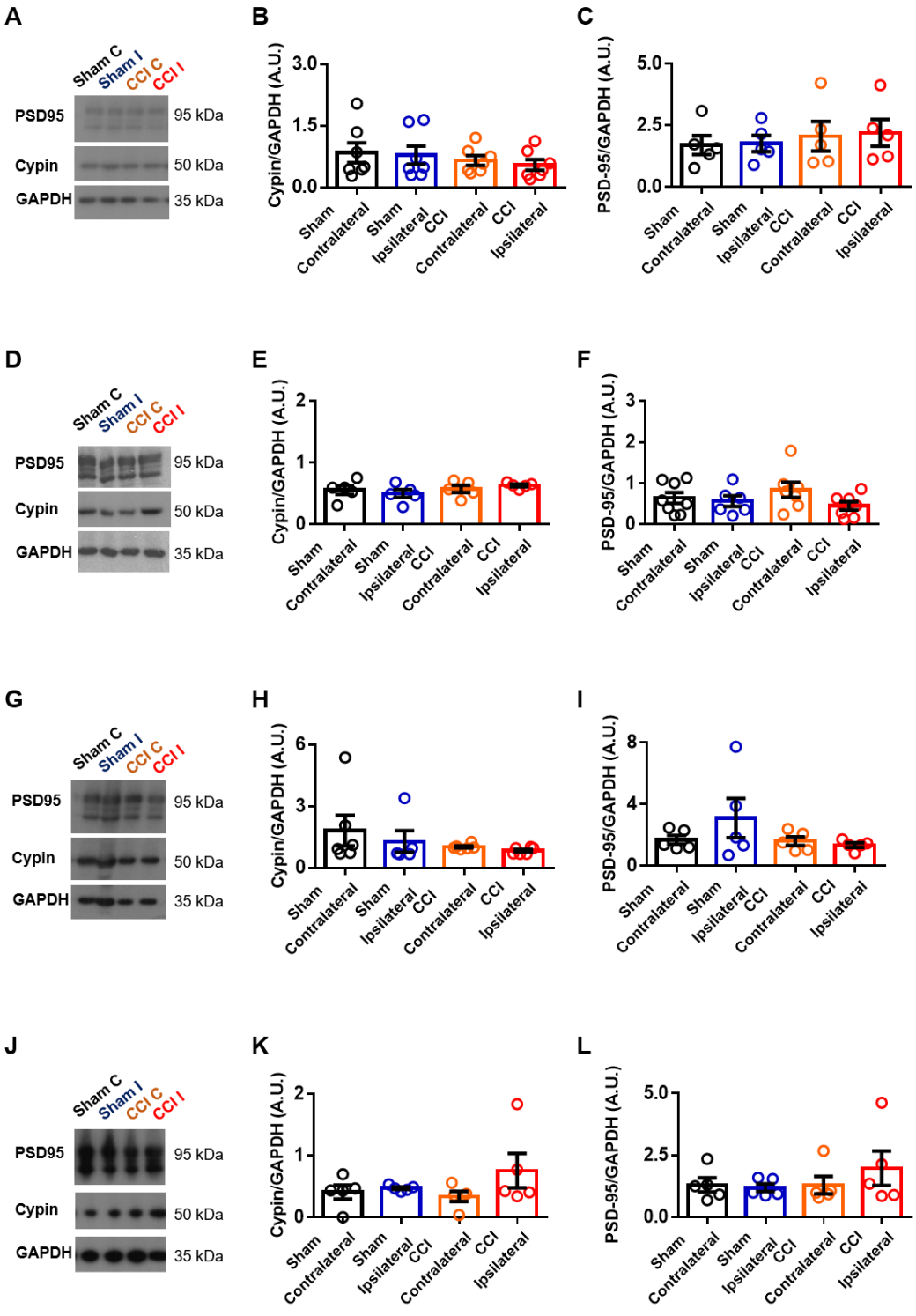

Figure 2.6. Cypin and PSD-95 expression in mouse hippocampus following mild CCI.

A,D,G,J. Representative Western blot bands for PSD-95, cypin, and GAPDH in mouse

hippocampus at 2hrs, 1, 7, and 14 days post mild CCI. *B,C,E,F,H,I,K,L.* Quantitative analysis of band intensity normalized to GAPDH shows elevated cypin protein levels at 7 days post injury in the contralateral hemisphere. Western blot bands are representative from at least five replicates of the experiment. *p*-values determined by one-way ANOVA followed by Tukey-Kramer multiple comparisons test. Error bars indicate ± SEM.

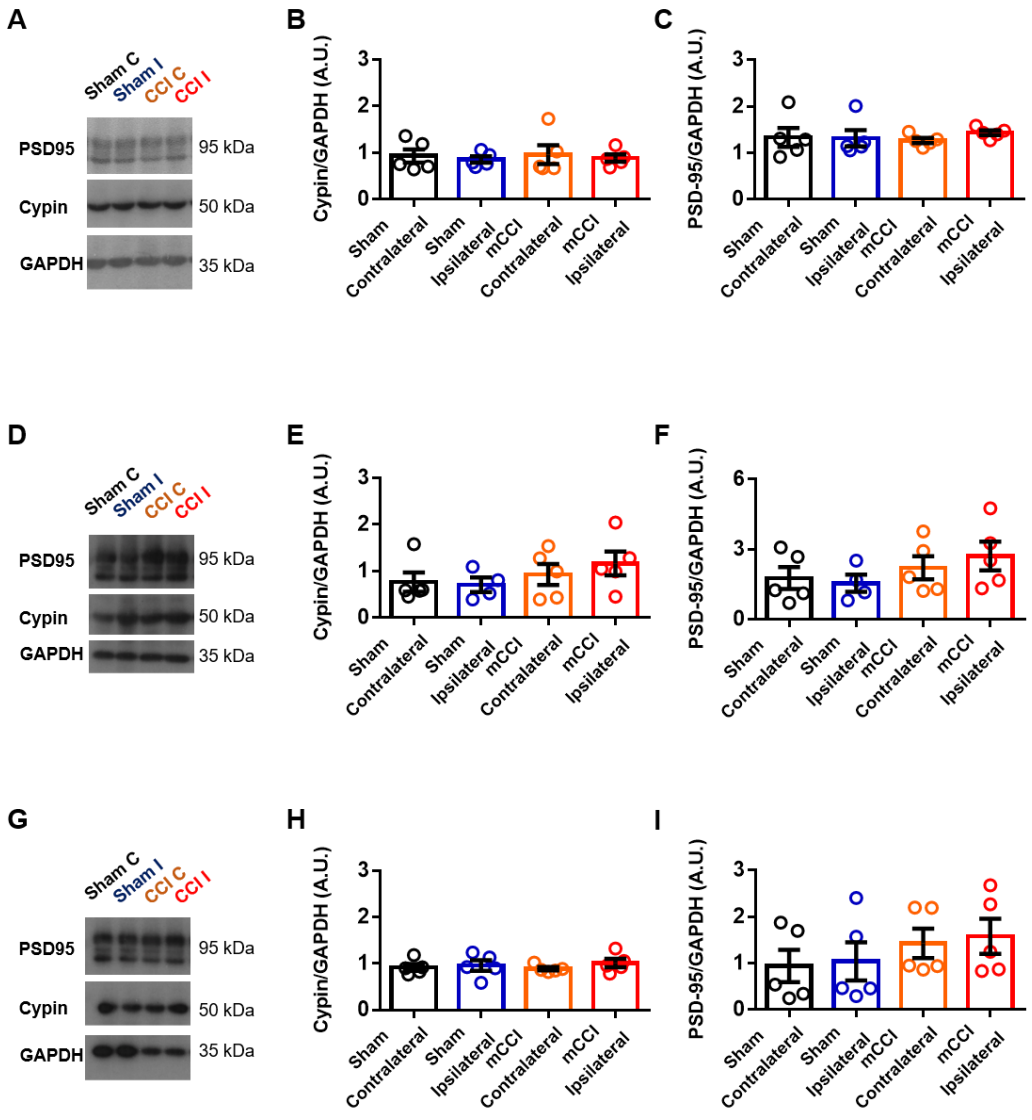

Figure 2.7. Cypin and PSD-95 expression in mouse cortex following moderate CCI. *A,D,G.* Representative Western blot bands for PSD-95, cypin, and GAPDH in mouse hippocampus at 1, 7, and 14 days post moderate CCI. *B,C,E,F,H,I.* Quantitative analysis of band intensity normalized to GAPDH shows elevated PSD-95 protein levels at 14 days post injury in ipsilateral and contralateral hemispheres. Western blot bands are representative from at least five replicates of the experiment. *p*-values determined by one-way ANOVA followed by Tukey-Kramer multiple comparisons test. Error bars indicate ± SEM.

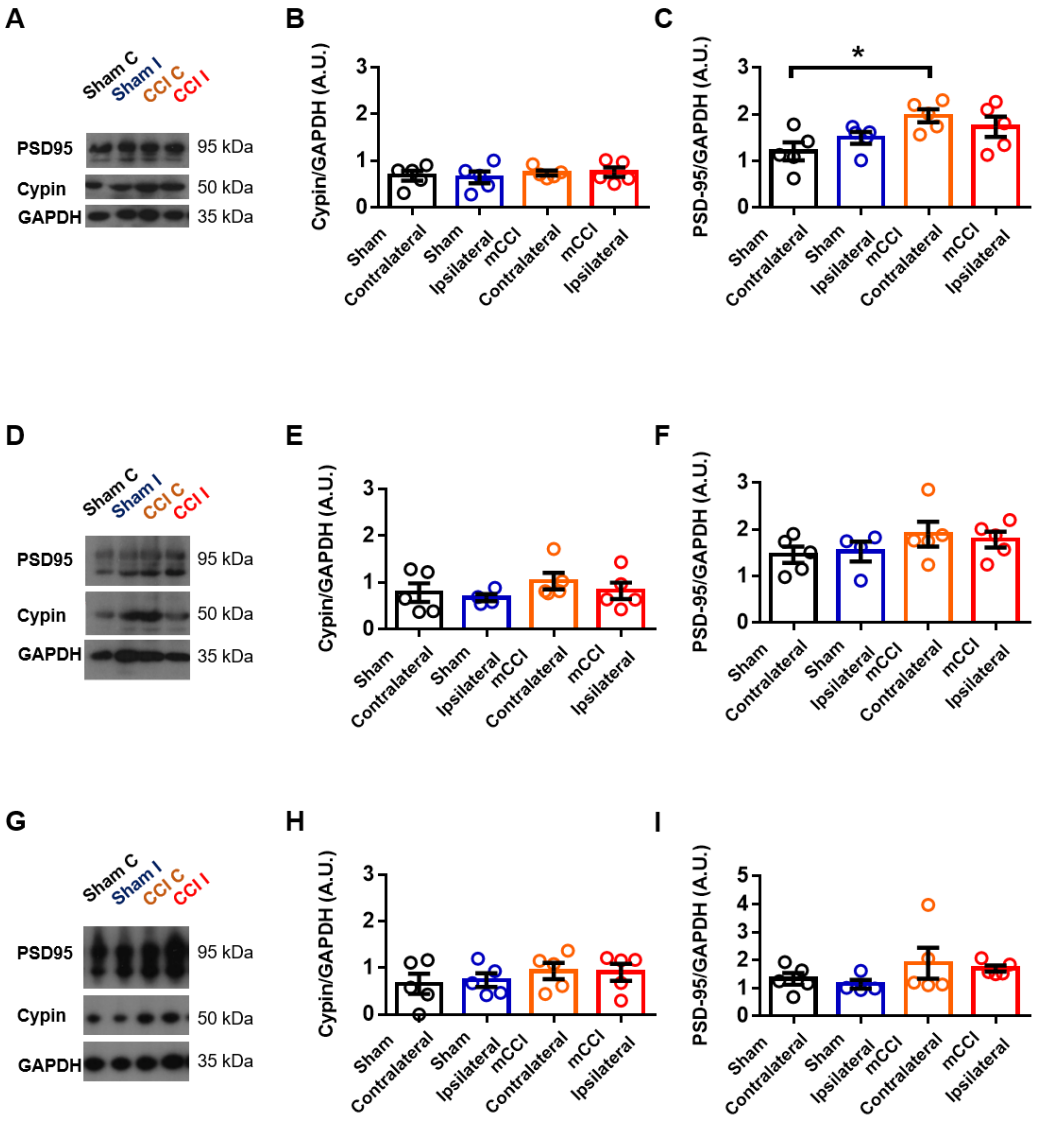

Figure 2.8. Cypin and PSD-95 expression in mouse hippocampus following moderate CCI. *A,D,G.* Representative Western blot bands for PSD-95, cypin, and GAPDH in mouse hippocampus at 1, 7, and 14 days post moderate CCI. *B,C,E,F,H,I.* Quantitative analysis of band intensity normalized to GAPDH shows elevated PSD-95 protein levels at 1 day post injury in the contralateral hemisphere. Western blot bands are representative from at least five replicates of the experiment. *$p<0.05$ determined by one-way ANOVA followed by Tukey-Kramer multiple comparisons test. Error bars indicate ± SEM.

2.2.3 Small molecule probes modulate cypin GDA activity

In order to select compounds that modulate cypin we obtained 288 compounds to screen for their effects on cypin's guanine deaminase activity in cypin expressing COS-7 cells lysates. We normalized the activity levels of all compounds so that average activity was 1 and found several positive and negative regulators (Eric Sweet, doctoral dissertation).
A subset of the compounds had a significant effect on cypin's GDA activity that was either 1 (inhibitors) or 2 (activators and inhibitors) standard deviations away from the normalized average, and these were selected for further testing.

2.2.3 Analysis of cypin and PSD-95 expression following treatment with cypin modulators post CCI

To further investigate a subset of previously screened cypin activators and inhibitors on their ability to modulate cypin, we analyzed cypin and PSD-95 protein levels from brain tissue from mice injected with 200μM DMSO (vehicle), H9 (activator) or B9 (inhibitor) directly into the hippocampus following sham surgery or moderate CCI. Interestingly, treatment with H9 resulted in elevated PSD-95 protein in the cortex at 1 day following injury (Figure 2.9C). Treatment with B9 resulted in no significant change (Figures 2.9E, 2.10C,F). Taken together, these data show that small molecule probes that modulate the enzymatic activity of cypin have no effect on cypin expression; however, increasing cypin

activity with the H9 may result in synapse restructuring as shown by increased PSD-95 expression.

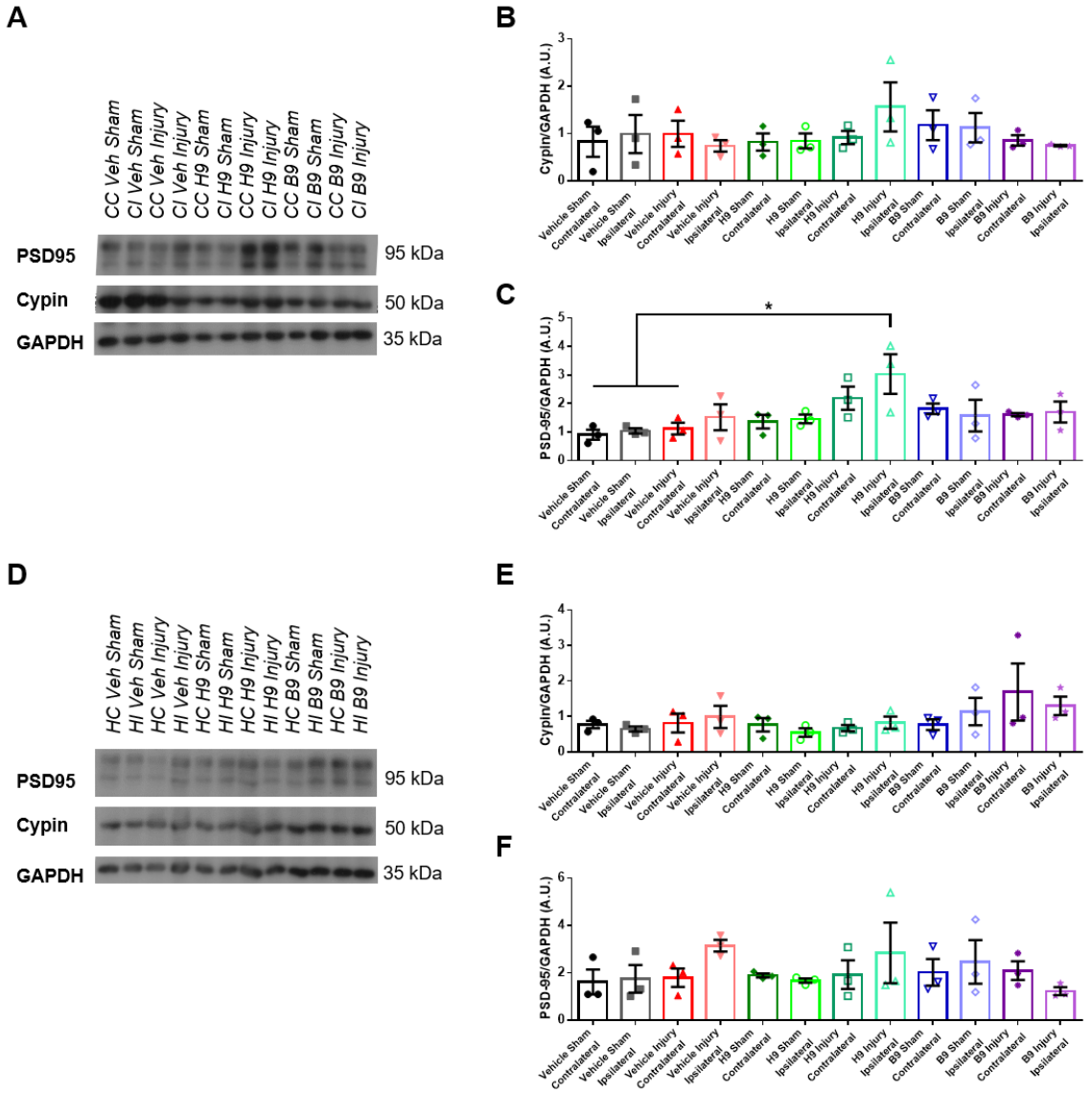

Figure 2.9. Cypin and PSD-95 expression in mouse cortex and hippocampus 1 day following moderate CCI. *A,D.* Representative Western blot bands for PSD-95, cypin, and GAPDH in mouse cortex (*A*) and hippocampus (*D*) at 1 day post moderate CCI. *B,C,E,F.* Quantitative analysis of band intensity normalized to GAPDH shows elevated PSD-95

protein levels at 1 day post-injury in the injured ipsilateral hemisphere form mice treated with H9. Western blot bands are representative from at three replicates of the experiment. *p<0.05 determined by one-way ANOVA followed by Tukey-Kramer multiple comparisons test. Error bars indicate ± SEM.

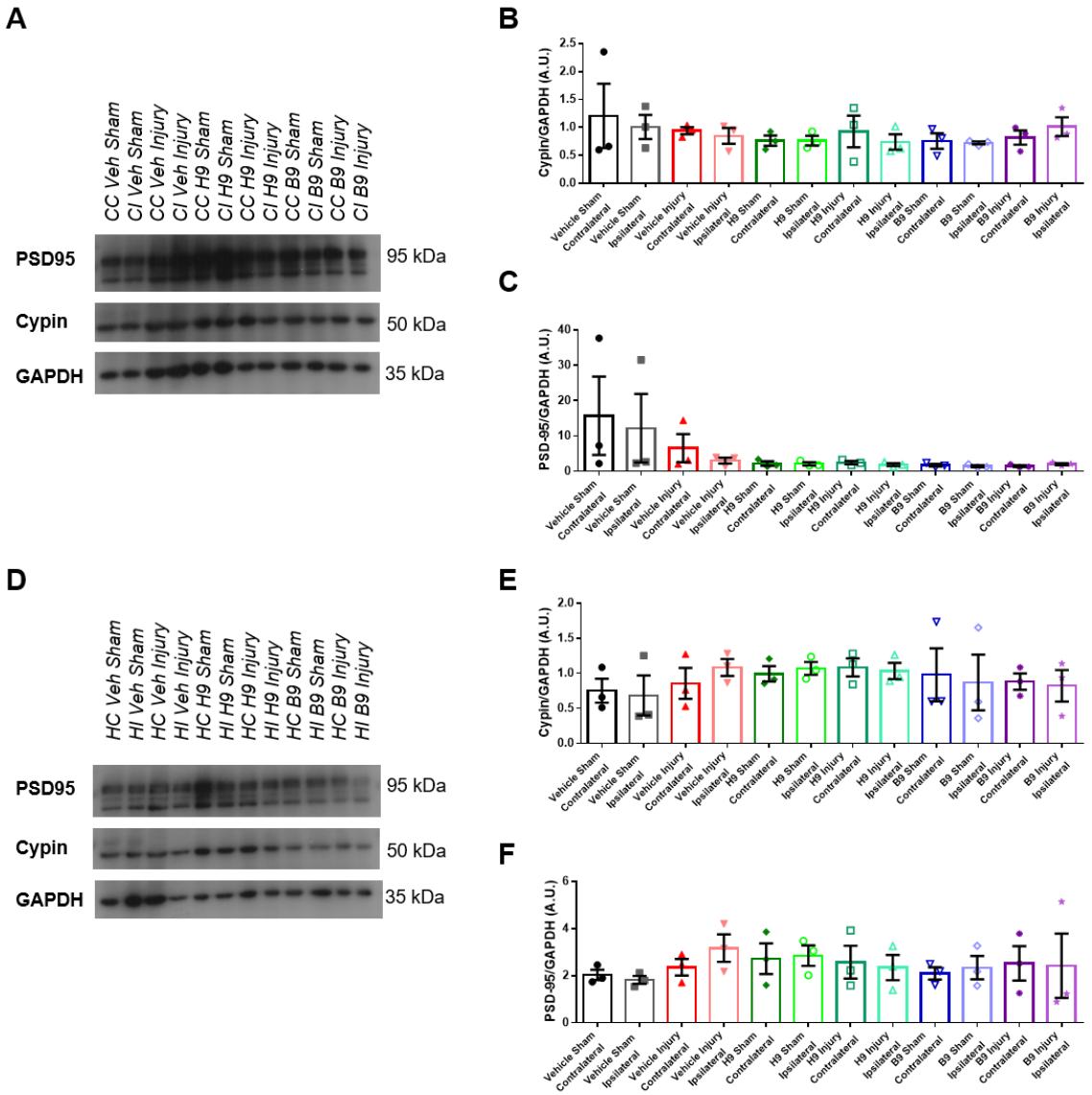

Figure 2.10. Cypin and PSD-95 expression in mouse cortex and hippocampus 7 days following moderate CCI. *A,D.* Representative Western blot for PSD-95, cypin, and

GAPDH in mouse cortex (*A*) and hippocampus (*D*) at 7 days post-moderate CCI. *B,C,E,F.* Quantitative analysis of band intensity normalized to GAPDH shows no significant induction of cypin or PSD-95 protein expression. Western blot bands are representative from at three replicates of the experiment. *p*-values determined by one-way ANOVA followed by Tukey-Kramer multiple comparisons test. Error bars indicate ± SEM.

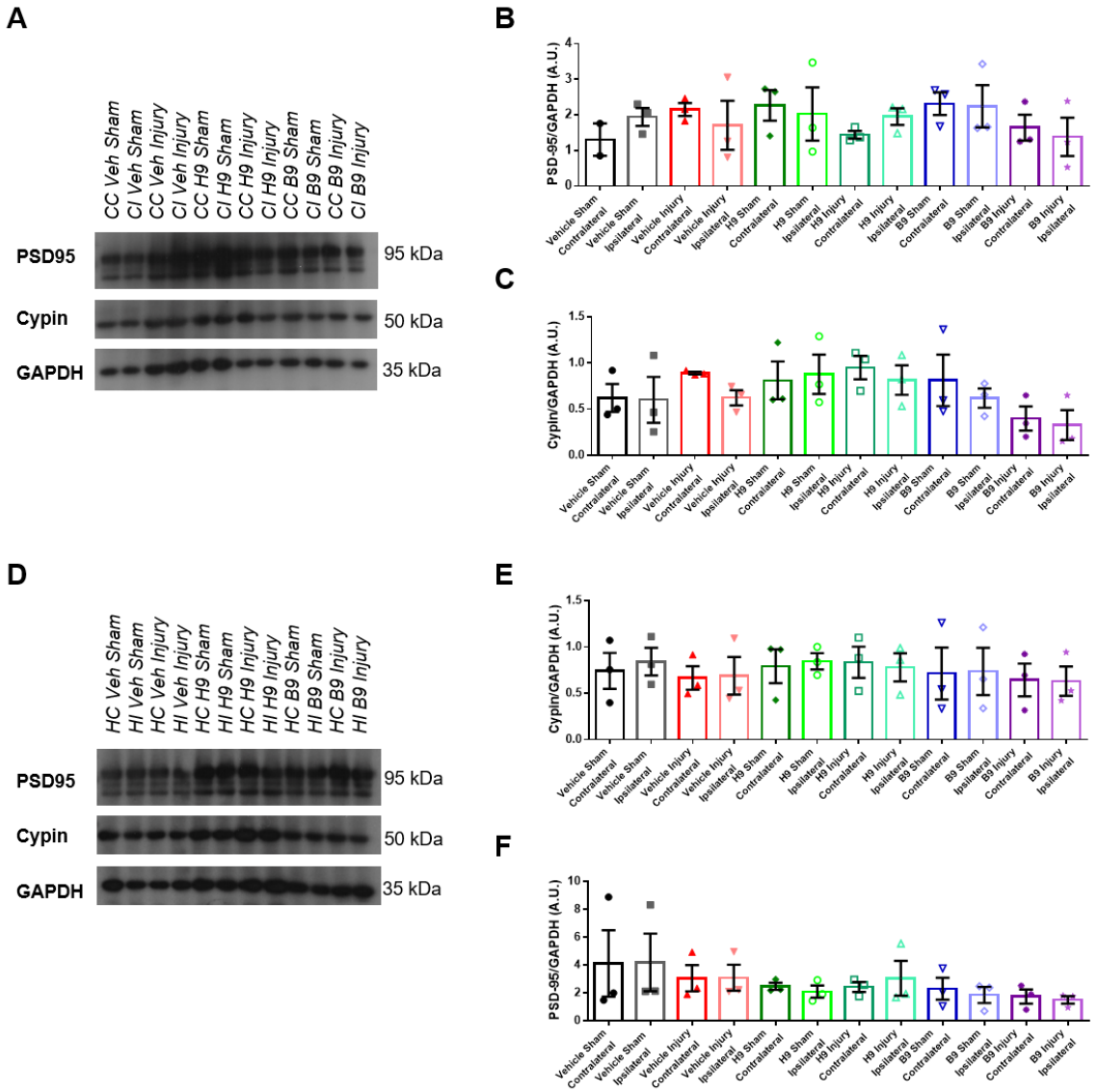

Figure 2.11. Cypin and PSD-95 expression in mouse cortex and hippocampus 14 days following moderate CCI. *A,D.* Representative Western blot bands for PSD-95, cypin, and

GAPDH in mouse cortex (*A*) and hippocampus (*D*) at 14 days post moderate CCI. *B,C,E,F.* Quantitative analysis of band intensity normalized to GAPDH shows no significant induction of cypin or PSD-95 protein expression. Western blot bands are representative from at three replicates of the experiment. *p*-values determined by one-way ANOVA followed by Tukey-Kramer multiple comparisons test. Error bars indicate ± SEM.

2.2.4 Cypin activators prevent NMDA-induced neuronal loss

In the light of our previous report showing a neuroprotective function for cypin in neuronal survival in response to NMDA-induced injury[43], we tested cypin activators H9 and G5, the inhibitor B9, and the neutral compound G6 for their effects on neuronal survival following injury. Pretreatment of cultures with H9 or G5 resulted in 100% survival after NMDA-induced injury, while B9 and G6 had no neuroprotective effect (Figure 2.12), suggesting a neuroprotective function for cypin activation. Interestingly, treatment with B9 alone caused 25% neuronal death, and these data demonstrate a detrimental effect of cypin inhibition (Figure 2.12).

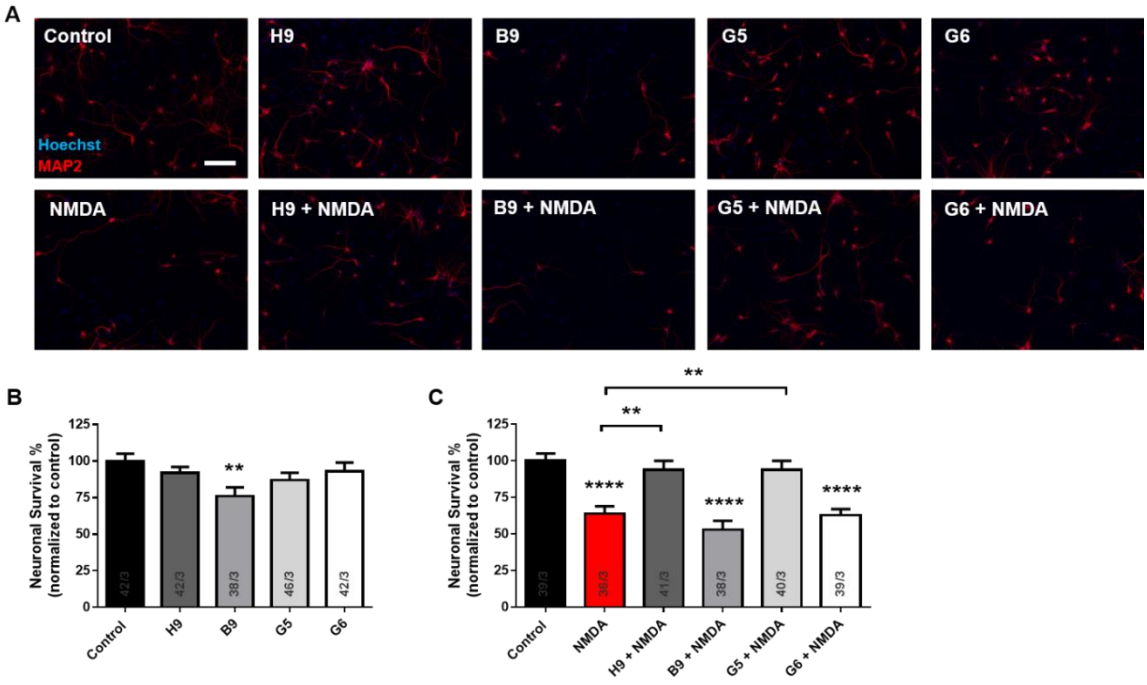

Figure 2.12. Pretreatment of neuronal cultures with H9 and G5 prevents neuronal death in response to NMDA-induced injury. *A.* Representative images showing neurons immunostained for the neuronal marker, MAP2, and co-stained with nuclear dye, Hoechst, after treatment with 0.1% DMSO (control), 20 µM NMDA, with/without 48h pretreatment with 20µM H9, B9, G5, or G6. Scale bars: 100µm. *B-C.* Quantitative analysis of neuronal survival expressed as percent live control neurons. Cypin activators, H9 and G5, prevented neuronal loss, while the inhibitor, B9, and the neutral compound, G6, had no beneficial effect. Additionally, B9 alone induced approximately 25% neuronal death. Data represent 36-46 samples from three separate trials. $^{**}p<0.01$, $^{***}p<0.005$, $^{****}p<0.001$ determined by one-way ANOVA followed by Tukey-Kramer multiple comparisons test. Error bars indicate ± SEM.

Next, we tested the specificity of cypin modulators using neurons with cypin knocked down or overexpressed. Similar to published data[43], cypin knockdown reduces neuronal viability by approximately 75% (Figure 2.13). Cypin knockdown leads to loss of neuroprotective function of H9 and G5, suggesting direct or indirect drug specificity and the importance of cypin for the observed neuroprotection in control neurons after injury (Figure 2.13). Interestingly, cypin overexpression alone resulted in resistance to NMDA-induced neurotoxicity, an effect blocked with B9 pretreatment (Figure 2.14). These data suggest that cypin plays a significant role in neuroprotective mechanisms following NMDA-induced injury, and that there is a neuroprotective effect of cypin activation by H9 or G5.

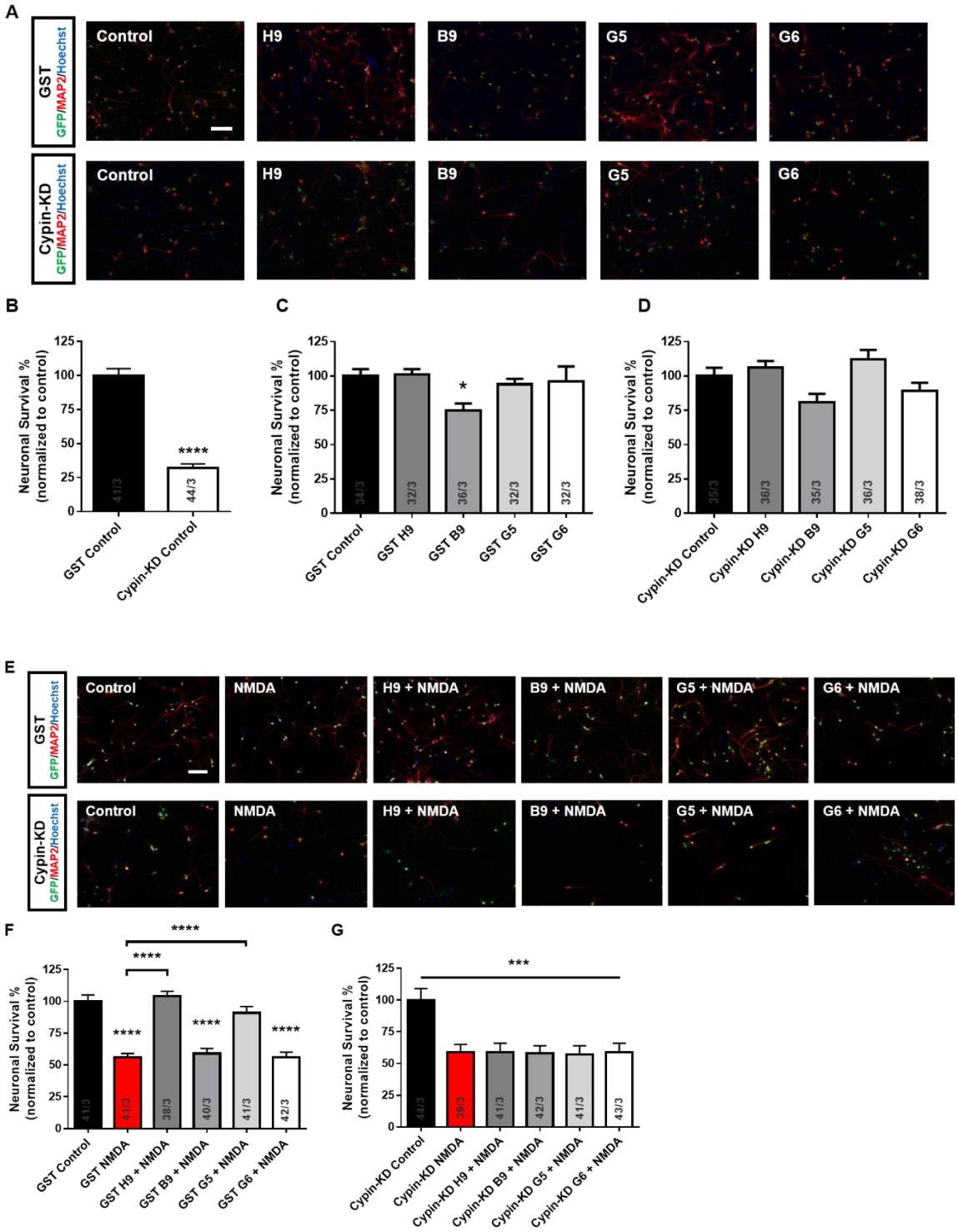

Figure 2.13. Cypin knockdown abolishes neuroprotective activity of H9 and G5. *A,E.* Representative images showing neurons immunostained for the neuronal marker, MAP2,

GFP, and co-stained with nuclear dye, Hoechst, after treatment with 0.1% DMSO (control), 20 μM NMDA, with/without 48h pretreatment with 20μM H9, B9, G5, G6. Scale bars: 100μm. *B-D,F-G.* Quantitative analysis of neuronal survival expressed as percent live control neurons. Cypin activators, H9 and G5, prevented neuronal loss after injury, while the inhibitor, B9, and the neutral compound, G6, had no beneficial effect in control cultures. Cypin knockdown induced 75% cell death, and abolished neuroprotective effects of H9 and G5. Data represent 39-43 samples from three separate trials. $^{**}p<0.01$, $^{***}p<0.005$, $^{****}p<0.001$ determined by one-way ANOVA followed by Tukey-Kramer multiple comparisons test. Error bars indicate ± SEM.

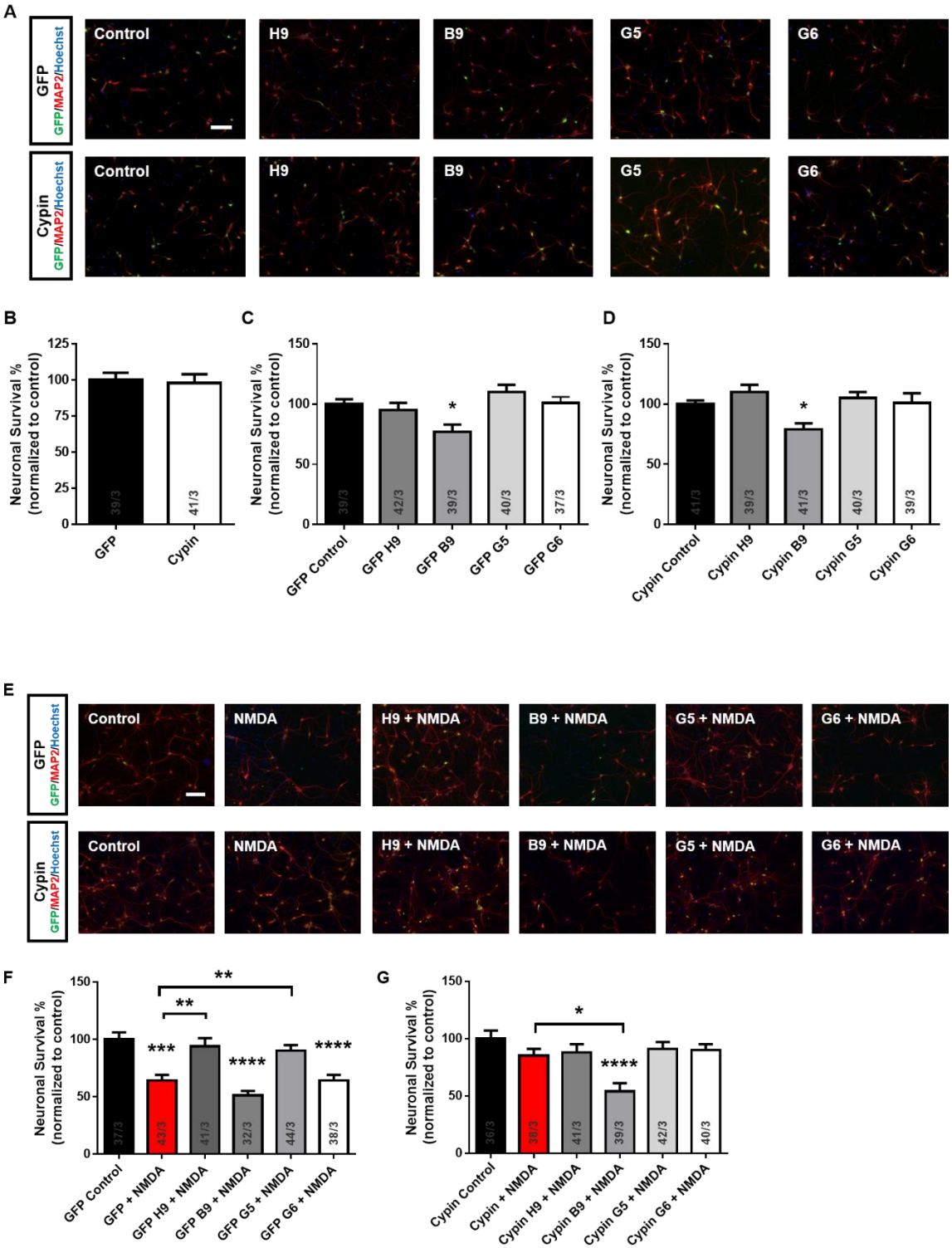
A
GFP
GFP/MAP2/Hoechst
Cypin
GFP/MAP2/Hoechst
Control
H9
B9
G5
G6
B
C
D
Neuronal Survival %
(normalized to control)
GFP
Cypin
GFP Control
GFP H9
GFP B9
GFP G5
GFP G6
Cypin Control
Cypin H9
Cypin B9
Cypin G5
Cypin G6
E
NMDA
H9 + NMDA
B9 + NMDA
G5 + NMDA
G6 + NMDA
F
G
GFP + NMDA
GFP H9 + NMDA
GFP B9 + NMDA
GFP G5 + NMDA
GFP G6 + NMDA
Cypin + NMDA
Cypin H9 + NMDA
Cypin B9 + NMDA
Cypin G5 + NMDA
Cypin G6 + NMDA

Figure 2.14. Pretreatment with H9 and G5 prevent neuronal death in response to NMDA-induced injury. *A.* Representative images showing neurons immunostained for the neuronal marker, MAP2, GFP, and co-stained with nuclear dye, Hoechst, after treatment with 0.1% DMSO (control), 20 µM NMDA, with/without 48h pretreatment with 20µM H9, B9, G5, G6. Scale bars: 100µm. *B-C.* Quantitative analysis of neuronal survival expressed as percent live control neurons. Cypin activators, H9 and G5, prevented neuronal loss after injury, while the inhibitor, B9, and the neutral compound, G6, had no beneficial effect in control cultures. Cypin overexpression prevented neuronal death, and this effect was abolished by B9. Data represent 32-44 samples from three separate trials. *p<0.05, **p<0.01, ***p<0.005, ****p<0.001 determined by one-way ANOVA followed by Tukey-Kramer multiple comparisons test. Error bars indicate ± SEM.

2.2.5 Cypin activators prevent injury induced loss of neuronal communication

To investigate functional changes following injury and cypin modulation, we recorded mEPSCs following NMDA-induced injury. Neurons pretreated with H9 or G5 displayed no decrease in frequency or amplitude of mEPSC that is normally observed after NMDA-induced injury (Figure 2.15). Neurons transduced with cypin knockdown lentiviral vectors and treated with NMDA, however, displayed a decrease in frequency and amplitude of mEPSCs, suggesting loss of neuroprotection after cypin knockdown (Figure 2.16). Interestingly, treatment with H9 alone significantly increased the frequency of mEPSCs in control neurons, and this effect was lost when cypin was knocked down (Figure 2.16). On the other hand, neurons overexpressing cypin showed no decrease in either frequency or

amplitude of mEPSCs following injury (Figure 2.17), thereby preventing changes induced by injury. However, when neurons that overexpress cypin were pretreated with B9, no protection from injury occurred (Figure 2.17). Pretreatment of control neurons with H9 or G5 increased frequency of mEPSCs, consistent with cypin overexpression (Figure 2.17).

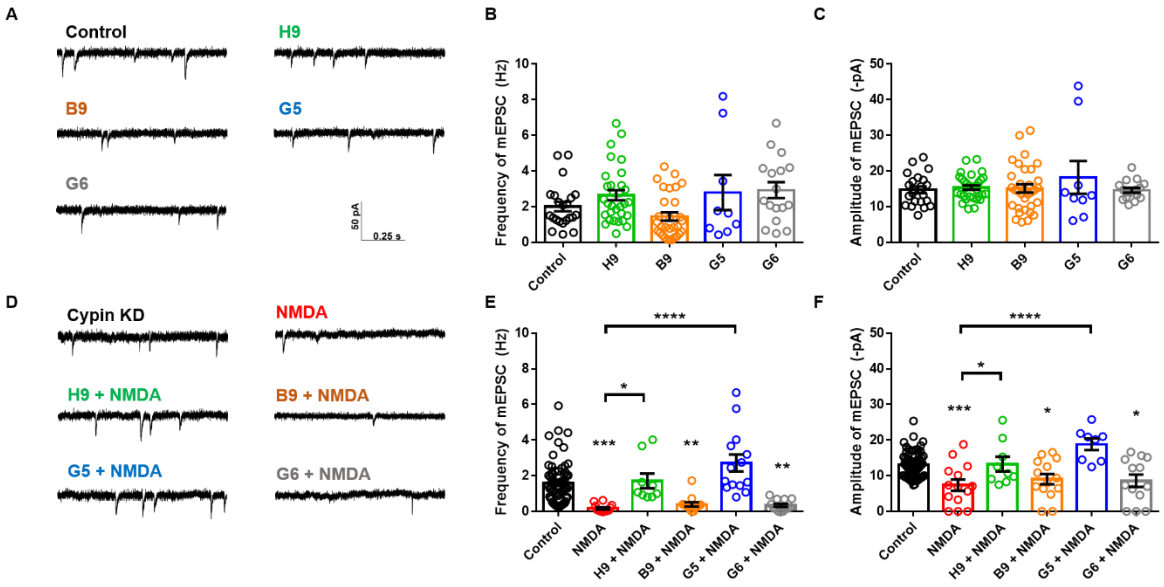

Figure 2.15. Cypin activators, H9 and G5, but not the inhibitor, B9, or the neutral compound, G6, prevent loss of neuronal activity following NMDA-induced injury. *A.* Representative traces of mEPSCs recorded from rat hippocampal neurons treated with <0.1% DMSO (control; n=22), 20µM: H9, (n=32), B9 (n=32), G5 (n=9), or G6 (n=17). *B-C.* Bar graph analysis of mEPSC frequency and amplitude following 48 hour baseline drug treatment. *D.* Representative traces of mEPSCs recorded from rat hippocampal neurons treated with <0.1% DMSO (control; n=24), 20µM: NMDA (n=15), H9 + NMDA (n=9), B9 + NMDA (n=14), G5 + NMDA (n=14), and G6 + NMDA (n=13). *E-F.* Bar graph analysis of mEPSC frequency and amplitude following 48 hour drug treatment, 5 minute 20µM NMDA-induced injury, and two hour recovery period. Pretreatment with cypin

activators prevents decrease in frequency and amplitude induced by NMDA injury while the inhibitor and neutral compound have no beneficial effect. *p<0.05, **p<0.01, ***p<0.005, ****p<0.001 determined by one-way ANOVA followed by Tukey-Kramer multiple comparisons test. Error bars indicate ± SEM.

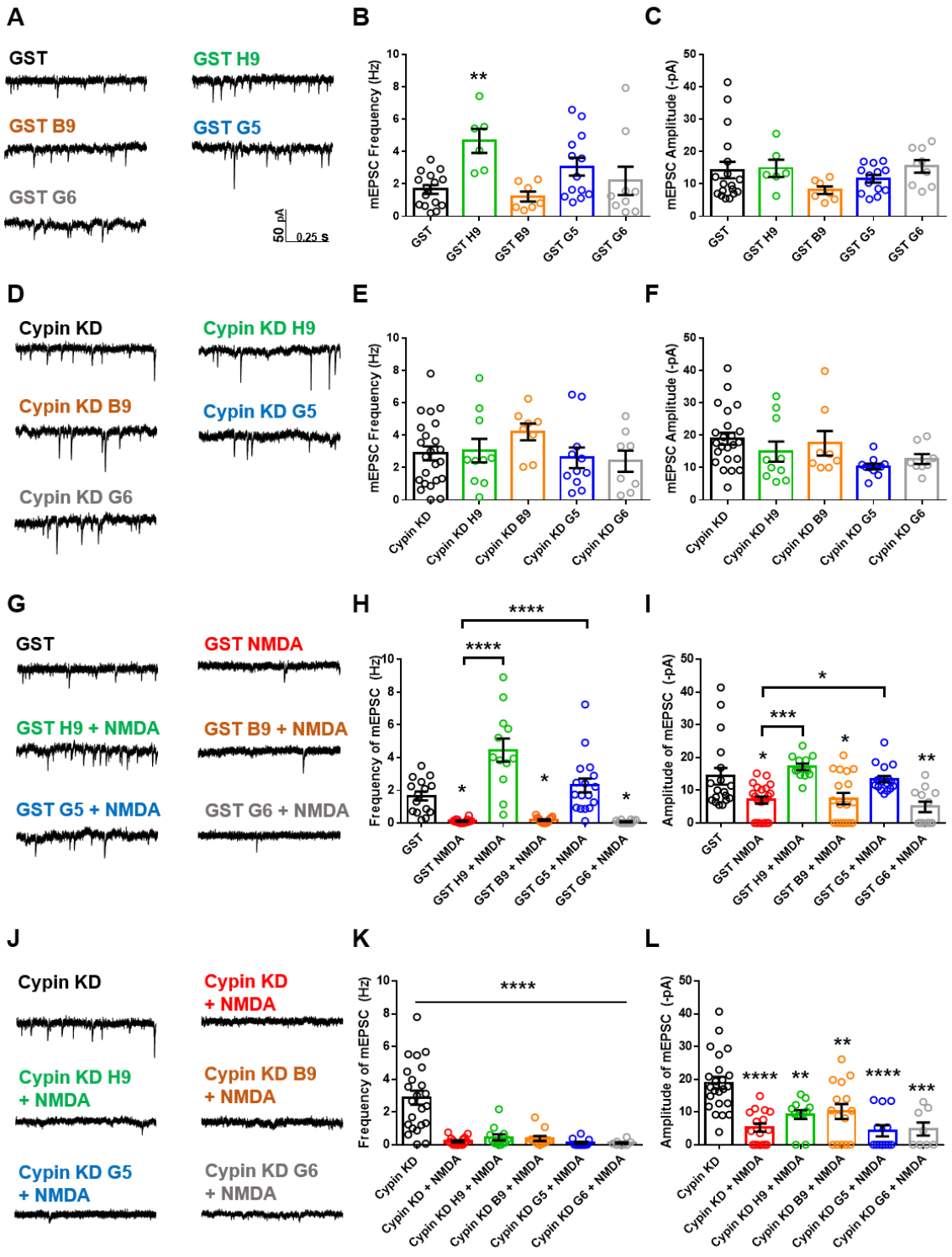

Figure 2.16. The neuroprotective function of cypin activators is dependent on cypin expression. *A,D.* Representative traces of mEPSCs recorded from control rat hippocampal

neurons or neurons with cypin knockdown treated with <0.1% DMSO (control; n=17/23), 20μM: H9, (n=6/8), B9 (n=7/8), G5 (n=13/11), or G6 (n=9/8). *B-C,E-F.* Bar graph analysis of mEPSC frequency and amplitude following 48 hour baseline drug treatment. Pretreatment with H9 increases the frequency of mEPSCs in control neurons with no change to amplitude. *G,J.* Representative traces of mEPSCs recorded from rat hippocampal neurons treated with <0.1% DMSO (control; n=17/23), 20μM: NMDA (n=19/16), H9 + NMDA (n=12/12), B9 + NMDA (n=15/11), G5 + NMDA (n=17/12), and G6 + NMDA (n=12/8). *H-I, K-L.* Bar graph analysis of mEPSC frequency and amplitude following 48 hour drug treatment, 5 minute 20μM NMDA-induced injury, and two hour recovery period. Treatment with cypin activators prevents the decrease in frequency and amplitude induced by NMDA injury in control neurons, while cypin knockdown causes a loss of function and subsequent decrease of mEPSC frequency and amplitude. *p<0.05, **p<0.01, ***p<0.005, ****p<0.001 determined by one-way ANOVA followed by Tukey-Kramer multiple comparisons test. Error bars indicate ± SEM.

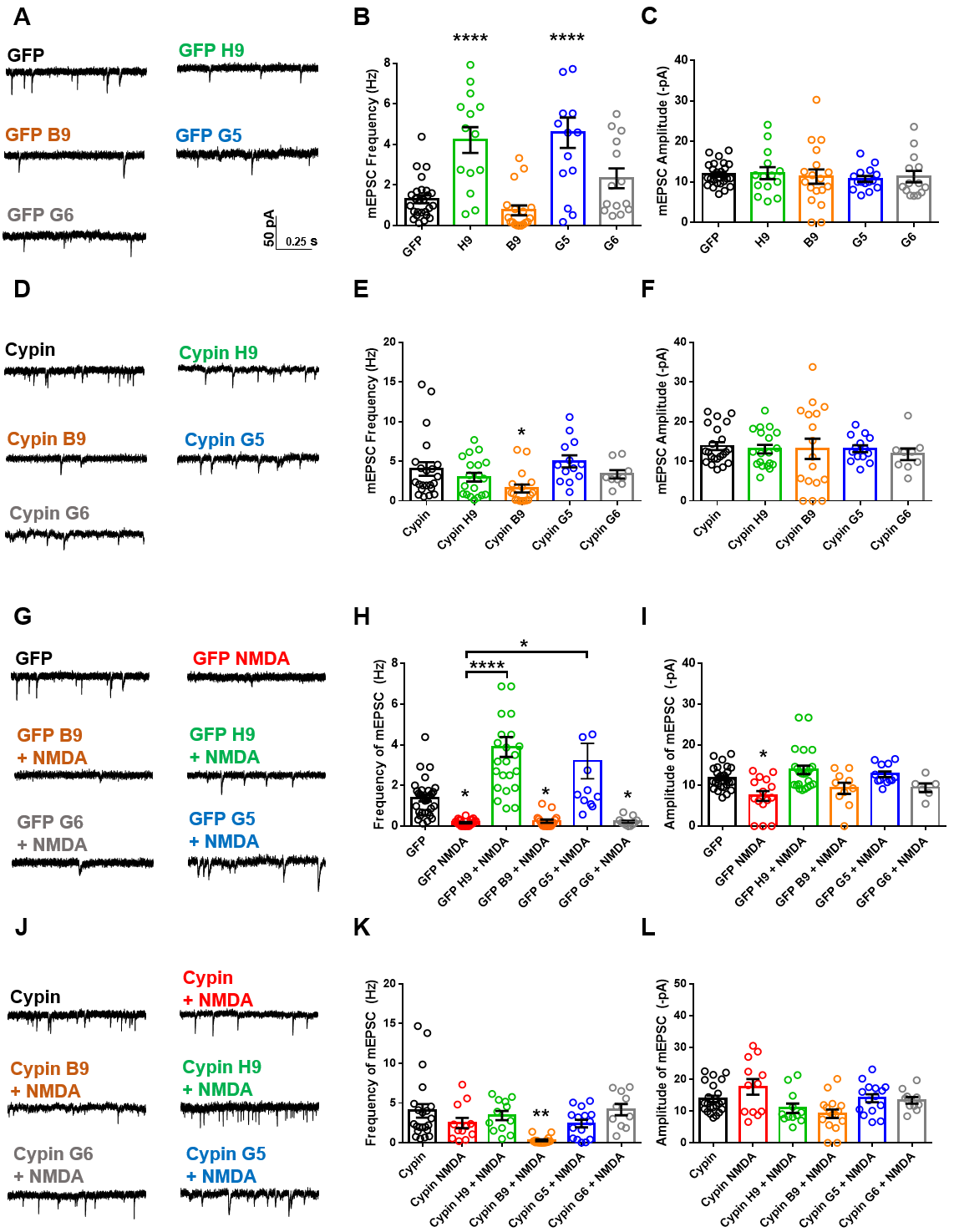

Figure 2.17. Cypin overexpression prevents NMDA-induced injury. *A,D.* Representative traces of mEPSCs recorded from rat hippocampal neurons overexpressing

GFP (control) or cypin treated with <0.1% DMSO (control; n=26/22), 20μM: H9, (n=14/21), B9 (n=18/17), G5 (n=15/13), or G6 (n=17/9). *B-C,E-F*. Bar graph analysis of mEPSC frequency and amplitude following 48 hour baseline drug treatment. H9 and G5 increased frequency of mEPSCs in control neurons with no change to amplitude. *G,J*. Representative traces of mEPSCs recorded from rat hippocampal neurons treated with <0.1% DMSO (control; n=32/22), 20μM: NMDA (n=23/12), H9 + NMDA (n=24/12), B9 + NMDA (n=17/16), G5 + NMDA (n=12/15), and G6 + NMDA (n=11/10). *H-I, K-L*. Bar graph analysis of mEPSC frequency and amplitude following 48 hour drug treatment, 5 minute 20μM NMDA-induced injury, and two hour recovery period. Pretreatment with cypin activators prevents the decrease in frequency and amplitude induced by NMDA injury in control neurons, while cypin overexpression alone prevents the decrease of frequency and amplitude of mEPSCs, an effect blocked by pretreatment with B9. *p<0.05, **p<0.01, ****p<0.001 determined by one-way ANOVA followed by Tukey-Kramer multiple comparisons test. Error bars indicate ± SEM.

2.3 Discussion

Traumatic brain injury (TBI) causes widespread neuronal damage and dysfunction, leading to cognitive dysfunction, which severely impairs the lives of affected individuals.[40-42,49] Patients with TBI often times experience deficits in learning and memory, which vary depending on the severity of injury.[40-42,49] Although TBI has been studied for many years, and its effects on learning and memory are well known, the molecular mechanisms of how TBI affects these cognitive functions are still largely unknown. The hippocampus is a

structure located in the medial temporal lobe of the brain, is a part of the limbic system, and has been extensively described for its critical function in learning, formation of short and long-term memories, and spatial recognition.[50,51] Long-term potentiation (LTP) is a process of strengthening synaptic connections between neurons critical for formation of long-term memories.[50-52] Induction of LTP is dependent upon activation of NMDA receptors, and downstream signaling effectors, CaMKII, PKC, and PKMz, leading to an increase in activation and synaptic localization of AMPA receptors, while the maintenance phase of LTP is dependent upon protein expression and proper function of the proteasome.[50-53] TBI disrupts both induction and maintenance phases of LTP, leading to deficits in formation of long-term memory and cognitive function.[47,48,54,55]

Cypin is a guanine deaminase, which promotes microtubule assembly and dendrite branching.[56,57] Cypin also binds PSD-95 via its PDZ-binding motif affecting trafficking of PSD-95, and effectively AMPA and NMDA receptors, to the postsynaptic site.[56,57] In this work, we used multiple approaches to determine the function of cypin in healthy and injured neurons. We found that cypin overexpression increases the frequency of mEPSCs while knockdown increases amplitude. These data suggest that cypin functions at both pre- and postsynaptic sites since frequency changes are generally associated with neurotransmitter release probability from the presynaptic site, while changes in amplitude are explained by receptor composition at the postsynaptic site.[58] Our laboratory previously reported that cypin binds zinc via its His82, His84, His240, His279, and Asp330 residues[59], and zinc imbalance has been shown to increase the amplitude of mEPSCs (in a concentration dependent manner) and is likely to be involved in a number of psychiatric diseases, such as epilepsy, spreading depression, and ischemia.[60-62] It is possible that cypin

knockdown leads to increases in synaptic zinc, which may be responsible for the observed increase in mEPSC amplitude. Additionally, snapin was previously found to bind to the CRMP homology domain of cypin via the carboxyl-terminal coiled-coil domain of snapin, and decrease dendritic branching.[38] At the presynaptic site snapin binds the SNARE complex through SNAP-25 and increases binding of synaptotagmin to the SNARE complex following cAMP-dependent phosphorylation, effectively leading to vesicle exocytosis and neurotransmitter release.[39] Studies investigating effect of snapin manipulation on neuronal electrophysiology and vesicle release dynamics show that snapin knockdown induces a decrease in mEPSC frequency and kinetics, as well as loss of homeostatic modulation of presynaptic vesicle release, while phospho-mimetic mutant of snapin increased exocytosis in chromaffin cells.[39] Based on our results, it is possible then that cypin increases trafficking of snapin to the presynapse leading to increased vesicle priming and release, effectively increasing mEPSC frequency. Alternatively, increases in mEPSC frequency and bursting synchrony can be explained by the ability of cypin to stabilize microtubules and increase dendritic branching, resulting in a greater number of synaptic connections.

Western blot analysis of brain tissue from mice subjected to mild or moderate CCI revealed induction of cypin protein expression in the cortex at 1 day post injury; however, this induction was not observed at 2 hours, 7 days, or 14 days following injury. This transient increase suggests that cypin might be involved in the early stages of injury response; however, its precise function is currently unknown. Nevertheless, we decided to take advantage of the guanine deaminase activity of cypin to potentially increase uric acid (UA) production via the use of small molecule probes. UA is

the product of purine catabolism and is an effective antioxidant due to its scavenger action on free radicals and acts upon astrocytes to upregulate glutamate transporters.[24-27] Peroxynitrite-induced cytotoxicity in an *in vitro* injury model has been shown to decrease in response to UA.[63-66] In a glutamate-induced injury model of SCI, UA decreased cell death in mixed spinal cord motor neurons and glial cultures.[63-66] *In vivo* evidence suggests that UA administered at the time of and after injury improves recovery from spinal cord compression injury.[63-66] The body of evidence shows, therefore, that UA effectively protects neurons *in vitro* and *in vivo* against the secondary injury, whether it is glutamate-induced or due to inflammatory cascades. Morphological and electrophysiological analysis revealed that cypin activators do, indeed, prevent NMDA-induced injury *in vitro*, an effect not observed with the use of cypin inhibitor or neutral compound. Additionally, we show that these compounds are dependent on the expression of cypin as cypin knockdown resulted in loss of neuroprotection. It is possible then, that these compounds act directly on cypin improving its GDA activity or dendritic branching, and decrease trafficking of PSD-95 or synapse-associated protein 102 (SAP-102) to the presynaptic site.[38] SAP-102 has been previously found to bind NMDA receptor NR2B subunit, which is highly permeable to calcium, a critical secondary messenger following secondary injury.[67] Decreased trafficking of SAP-102 induced by indirect effect of cypin activators might be responsible for observed neuroprotection and recovery of neuronal electrophysiology *in vitro*. Although these compounds show great promise, they have several limitations. At this time, we do not know whether our activators, inhibitor, or the neutral compound are specific to cypin, have an indirect effect, or nonspecific activity. We also do not know the pharmacokinetics, pharmacodynamics, or binding affinity, all of which limit their potential

therapeutic use *in vivo*. Given our data thus far, it would be of great value to perform these studies in order to further characterize these compounds and validate them for use *in vivo*. Interestingly, neuronal death and mEPSC analysis show that cypin overexpression alone is neuroprotective in an NMDA-induced injury model of TBI. This phenotype can be explained by the ability of cypin to bind zinc and prevent its neurotoxic effect after injury[59], as well as cypin's GDA activity resulting in increased UA production.

Taken together, these data show that cypin is an attractive target for modulation following brain injury and the availability of small molecule compounds presents a viable therapeutic avenue.

2.4 Methods

2.4.1 Primary cortical neuron culture and injury

Neuronal cultures were plated from hippocampi of rat embryos at 18 days gestation on glass coverslips (12 mm diameter; 176,911 cells/cm^2 for electrophysiology and Sholl analysis, 47,244 cells/cm^2 for immunocytochemistry) previously coated with poly-D-lysine (Sigma-Aldrich) in full Neurobasal medium (Life Technologies, Grand Island, NY) supplemented with B-27 (Life Technologies) and GlutaMax (Life Technologies). At day *in vitro* (DIV) 7, cultures were transduced with pHUUG-GST-shRNA, pHUUG-Cypin-shRNA, GFP, or cypin overexpression lentiviral vectors, at DIV14 cultures were treated with 20μM of each cypin modulator, and at DIV16 cultures were treated with NMDA in 0.1% DMSO for 5 minutes or vehicle, and allowed either 2 hours of recovery before electrophysiological experiments, or 24 hours before immunocytochemistry.

2.4.2 Drugs

N-methyl-D-aspartate (NMDA) was purchased from Sigma-Aldrich (St. Louis, MO). RAD001 and MK2206 were purchased from Selleckchem (Houston, TX). Dimethyl sulfoxide (DMSO) was purchased from Thermo Fisher Scientific (Waltham, MA). Small molecule cypin modulators were purchased from Fox Chase Chemical Diversity Center, Inc. (Doylestown, PA).

2.4.3 Western Blot analysis

Protein concentration was measured by a standard Bradford assay. Proteins (15 µg per sample) were resolved on a 10% SDS-polyacrylamide gel and transferred to a polyvinylidene difluoride membrane. Membranes were blocked in 5% bovine serum albumin (BSA) in TBS-T (50 mM Tris, 150 mM NaCl, pH 7.6) for 1 hour and incubated in primary antibodies overnight at 4^0C. Membranes were then incubated for 1 hour in secondary HRP-conjugated antibodies and subjected to HyGlo Western Blotting Detection System (Denville Scientific, Holliston, MA).

2.4.4 Immunocytochemistry

Cortical neurons were grown for 16 days in culture, and treated as previously described, on coverslips coated with poly-D-lysine, and after immunostaining, coverslips were mounted on glass slides using Fluoromount G (Southern Biotechnology) and then imaged.

Cultures were fixed in 4% paraformaldehyde in phosphate-buffered saline (PBS) for 10 min, permeabilized with 0.1% Triton X-100 in PBS + 5% normal goat serum, and immunostained with mouse anti-MAP2 (1:500) from Rockland and anti-GFP (1:500) from EMD Millipore followed by secondary antibodies conjugated to Alexa-Fluor® 488 (Invitrogen, 1:250) or Alexa-Fluor® 555 (Invitrogen, 1:250). Nuclei were stained with Hoechst dye (1:1000). Neurons were visualized by immunofluorescence under a 10X objective on an EVOS FL microscope. Only neurons positive for MAP2 immunostaining and Hoechst staining were counted and used for statistical analysis.

2.4.5 Electrophysiology

Whole cell patch-clamp recordings were performed on the soma of cortical neurons. For recordings, cells were bathed in artificial cerebrospinal fluid containing (in mM): 140 NaCl, 5 KCl, 2 $CaCl_2$, 2 $MgCl_2$, 10 HEPES, and 10 glucose (pH 7.4 adjusted with NaOH; 290-310 mOsmol). Recording electrodes (3 –5 MΩ) contained a K^+-based internal solution composed of (in mM): 126 K-gluconate, 4 KCl, 10 HEPES, 4 ATP-Mg, 0.3 GTP-Na_2, and 10 phosphocreatine (pH 7.2; 280 –300 mOsmol). Miniature excitatory postsynaptic currents (mEPSCs) were recorded in presence of 1 µM tetrodotoxin (to block the action potentials) in the external solution, and 10 µM QX-314 (Tocris, R & D Systems; Minneapolis, MN) in the internal solution, $GABA_A$-mediated neurotransmission was blocked with 50 µM picrotoxin (Tocris, R & D Systems; Minneapolis, MN) as previously described. The membrane potential was held at -70mV throughout all experiments. Data were amplified and filtered at 2 kHz by a patch-clamp amplifier (Multiclamp 700B), digitalized (DIGIDATA 1440A), stored, and analyzed by pCLAMP (Molecular Devices;

Union City, CA). Data were discarded when the input resistance changed >20% during recording.

2.4.6 Statistics

Western blot, survival and electrophysiological data were analyzed for changes in treatment conditions when compared to control cells treated with vehicle or injured. Data were analyzed with ANOVA followed by Tukey-Kramer's multiple comparisons test using InStat and Prism software (GraphPad). p values <0.05 were considered significant.

2.5 Acknowledgments

I would like to thank Sara A. McEwan, Mihir V. Patel, Nick Cuccolo, the Meaney group at the University of Pennsylvania, and Dr. Bonnie Firestein for their tremendous work on this project.

Chapter 3: Role of Akt-independent mTORC1 and GSK3β signaling in sublethal NMDA-induced injury and the recovery of neuronal electrophysiology and survival

The work in this chapter has been previously published in the following article: Swiatkowski P, Nikolaeva I, Kumar G, Zucco A, Akum BF, Patel MV, D'Arcangelo G, Firestein BL (2017). Role of Akt-independent mTORC1 and GSK3β signaling in sublethal NMDA-induced injury and the recovery of neuronal electrophysiology and survival. *Scientific Reports* 7(1):1539.

3.1 Introduction

Brain trauma, caused by either mechanical injury or oxygen deprivation, leads to the stimulation or suppression of a large number of molecular signaling cascades within the brain, and overall disruption of neuronal electrophysiology.[68-70] Following the initial physical damage, an almost immediate release of excitotoxic levels of amino acids, such as glutamate and aspartate, occurs in the surrounding tissues, exacerbating cell death.[71] Glutamate-induced toxicity is a common mechanism of secondary injury in both neurodegenerative disorders and neuronal injury, such as traumatic brain injury, stroke, or epilepsy.[72-76] Glutamate receptor blockers have failed to improve recovery from the secondary damage in human clinical trials, leaving researchers to examine other pathways affected by injuries.

One pathway that undergoes a dramatic increase in signaling activity after injury is the PI3K/Akt/mTORC1 pathway[77-79] and has become a focus for drug development for the treatment of central nervous system injuries.[80] The PI3K/Akt/mTOR pathway plays an essential role in cellular growth and repair of neurons and is susceptible to modulation through glutamate receptor-mediated signaling. Excitatory levels of amino acids stimulate pathway activity, while excitotoxic levels of amino acids lead to pathway suppression.[81-83] While many studies have focused on teasing out the role of the PI3K/Akt/mTOR pathway in damage and repair, the results of these experiments have yielded conflicting results on whether activation of PI3K/Akt/mTOR signaling is beneficial or detrimental for neuronal and functional recovery.[84,85] Additional research at the cellular level is needed to discern the molecular and functional roles of PI3K/Akt/mTOR pathway signaling following injury.

At the cellular level, dendrites undergo morphological changes after exposure to excitotoxic levels of glutamate.[86-89] These alterations, including spine retraction and varicosity formation, also occur *in vivo* after injury.[90-95] Not much is known about the mechanisms underlying spine retraction and recovery; however, actin is thought to contribute to spine loss[96,97] but not to spine recovery.[98] Since actin has been linked to activation of the PI3K/Akt/mTOR pathway in local cue-induced axonal protein synthesis[99], it is of interest to study how this pathway regulates synaptic function after injury.

To study how glutamate receptor-mediated injury affects electrophysiological properties and neuronal cell survival, cultured rat cortical neurons were exposed to a sublethal concentration of NMDA. This treatment models secondary damage caused by mechanical,

ischemic, or neurodegenerative injury. To test whether the PI3K/Akt/mTOR pathway plays a role in the response to NMDA, neurons were exposed to specific pharmacological agonists and inhibitors, some of which are currently in clinical trials for other diseases, such as certain cancers[100-102], involving aberrant activity of this signaling pathway (Figure 3.1). In the present study, we find that exposure of cultured neurons to sublethal levels of NMDA does not induce activation or suppression of the PI3K/Akt/mTOR pathway; however, inhibition of mTORC1 and GSK3β prior to mild excitotoxic damage aids in recovery of normal electrophysiology and survival. In contrast, inhibition of Akt does not rescue excitotoxic damage, suggesting that NMDA-mediated changes to electrophysiology and survival are independent of Akt activity, and rather, depend on selective basal activity of mTORC1 and GSK3β kinases. Together, these data demonstrate the importance of mTORC1 and GSK3β in mediating neuronal dysfunction following excitotoxic injury.

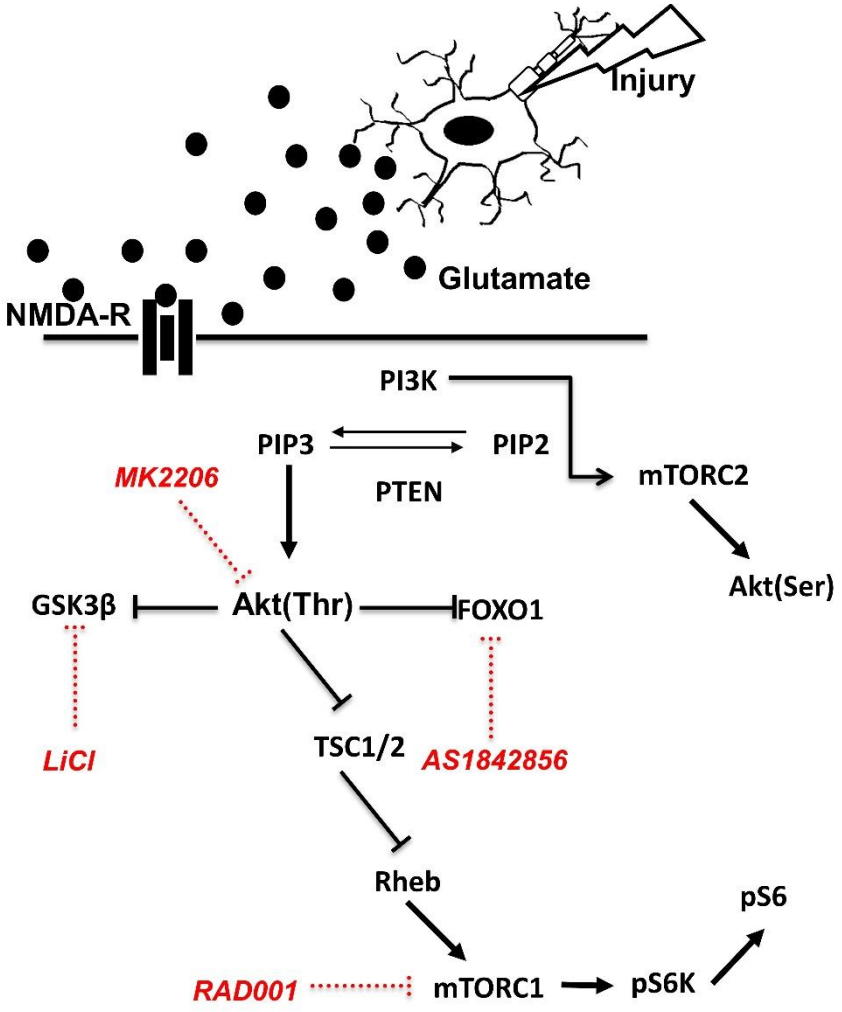

Figure 3.1. Schematic model of the PI3K/Akt/mTOR signaling pathway and pharmacological compounds used to modulate its activity.

PI3K activity causes the conversion of PIP2 to PIP3, which then leads to the activation of Akt via PDK1-mediated phosphorylation on threonine 308. Additional mTORC2-dependent phosphorylation on serine 473 contributes to full Akt kinase activity. Phosphorylated Akt subsequently targets GSK3β, FOXO1, and TSC1/2 for inhibition by phosphorylation of specific residues. Suppression of TSC1/2 leads to activation of Rheb,

mTORC1, and downstream targets. MK2206 inhibits Akt kinase activity, RAD001 inhibits mTORC1 activity, LiCl inhibits GSK3β activity, and AS1842856 inhibits FOXO1 function.

3.2 Results

3.2.1 Inhibition of mTORC1 signaling before injury leads to preserved acute neurotransmission in injured neurons

While the long term effects of excitotoxic damage on neuronal physiology are well-characterized, evidence showing acute effects is lacking. Rat cortical neuron cultures were treated on day *in vitro* (DIV) 14 with 20 μM NMDA for 5 minutes to mimic sublethal excitotoxicity as we previously described.[103-105] Electrophysiological analysis revealed that neurons treated with NMDA display a decrease in both frequency and amplitude of spontaneous excitatory postsynaptic currents (sEPSCs; Figure 3.2B-C) at 2 hours following sublethal excitotoxic insult. As expected, NMDA-induced decrease in sEPSC frequency was not observed when neuronal cultures were co-treated with APV (Figure 3.2B), an NMDA receptor antagonist. Interestingly, NMDA-induced decrease in amplitude was not blocked by APV, suggesting that excitotoxicity induced by synaptic NMDA receptors is, in part, responsible for the observed acute decline in neuronal activity.[106,107]

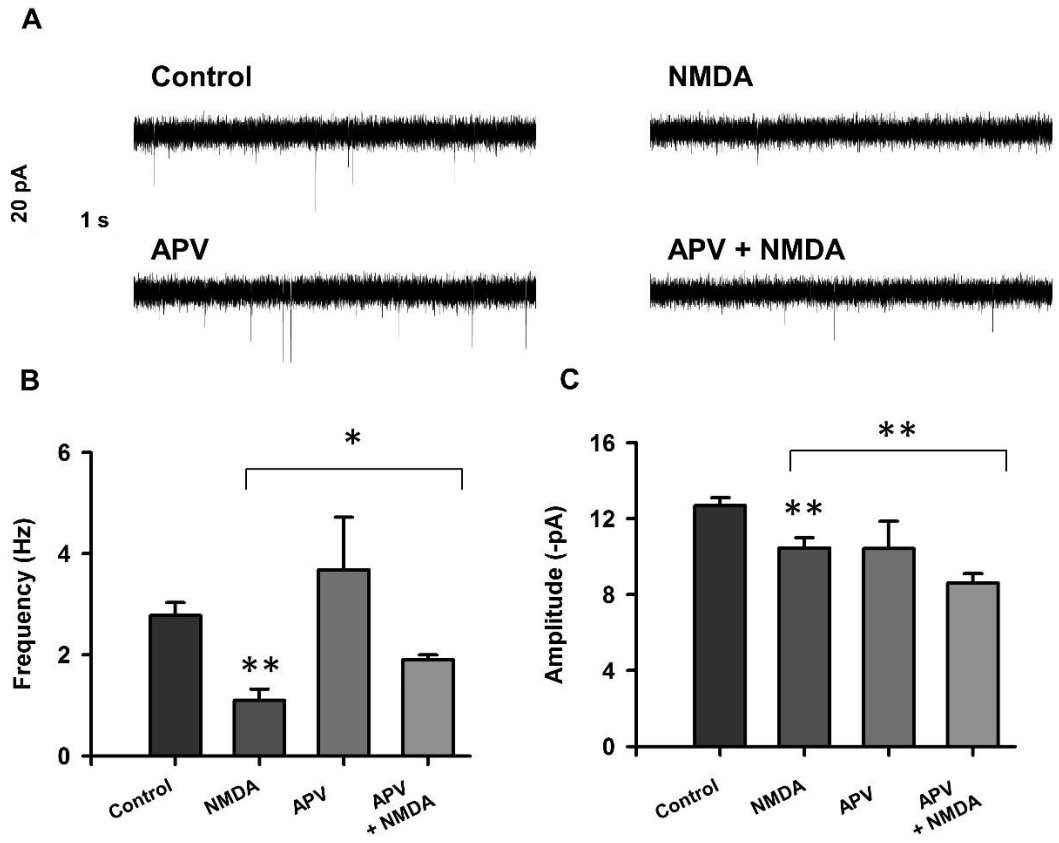

Figure 3.2. Excitotoxic injury leads to decreased sEPSC frequency and amplitude. *A.* Representative traces of sEPSCs recorded from rat cortical neurons treated with vehicle (control; n=74), 20µM NMDA (n=38), 20µM APV (n=6), or APV + NMDA (n=7). *B-C.* Bar graph analysis of sEPSC frequency and amplitude following 4 hour drug treatment followed by 5 minute 20µM NMDA-induced injury and 2 hour recovery period. Data from NMDA treatment are compared to control. * $p<0.05$, ** $p<0.01$ determined by one-way ANOVA followed by Tukey-Kramer multiple comparisons test. Error bars indicate ± SEM.

To investigate the role of mTORC1 signaling on the disruption of neuronal activity in our injury paradigm, we recorded sEPSCs from control or injured neurons exposed to

RAD001, an inhibitor of mTORC1 (Figure 3.1). Cultures were treated with 5 μM RAD001 for four hours, followed by a five minute treatment with 20μM NMDA to induce injury, and a two hour recovery period. We found that treatment with RAD001 alone increased the baseline frequency of sEPSCs (Figure 3.3A-B). In our injury paradigm, RAD001 prevented NMDA-induced decreases in sEPSC frequency, suggesting that mTORC1 activity is detrimental for neuronal electrophysiology post-NMDA-induced injury (Figure 3.3D-F). In addition, it should be noted that the apparent prevention observed with RAD001 on the effects of NDMA treatment might be ascribed to the effect of RAD001 on basal sEPSCs, consistent with a permissive role for mTORC1 in NMDA-induced changes to frequency.

We then asked whether other proteins in the PI3K/Akt/mTOR signaling pathway play a role in electrophysiological changes induced by NMDA-induced excitotoxicity. First, to demonstrate the effect of altering Akt activity on neuronal electrophysiology *in vitro*, we treated our cultures with 2 μM MK2206, an Akt inhibitor (Figure 3.1), and recorded from these cultures. Treatment did not affect baseline amplitude or frequency of sEPSCs (Figure 3.3A-C). We then subsequently subjected cultures treated with MK2206 to NMDA-induced injury. As described above, NMDA-induced excitotoxic damage led to a decrease in frequency and amplitude of sEPSCs two hours post-injury; however, treatment with MK2206 had no effect on sEPSC frequency and amplitude (Figure 3.3D-F), suggesting that Akt activity does not play a role in the disruption of electrophysiological function due to NMDA-mediated injury. Taken together, these data suggest that mTORC1,

but not Akt, activity in excitotoxic conditions mediates deleterious effects and that inhibition of mTORC1 partially prevents changes in neuronal electrophysiology.

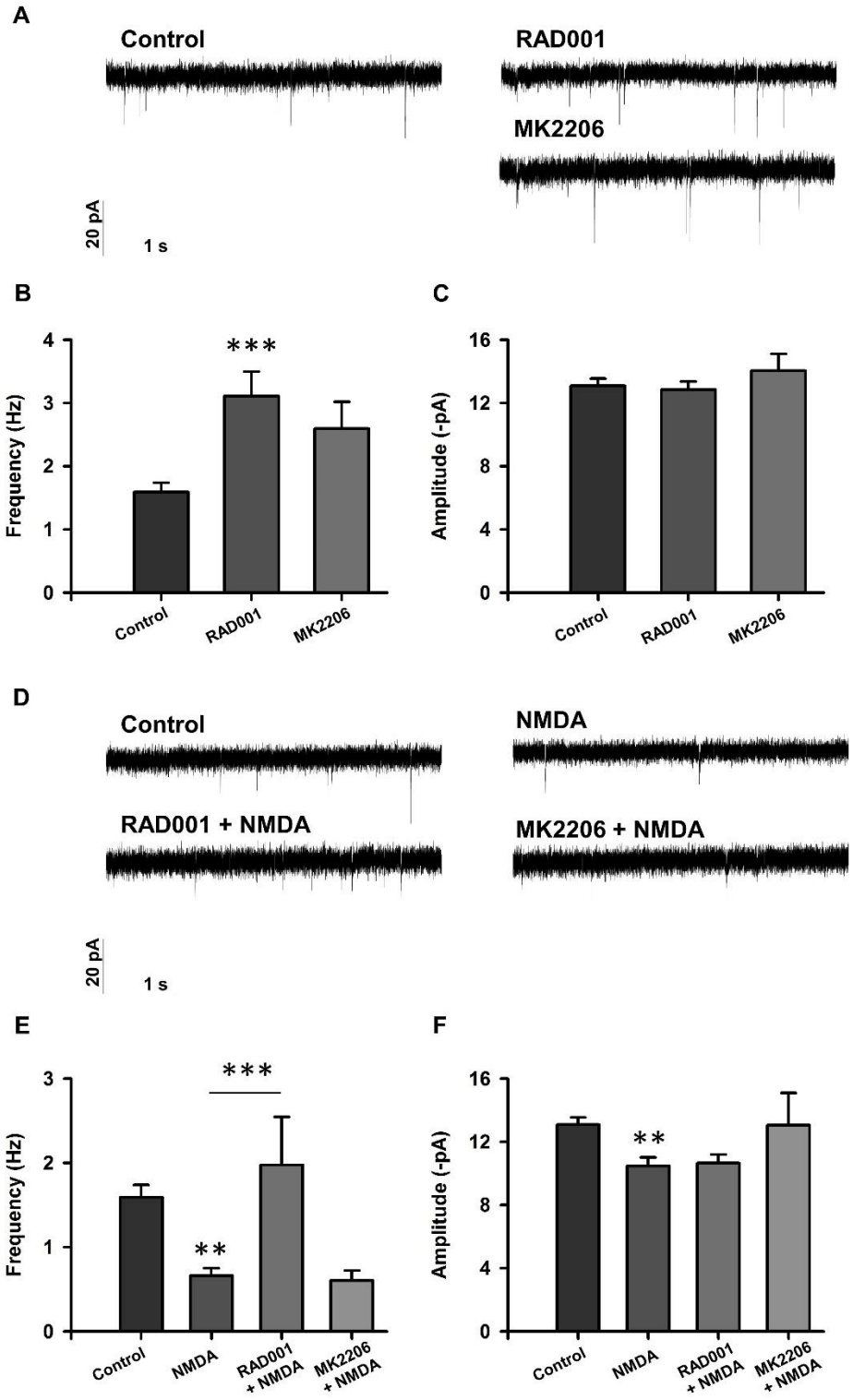

Figure 3.3. mTORC1, but not Akt, inhibition restores acute electrophysiology following injury. *A.* Representative traces of sEPSCs recorded from rat cortical neurons treated with <0.1% DMSO (control; n=67), 5μM RAD001 (n=37), or 2μM MK2206 (n=29). *B-C.* Bar graph analysis of sEPSC frequency and amplitude following 4 hour baseline drug treatment and 2 hour recovery period. *D.* Representative traces of sEPSCs recorded from rat cortical neurons treated with <0.1% DMSO (control; n=67), 20μM NMDA (n=35), RAD001 + NMDA (n=16), and MK2206 + NMDA (n=13). *E-F*. Bar graph analysis of sEPSC frequency and amplitude following 4 hour drug treatment, 5 minute 20μM NMDA injury, and 2 hour recovery period. $^{**}p<0.01$, $^{***}p<0.005$ determined by one-way ANOVA followed by Tukey-Kramer multiple comparisons test. Error bars indicate ± SEM.

3.2.2 *mTORC1, but not Akt, inhibition is beneficial for neuronal function 24h after injury*

Our electrophysiology data recorded from neurons shortly following injury demonstrate that inhibition of mTORC1 aids in preventing alterations in neuronal electrophysiology following excitotoxic injury. To address whether the effects of this manipulation confer any long-term effects on sEPSC frequency or amplitude, as this is clinically relevant, we performed our experiments 24 hours following drug treatment and NMDA-induced injury. Both frequency and amplitude of sEPSCs were significantly decreased 24 hours after injury (Figure 3.4D-E), suggesting long-term detrimental effects of excitotoxic damage on neuronal electrophysiology. At this time point, treatment with RAD001 alone resulted in no changes to baseline electrophysiology (Figure 3.4A-C).

However, treatment with RAD001 prevented NMDA-induced decreases in both sEPSC frequency and amplitude, whereas treatment with MK2206 had no effect (Figure 3.4D-F). Taken together, these data suggest that NMDA-mediated excitotoxicity induces long-term damage to neuronal electrophysiology and that mTORC1 inhibition improves neurotransmission both acutely (two hours) and longer-term (24 hours) following injury. Akt inhibition, on the other hand, is not effective in preserving normal electrophysiology after injury.

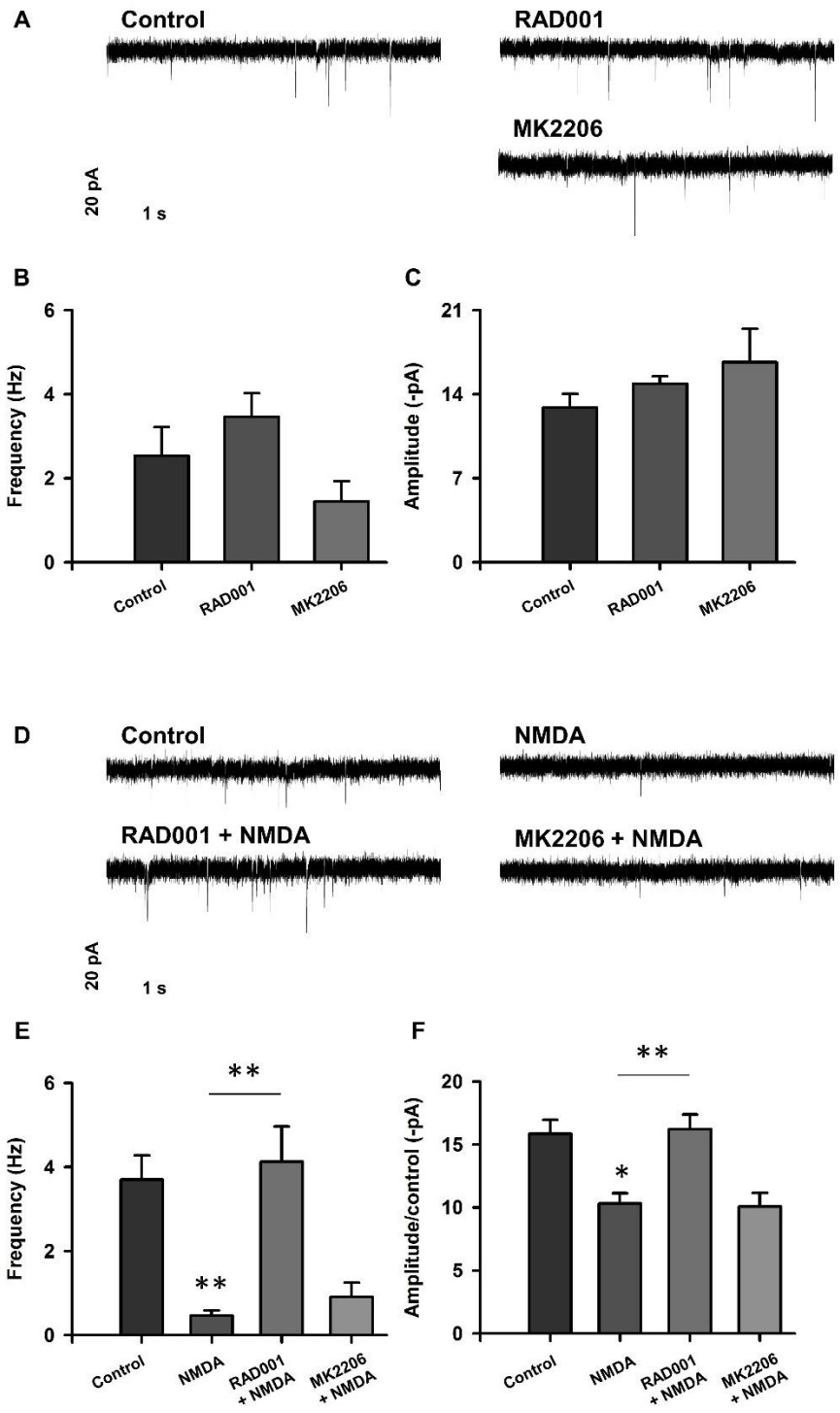

Figure 3.4. Inhibition of mTORC1, but not Akt, restores electrophysiology 24 hours following injury. *A.* Representative traces of sEPSCs recorded from rat cortical neurons treated with <0.1% DMSO (control; n=16), 5μM RAD001 (n=7), 2μM MK2206 (n=7). *B-*

C. Bar graph analysis of sEPSC frequency and amplitude following 4 hour baseline drug treatment and 24 hour recovery period. *D.* Representative traces of sEPSCs recorded from rat cortical neurons treated with <0.1% DMSO (control; n=29), 20μM NMDA (n=14), RAD001 + NMDA (n=14), and MK2206 + NMDA (n=15). *E-F*. Bar graph analysis of sEPSC frequency and amplitude following 4 hour drug treatment, 5 minute 20μM NMDA injury, and 24 hour recovery period. *p<0.05, **p<0.01 determined by one-way ANOVA followed by Tukey-Kramer multiple comparisons test. Error bars indicate ± SEM.

3.2.3 The role of FOXO1 and GSK3β in recovery of neuronal electrophysiology following NMDA-induced injury

Our data presented above suggest that Akt does not play a major role in mediating the effects resulting from NMDA-induced excitotoxicity, however one of its targets (mTORC1) does. To explore the role of other signaling molecules downstream of Akt, we investigated FOXO1, a transcription factor critical for cell survival and metabolism[108], and GSK3β, a ubiquitous enzyme implicated in glycogen metabolism and cell survival.[109] Both FOXO1 and GSK3β are phosphorylated and are functionally inhibited by Akt (Figure 3.1). Additionally, FOXO1 is activated in a stress response leading to inhibition of mTORC1 and activation of Akt in order to preserve energy homeostasis (Figure 3.1).[110-112]

To investigate how manipulation of these Akt downstream targets affects neuronal electrophysiology, we treated neurons with AS1842856, a FOXO1 inhibitor (Figure 3.1), for 24 hours or LiCl, a GSK3 inhibitor (Figure 3.1), for four hours prior to injury. While treatment with AS1842856 resulted in decreased baseline sEPSC frequency two hours

following treatment (Figure 3.5A-C), but not 24 hours after treatment (Figure 3.6A-C), inhibition of FOXO1 had no effect on NMDA-induced electrophysiological changes by two or 24 hours post-injury (Figures 3.5D-F and 3.6D-F). In contrast, inhibition of GSK3 with LiCl had no effect on baseline neurotransmission (Figures 3.5A-C and 3.6A-C) but prevented NMDA-induced changes to sEPSCs to control, uninjured amplitude and frequency at two hours, and partial recovery at 24 hours following injury (Figures 3.5D-F and 3.6D-F). The partial recovery at 24 hours may represent the fact that inhibition of GSK3 early is not sufficient to maintain full recovery of sEPSCs at this time point.

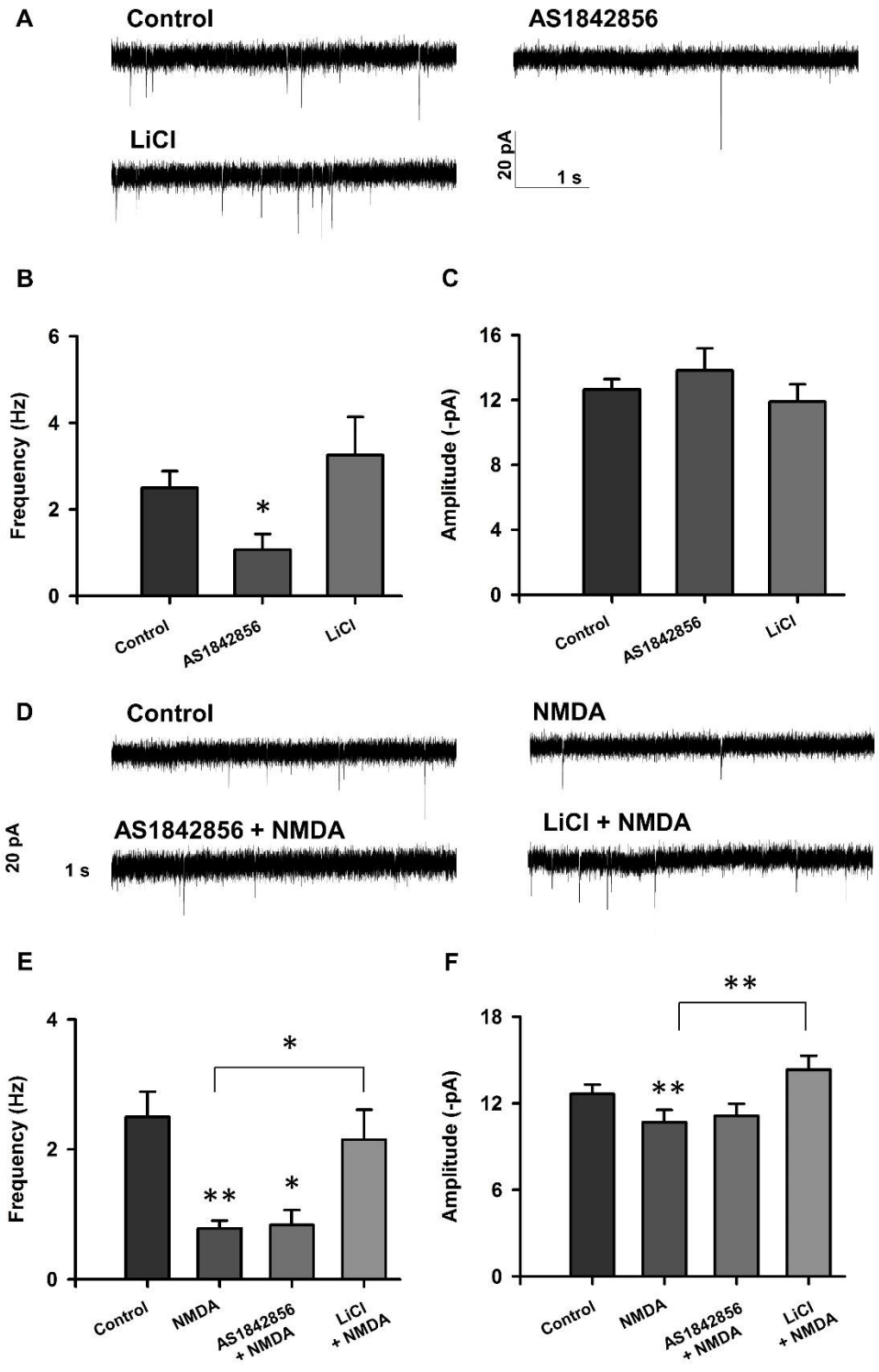

Figure 3.5. Inhibition of GSK3β, but not FOXO1, results in improved electrophysiology 2 hours following injury. *A.* Representative traces of sEPSCs recorded

from rat cortical neurons treated with <0.1% DMSO (control; n=34), 1µM AS1842856 (n=15), 10mM LiCl (n=16). *B-C.* Bar graph analysis of sEPSC frequency and amplitude following 4 hour baseline drug treatment and 2 hour recovery period. *D.* Representative traces of sEPSCs recorded from rat cortical neurons treated with <0.1% DMSO (control; n=34), 20µM NMDA (n=22), AS1842856 + NMDA (n=12), LiCl + NMDA (n=18). *E-F.* Bar graph analysis of sEPSC frequency and amplitude following 4 hour drug treatment, 5 minute 20µM NMDA-induced injury, and two hour recovery period. **p*<0.05, ***p*<0.01 determined by one-way ANOVA followed by Tukey-Kramer multiple comparisons test. Error bars indicate ± SEM.

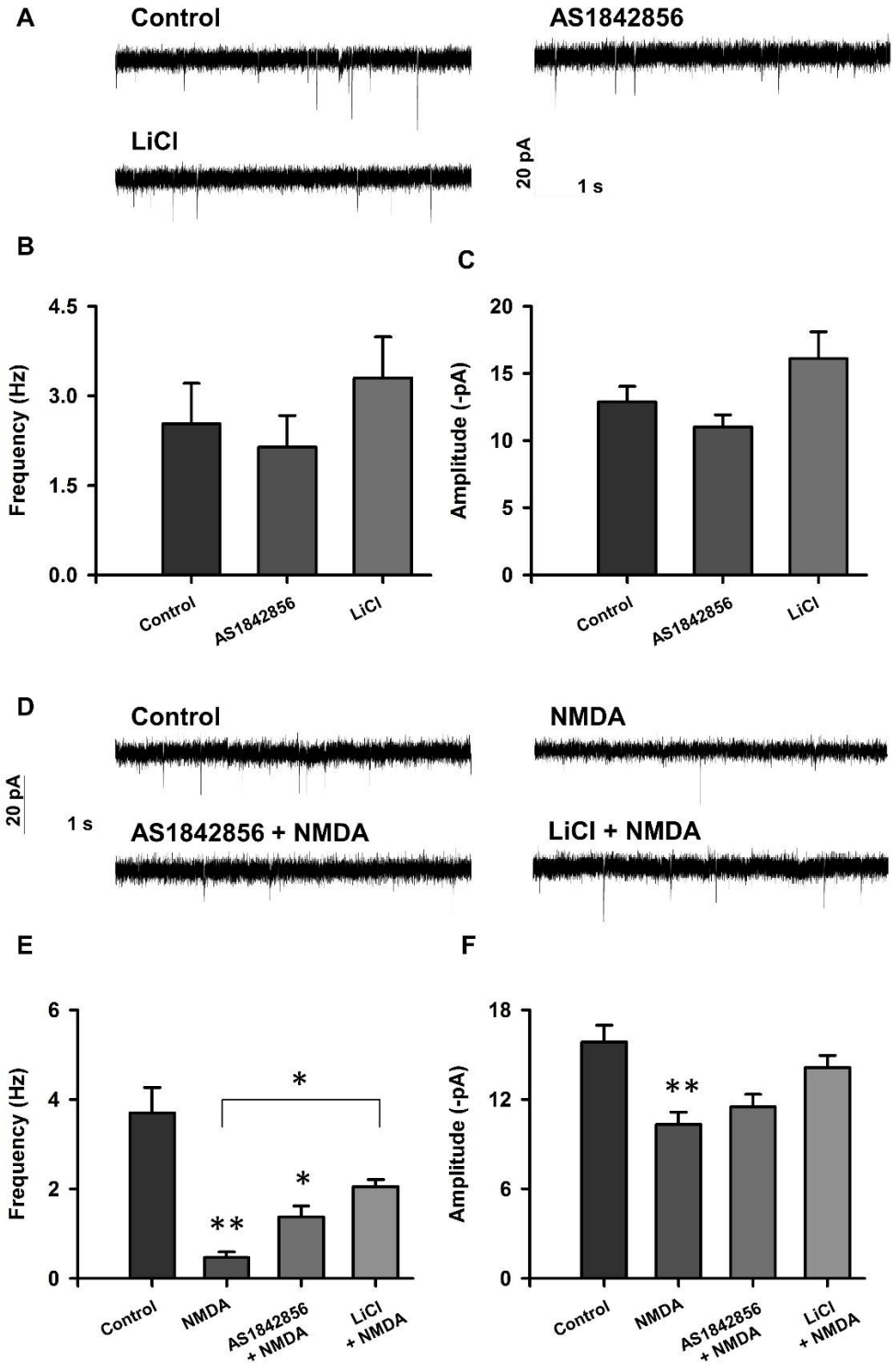

Figure 3.6. Inhibition of GSK3β results in recovery of electrophysiology 24 hours following NMDA-induced injury. *A.* Representative traces of sEPSCs recorded from rat

cortical neurons treated with <0.1% DMSO (control; n=16), 1μM AS1842856 (n=16), 10mM LiCl (n=10). *B-C.* Bar graph analysis of sEPSC frequency and amplitude following 4 hour baseline drug treatment and 24 hour recovery period. *D.* Representative traces of sEPSCs recorded from rat cortical neurons treated with <0.1% DMSO (control; n=29), 20μM NMDA (n=14), AS1842856 + NMDA (n=9), LiCl + NMDA (n=27). *E-F*. Bar graph analysis of sEPSC frequency and amplitude following 4 hour drug treatment, 5 minute 20μM NMDA-induced injury, and 24 hour recovery period. *p<0.05, **p<0.01 determined by one-way ANOVA followed by Tukey-Kramer multiple comparisons test. Error bars indicate ± SEM.

3.2.4 The roles of mTOR pathway components in NMDA-induced changes to mEPSCs and sEPSCs are identical

Since the observed decreases in sEPSC frequency and amplitude after NMDA treatment might be attributed to changes in neuronal excitability, we recorded miniature-EPSCs (mEPSCs), which are independent of action potentials. Analysis of mEPSCs revealed that NMDA-induced changes are almost identical to the decreased frequency and partially decreased amplitude observed at 2 hours following sublethal excitotoxic insult (Figure 3.7D-F). Neurons co-treated with mTORC1 and GSK3β inhibitors before injury did not show this reduction. Interestingly, treatment with either the Akt or FOXO1 inhibitor alone induced reduction of mEPSC frequency (Figure 3.7A-C).

Furthermore, we quantified any changes to dendritic arborization and number of synapses resulting from NMDA-induced injury or the inhibitors used in this study,

potentially providing mechanistic insight into observed changes in neuronal electrophysiology. Our data show that arborization of dendrites, which are MAP2-immunopositive, does not change in response to exposure to NMDA or inhibitors as evidenced by Sholl analysis (Figure 3.8). In addition, treatment with NMDA or inhibitors does not result in changes to the number of excitatory synapses, as determined by the number of axonal synaptophysin-positive clusters apposing dendritic PSD-95 clusters per 10 µm dendrite (Figure 3.9A). While these data show no effect on the number of synapses in our cultures by NMDA and inhibitors used in this study, electrophysiological data suggest that a subset of these synapses are dysfunctional.

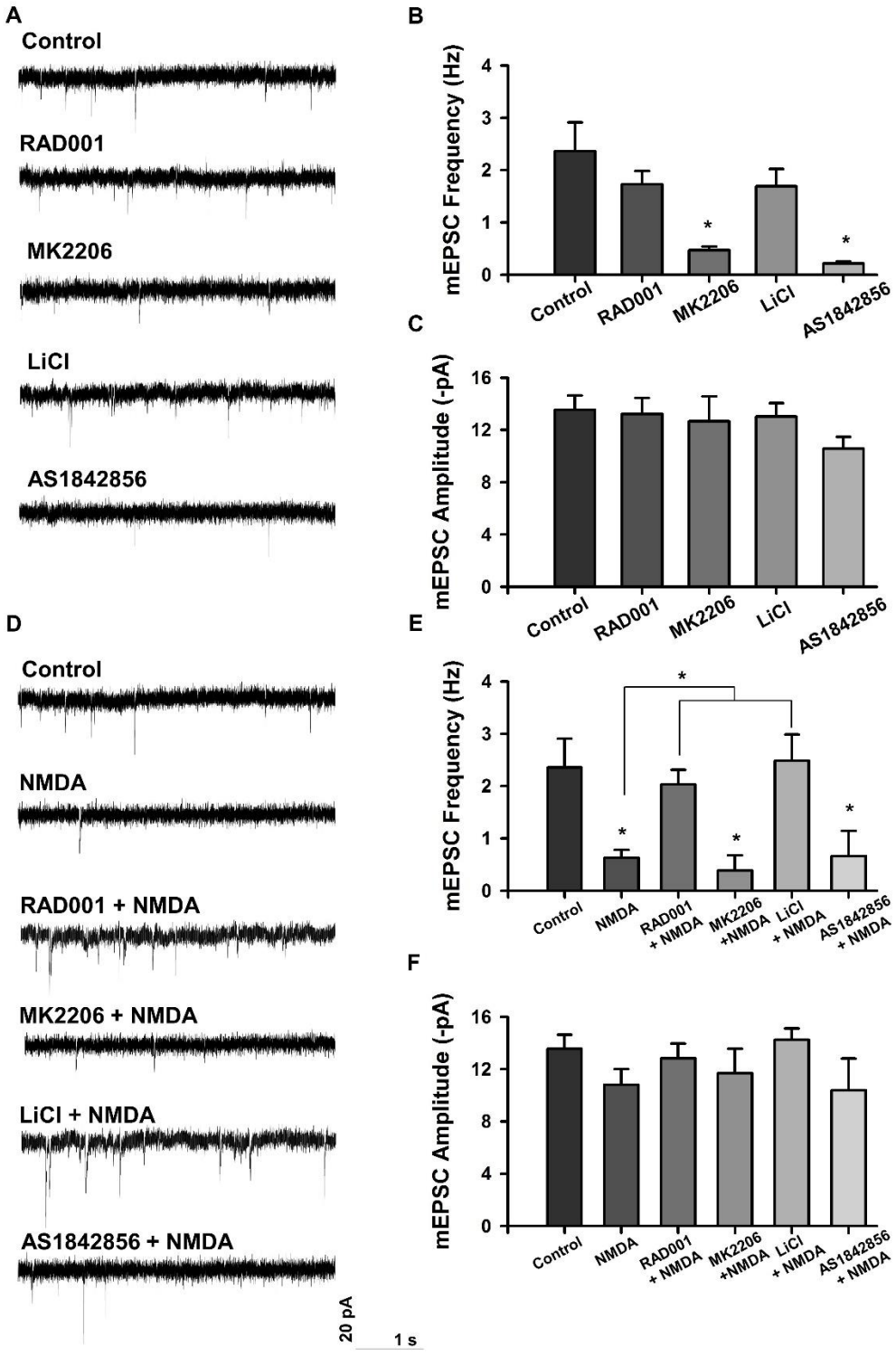

Figure 3.7. Inhibition of mTOR and GSK3β lead to improved frequency of mEPSCs 2 hours following NMDA-induced injury. *A,D.* Representative traces of mEPSCs

recorded from rat cortical neurons treated with <0.1% DMSO (control; n=12), 20μM NMDA (n=10), 5 μM RAD001 (n=12), 2 μM MK2206 (n=7), 10mM LiCl (n=7), 1 μM AS1842856 (n=7), RAD + NMDA (n=16), MK2206 + NMDA (n=7), LiCl + NMDA (n=12), and AS1842856 + NMDA (n=6). *B-C.* Bar graph analysis of sEPSC frequency and amplitude following 4 hour baseline drug treatments and 2 hour recovery period. *E-F.* Bar graph analysis of sEPSC frequency and amplitude following 4 hour drug treatment, 5 minute 20μM NMDA-induced injury, and two hour recovery period. mEPSC data suggest that deficits in neuronal electrophysiology at two hours following injury are independent of neuronal excitability. **p*<0.05 determined by one-way ANOVA followed by Tukey-Kramer multiple comparisons test. Error bars indicate ± SEM.

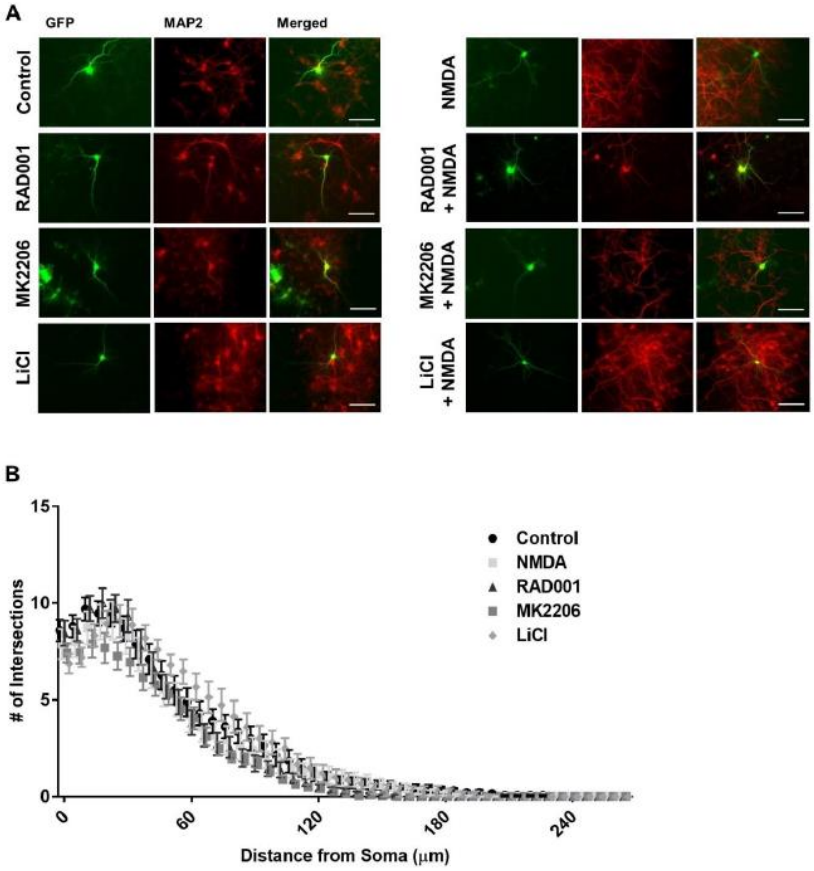

Figure 3.8. PI3K/Akt/mTOR pathway inhibitors do not affect dendritic arborization. Primary hippocampal neurons were transfected with cDNA encoding GFP on DIV 14. On DIV 20, neurons were treated with 0.1% DMSO (control), NMDA, RAD001, MK2206, LiCl, then medium with or without 20 μM NMDA. *A.* Representative images showing GFP fluorescence and neuron-specific MAP2 immunostaining. Scale bar: 100μm. *B.* Sholl analysis reveas no differences between treatment groups in number of intersections of dendrites. Each data set represents 20 neurons from three different trials. No difference between any condition and control was observed. *p* value determined by one-way ANOVA followed by Tukey-Kramer multiple comparisons test. Error bars indicate ± SEM.

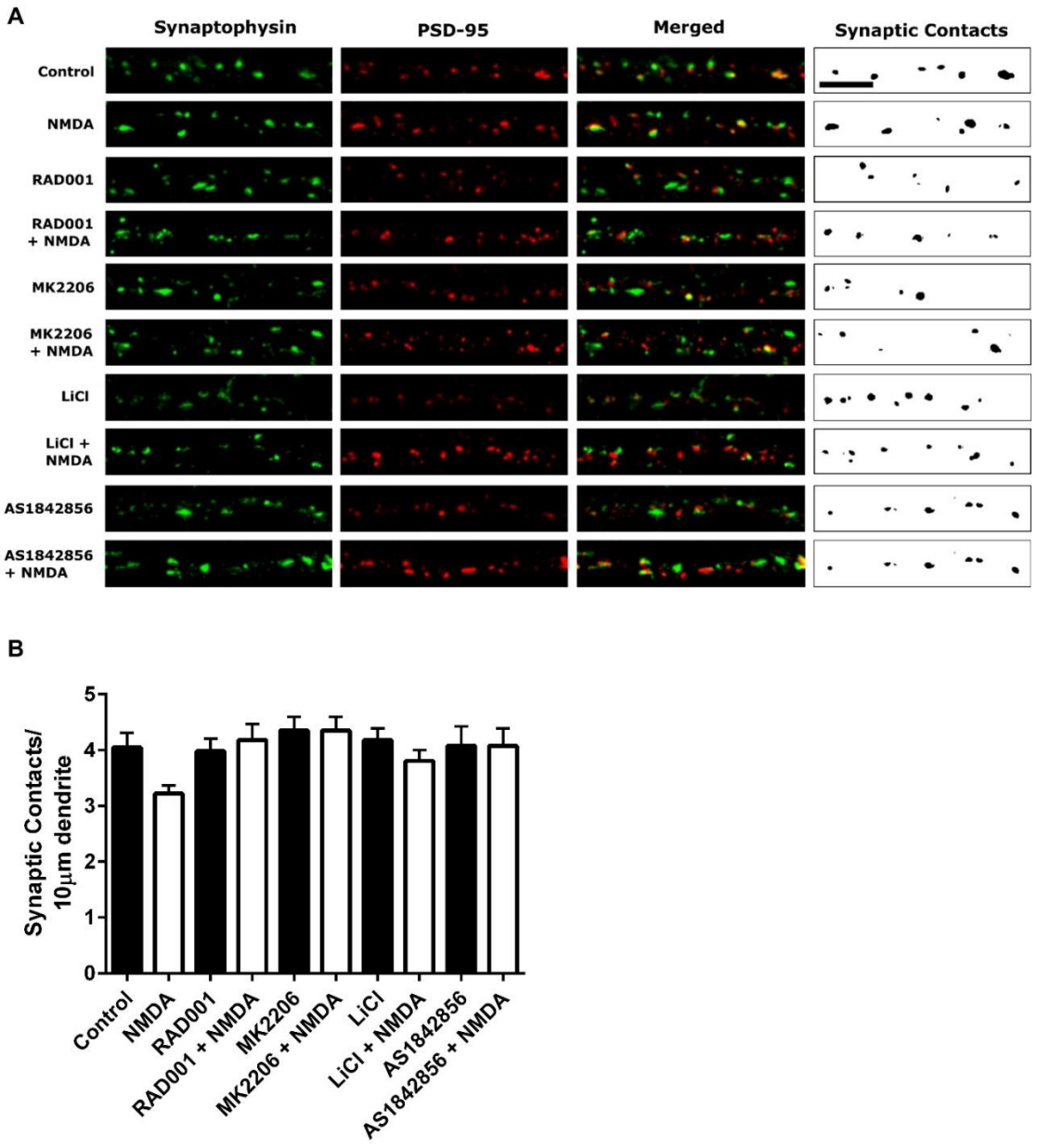

Figure 3.9. PI3K/Akt/mTOR pathway inhibitors do not affect synaptic clusters. On DIV 14, neurons were treated with 0.1% DMSO (control), 5 µM RAD001, 2 µM MK2206, or 10 mM LiCl, with or without 20 µM NMDA. A. Representative fluorescence images showing excitatory synapses with immunostaining for PSD-95 on dendrites and synaptophysin on axons. Merged panels show apposition of PSD-95 and synaptophysin immunostaining, and hence synaptic clusters, in yellow. Apposed clusters (excitatory

synapses) from merged panels are shown as binary images. B. Quantitation of excitatory synapses counted from 15-30 µm dendrite lengths. Each data set represents 20 neurons from three different trials. No difference between any condition and control was observed. *p* value determined by one-way ANOVA followed by Tukey's multiple comparisons test. Error bars indicate ± SEM. Scale bar= 5 µm.

Taken together, our data suggest that inhibition of GSK3 activity has a beneficial effect on function of cortical neurons after injury and may be a therapeutic target for managing the effects of excitotoxic damage. In addition, based on our data, GSK3 signaling is parallel to mTORC1 signaling in mediating synaptic and electrophysiological changes in response to NMDA-induced injury. Since Akt inhibition is not sufficient to suppress NMDA-induced effects, we propose that both mTORC1 and GSK3 function independently of Akt in this process.

3.2.5 Sublethal levels of NMDA do not activate the PI3K/Akt/mTOR pathway

To investigate whether the acute effects on neuronal physiology after sublethal NMDA-mediated injury are associated with activation of the PI3K/Akt/mTOR pathway, we performed Western blot analysis on protein extracts from cultures at two (Figure 3.10) and 24 hours after NMDA treatment. We found that NMDA treatment did not induce phosphorylation of Akt on threonine 308 (pAkt(Thr308)) or serine 473 (pAkt(Ser473)), ribosomal protein S6 on serine 235/236 (pS6), and GSK3β on serine 9 (pGSK3β) when compared to levels of total Akt, S6, and GSK3β (Figure 7; n=6). These data, in contrast to

published literature, show that sublethal exposure to NMDA does not activate PI3K/Akt/mTOR pathway at two and 24 hours.[113,114]

Since we observed a lack of activation of the PI3K/Akt/mTOR pathway by NMDA, we asked how selective modulation of the downstream targets of Akt affects different components of the PI3K/Akt/mTOR pathway and whether the data observed for mTOR and GSK3 involvement in NMDA-induced changes to electrophysiology suggest a permissive role for these effectors. We took a pharmacological approach to establish the role of individual kinases in NMDA-induced excitotoxicity. To confirm the specificity of our drug treatments in our culture conditions, we either pretreated cultures for four hours with 0.01% DMSO (as a vehicle control[103-105]), Akt inhibitor MK2206 (2 μM), mTORC1 inhibitor RAD001 (5 μM), GSK3β inhibitor LiCl (10mM) or pretreated cultures for twenty four hours with FOXO1 inhibitor AS1842856 (1 μM) and then either induced sublethal injury with 20μM NMDA for 5 minutes. Control cultures were treated with vehicle. Cultures were allowed to recover for 2 hours without the presence of these inhibitors, at which point, cells were lysed, and proteins were extracted for Western blot analysis. As expected, exposure of cultures to MK2206 resulted in significantly decreased levels of pAkt(Thr), pAkt(Ser), and pGSK3β (Figure 3.10B,C,G), and exposure of cultures to RAD001 resulted in decreased pS6 (Figure 3.10E). Furthermore, LiCl induced a modest increase in pGSK3β ($p=0.055$, Figure 3.10F), while exposure to AS1842854 resulted in decreased pAkt(Thr) and pGSK3β levels (Figure 3.10D,H).

To determine whether the effects observed on the PI3K/Akt/mTOR signaling pathway are maintained for a longer time period after NMDA exposure, we performed similar Western blot analysis of cellular extracts from cultures allowed to recover for 24

hours post-injury. We found that at this time point, phosphorylation levels of targets of the pathway were highly variable, and thus, the activation status of the signaling kinases could not be determined (data not shown).

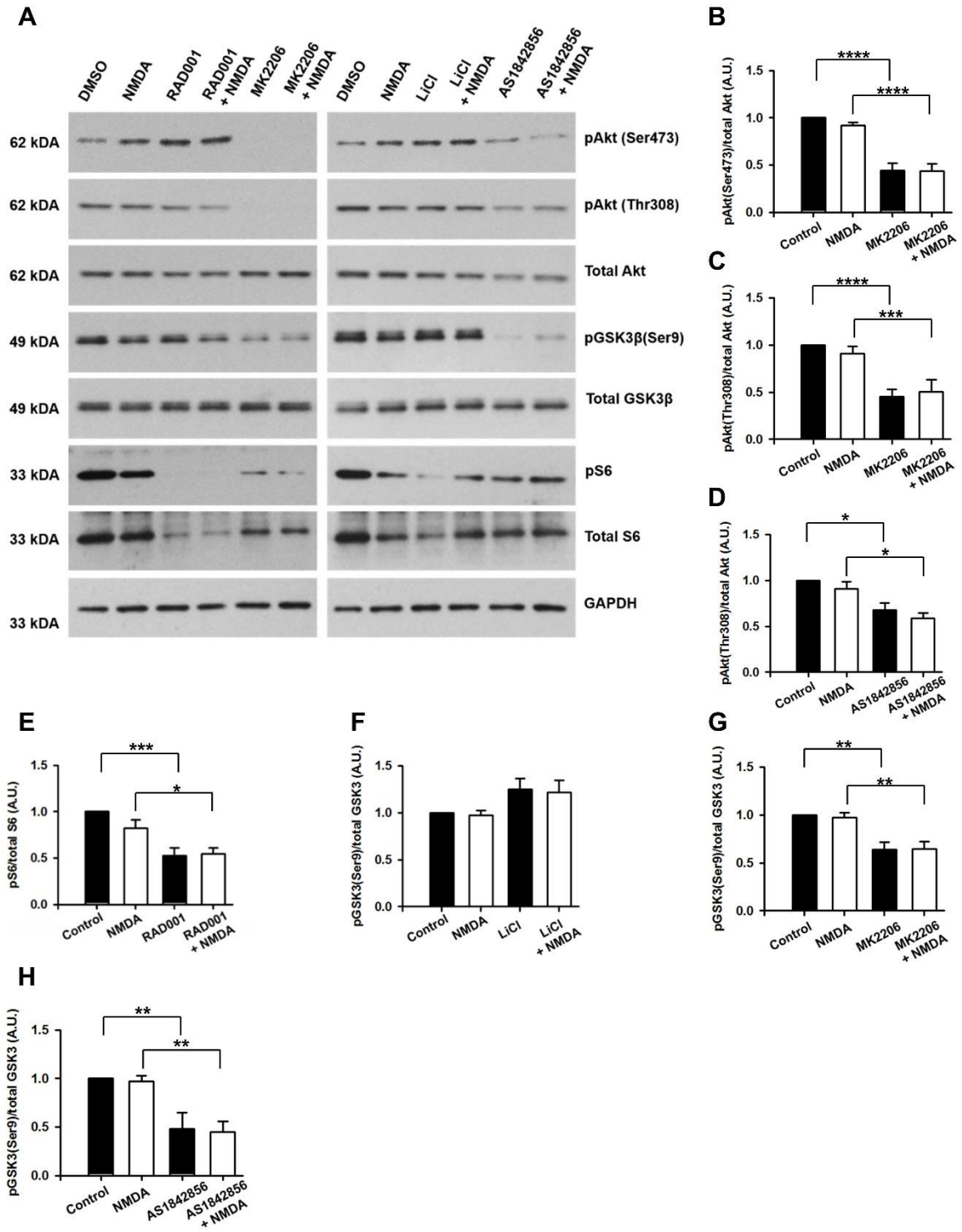

Figure 3.10. Sublethal excitotoxic injury does not induce phosphorylation of downstream targets of Akt at 2 hours after injury. *A.* Representative Western blot bands

showing phosphorylation of threonine 308 in Akt (pAkt(Thr308)) and serine 473 in Akt (pAkt(Ser473)) and total Akt, phosphorylation of S6 (pS6) and total S6, phosphorylation of serine 9 in GSK3β (pGSK3β(Ser9)) and total GSK3β, from cortical neuron cultures treated with 0.1% DMSO (control), NMDA (20μM), RAD001 (5 μM), MK2206 (2 μM), LiCl (10 mM), and AS18425856 (1 μM) and allowed to recover for two hours. *B-H.* Quantitative analysis of band intensity shows MK2206-induced inhibition of phosphorylation of Akt and GSK3β, RAD001-induced inhibition of phosphorylation of ribosomal protein S6, LiCl induced phosphorylation of GSK3β, and AS1842856-induced inhibition of phosphorylation of Akt and GSK3β. Western blot bands are representative from six replicates of the experiment. *p<0.05, **p<0.01, ***p<0.005, ****p<0.001 determined by two-way ANOVA followed by Tukey's multiple comparisons test. Error bars indicate ± SEM.

Taken together, our data suggest that exposure to sublethal levels of NMDA does not change the activation state of the PI3K/Akt/mTORC1 signaling pathway and that the drugs used act to inhibit their intended targets under our experimental conditions. Furthermore, our data suggest that basal activity of mTOR and GSK3β acts permissively to allow NMDA to induce damage to neurons. This permissive role is supported by data that inhibition of GSK3 activity by LiCl (Figure 3.5) restores sEPSCs to control, uninjured amplitude and frequency but that GSK3β is not phosphorylated by NMDA-induced injury. Additionally, loss of some protection by LiCl after 24 hours also suggests that GSK3β may only play a permissive role within hours after injury.

4.2.6 Inhibition of mTORC1 and GSK3β promotes neuronal survival after NMDA treatment

The data presented thus far suggest a protective effect of RAD001 and LiCl treatment on neuronal electrophysiology both acutely and 24 hours after injury. Since these inhibitors did not change the phosphorylation state of Akt (Figure 3.10), we asked whether in addition to improved electrophysiology, these inhibitors improve neuronal survival after injury. Thus, we quantified the number of surviving neurons in our cultures at 24 hours after treatment with 0.01% DMSO (vehicle), RAD001 (5 μM), MK2206 (2 μM), LiCl (10 mM), AS1842856 (1 μM) and either NMDA or vehicle (as described above). Interestingly, NMDA treatment induced a 38% decrease in neuron count when compared to cultures treated with vehicle, while both RAD001 and LiCl prevented any substantial neuronal death (Figure 3.11A,B,D). In contrast, both MK2206 and AS1842856 induced death of control neurons and had no effect on survival of cultures treated with NMDA (Figure 3.11A,C,E).

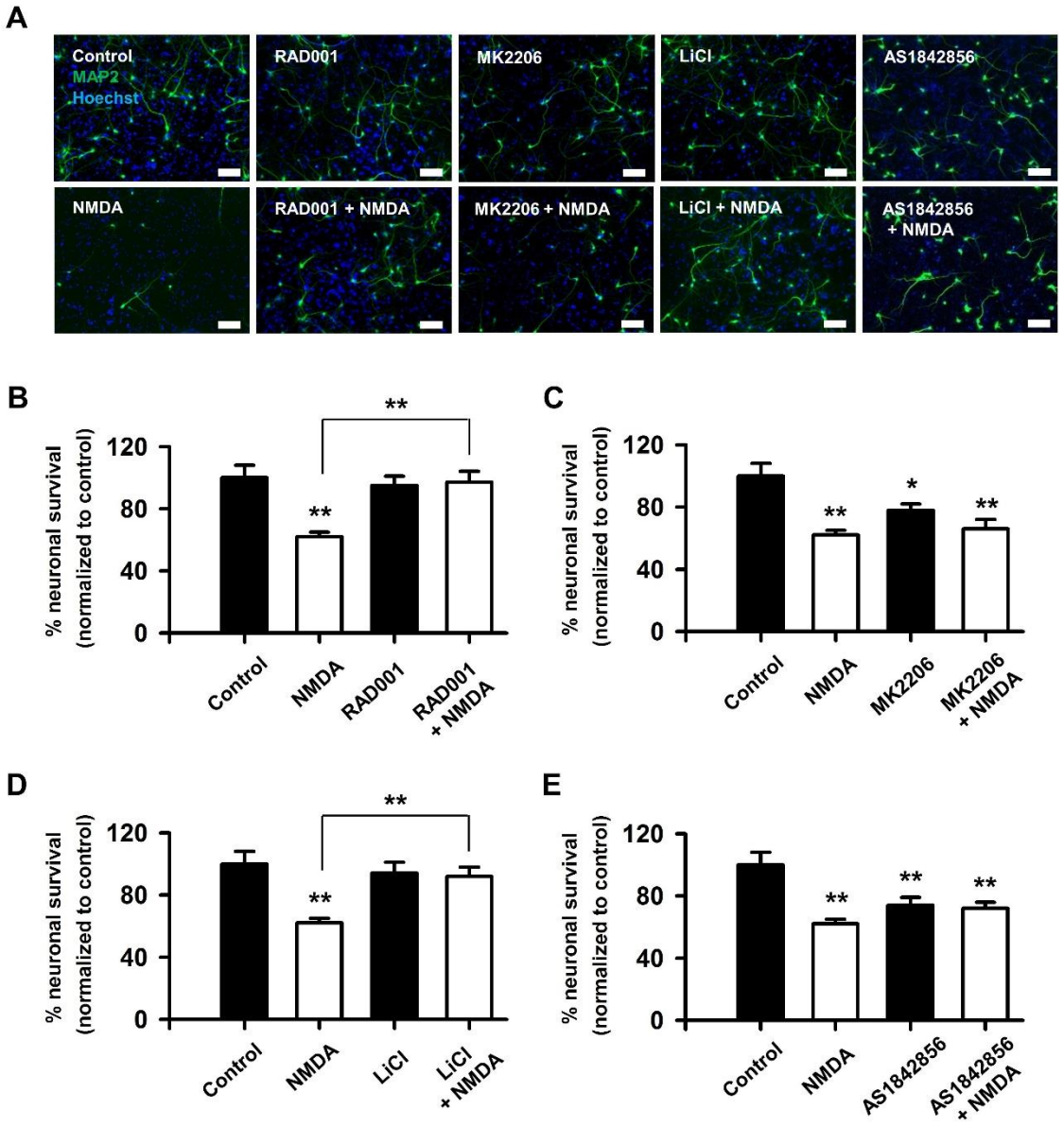

Figure 3.11. mTORC1 and GSK3β inhibitors protect neurons from NMDA-induced death. *A.* Representative images showing neurons immunostained for the neuronal marker, MAP2, and co-stained with nuclear dye, Hoechst, after treatment with 0.1% DMSO (control), 20 µM NMDA, 5 µM RAD001, 2 µM MK2206, 10 mM LiCl, 1 µM AS1842856, with or without 20 µM NMDA. Scale bars: 100µm. *B-E.* Quantitative analysis of neuron survival expressed as percent live control neurons. RAD001 or LiCl pretreatment

prevented NMDA-induced death. Data represent 38-53 samples from three separate trials. *p<0.05, **p<0.01 determined by one-way ANOVA followed by Tukey-Kramer multiple comparisons test. Error bars indicate ± SEM.

3.3 Discussion

Excessive release of glutamate from neurons occurs in response to tearing, stretching, or nutrient deprivation in the brain.[115,116] High levels of extracellular glutamate lead to overactivation of receptors, and in specific, NMDA receptors[117], on neighboring neurons and subsequent excitotoxicity.[105,116,117] This cellular mechanism underlies damage to neuronal networks due to injury, disease, and neurocognitive disorders. Existing treatment therapies employ NMDA antagonists to limit excitotoxic damage and aid in recovery of cellular and cognitive health of affected individuals. Unfortunately, many of the clinical trials ultimately fail, due to the importance of normal NMDA function in the brain.[118] Thus, the identification of alternative drug targets for the treatment of the damaged brain is of importance.

In the current study, we focused on the role of the Akt and its downstream signaling molecules in electrophysiological recovery and survival after injury. Glutamate release caused by excitotoxic damage has been previously associated with Akt inhibition and caspase-independent and dependent cell death.[115,119-123] In our experimental design, we treated cultures with a sublethal concentration of NMDA (20μM), as previously described[124], in order to mimic the secondary phase of trauma, excitotoxic injury. Our data demonstrate no activation of the PI3K/Akt/mTORC1 pathway two or twenty four hours

following exposure, which differs from previous reports that trauma induces this signaling pathway activation *in vivo*.[79,108,125] Our data may be different since our study employs cultured neurons treated with NMDA while other studies were performed *in vivo*. Furthermore, it is possible that NMDA increases activation of mTOR and GSK3β at time points that we did not analyze. Additionally, our paradigm simulates sublethal NMDA-induced injury while more severe injuries *in vivo* may show activation of components of the mTOR signaling pathway. Regardless, our data suggest an important, yet permissive, novel role for GSK3β, and an established role for mTOR, in mediating the effects of NMDA-induced injury.

While the long-term effects of glutamate-induced excitotoxicity generally involve epileptic seizures, disruption of long-term potentiation and depression, dysregulated sEPSCs, and miniature EPSCs[115,117,126], the acute effects of injury on neuronal electrophysiology are poorly characterized. In this study, we demonstrated that NMDA-induced sublethal damage causes a significant decrease in both frequency and amplitude of sEPSCs. This effect was partially recovered by APV, an NMDA antagonist, confirming the importance of NMDA receptors in mediating excitotoxic damage. Until now, the effect of PI3K/Akt/mTOR pathway manipulation on neuronal electrophysiology following injury, however, has remained largely unknown. Using the FDA approved drug RAD001, we report that inhibition of mTORC1 leads to recovery of frequency and partial recovery of amplitude of sEPSCs at two and 24 hours following injury. Additionally, RAD001 caused a significant increase in baseline activity, which in itself could be protective against upcoming injury by NMDA. Recovery is also seen upon manipulation of GSK3 but not FOXO1. GSK3β plays a role in control of several voltage-gated channels and ligand-gated

receptors.[127,128] It is important to note, however, that LiCl induced full recovery acutely, but only partial recovery 24 hours following injury (Figure 3.6D-F). In light of the fact that 20μM NMDA does not induce phosphorylation of GSK3β (Figure 3.10A,F), our results suggest that GSK3β may play a permissive role in allowing NMDA to induce damage hours after injury but that inhibition of GSK3β cannot fully rescue the neurons at later time points, such as 24 hours. Inhibition of GSK3 has been implicated in internalization of AMPA and NMDA receptors, potentially leading to a decrease in the amount of intracellular Ca^{2+} and reduced excitotoxicity.[129,130] These mechanisms may underlie the role of GSK3β in mediating neuroprotection. Here, we report that the use of the FDA approved and commonly used antipsychotic and GSK3 inhibitor, LiCl, leads to recovery of neuronal electrophysiology post-injury. We posit that this recovery is caused by either reduction of the extent of injury due to the reduced function of GSK3 in AMPA-mediated NMDA recycling from the postsynaptic density or a direct role of GSK3 in neuronal dysfunction after injury.

Changes to neuronal survival and spines have been characterized in several *in vivo* and *in vitro* models of excitotoxicity.[86,87,89] The PI3K/Akt/mTOR signaling cascade is a key player in dendrite and axon growth and repair[131], however, the role of this pathway in TBI, stroke, and other neurodegenerative diseases is either controversial or largely unknown.[78,125] Interestingly, our data demonstrate that MK2206, a potent Akt inhibitor, has no effect on neuronal survival, while RAD001 and LiCl, FDA approved mTORC1 and GSK3 inhibitors, respectively, cause a significant increase in neuronal survival after sublethal injury. Given that mTORC1 and GSK3β are both targeted by Akt, but mTORC1 is activated whereas GSK3β is inhibited by Akt-dependent phosphorylation events, these

results may appear contradictory. We speculate that inhibition of both mTORC1 and GSK3 (possibly GSK3α) is beneficial following NMDA-induced injury. Our data are most consistent with a model in which both mTORC1 and GSK3 are targeted by upstream signaling molecules other than Akt to mediate injury or launch repair and survival processes. For example, mTORC1 may be activated by the Ras/MEK/ERK pathway[132,133], or by phospholipase D.[134,135] mTORC1 could also be inhibited by AMP-activated protein kinase,[136-138] hypoxia-inducible REDD1 gene and the TSC1/2 complex.[139] Importantly, inhibition by REDD1 and TSC1/2 occurs in response to hypoxia[140-142], resulting in mTORC1 activation. mTORC1 can also be activated by elevated levels of amino acids through MAP3K3, representing an additional mechanism by which NMDA may act to regulate this kinase activity.[143] Similarly, NMDA exposure could regulate GSK3 activity independently of Akt, despite the fact that GSK3β is a well-known Akt target. Although less is known about how this may occur, there are reports reflecting such a pathway. In murine sensory neurons, regeneration is mediated by Akt-independent GSK3β inactivation.[144] In human non–small-cell lung cancer cell lines, degradation of cellular FLICE-inhibitory protein by celecoxib is mediated by GSK3 but not Akt[145], and in murine neuroblastoma cells, estradiol regulates GSK3β activity independent of Akt.[146] Furthermore, GSK3β has been extensively investigated for its role in cancer progression where it is reported to be under control of several different pathway including PI3K/Akt/mTOR, Ras/Raf/MEK/ERK, Wnt/β-catenin, Hedgehog, and Notch.[147] Thus, Akt-independent regulation of GSK3 by NMDA to alter electrophysiology and survival of neurons may represent a novel pathway by which neurons react to injury.

It is important to note that since mTORC1 appears to mediate a deleterious effect of NMDA-mediated injury, the therapeutic window for treatment with an mTORC1 inhibitor to counteract this effect is likely short. Similar to the failure of NMDA antagonists in clinical trials for traumatic brain injury, the targeting of deleterious pathways during injury requires timely inhibitor administration to prevent irreversible damage to occur. However, since suppression of GSK3 activity may be part of the recovery response of the cell to injury, the therapeutic window for stimulating repair and recovery responses may last days or even months. Therefore, pharmacological targeting of the GSK3 and mTORC1 pathways may distinct beneficial effects if initiated at different times before and after NMDA-induced injury.

Taken together, our data suggest a novel role for parallel mTORC1 and GSK3 signaling and manipulation on neuronal recovery following excitotoxic damage, a common secondary injury mechanism shared among multiple brain injuries and diseases. We show that mTORC1 and GSK3 inhibition result in recovery of both frequency and amplitude of sEPSCs two and 24 hours following injury. Since our data suggest that these pathways act in an Akt-independent manner, future studies aimed at elucidating the upstream molecular mechanisms governing neuronal recovery will provide details for precise manipulation of these signaling molecules in brain injury and disease.

3.4 Methods

3.4.1 Ethical approval

All methods using animals in this manuscript were approved by the Rutgers Institutional Animal Care and Use Committee in accordance with the Panel on Euthanasia of the AVMA.

3.4.2 Primary cortical neuron culture and injury

Neuronal cultures were plated from cortices of rat embryos at 18 days gestation on glass coverslips (12 mm diameter; 176,911 cells/cm^2 for electrophysiology and Sholl analysis, 47,244 cells/cm^2 for immunocytochemistry) or 6 well Falcon tissue culture plates (9.6 cm^2; 104,167 cells/cm^2 for Western blot analysis) previously coated with poly-D-lysine (Sigma-Aldrich) in full Neurobasal medium (Life Technologies, Grand Island, NY) supplemented with B-27 (Life Technologies) and GlutaMax (Life Technologies). At day *in vitro* (DIV) 14, cultures were treated with 20μM NMDA in 0.1% DMSO for 5 minutes, and allowed either 2 or 24 hours of recovery before electrophysiological experiments or Western blot analysis.

3.4.3 Antibodies

All antibodies, with the exception of mouse anti-actin (EMD Millipore, Billerica, MA) and Akt1/2/3 antibody for immunostaining (sc-8312, Santa Cruz Biotechnology), were purchased from Cell Signaling (Danvers, MA) and were used 1:1000 dilution. Catalogue numbers for each antibody are as follows: pAkt(Thr308) (Rb, 2965), pAkt(Ser473) (Rb,

9271), total Akt (Rb, 4691), pS6(Ser235/236) (Rb, 4858), total S6 (M, 2317), pGSK3β(Ser9) (Rb, 9323), total GSK3β (Rb, 9315).

3.4.4 Drugs

N-methyl-D-aspartate (NMDA) was purchased from Sigma-Aldrich (St. Louis, MO). RAD001 and MK2206 were purchased from Selleckchem (Houston, TX). AS1842856 was purchased from EMD Millipore (Billerica, MA). LiCl and dimethyl sulfoxide (DMSO) were purchased from Thermo Fisher Scientific (Waltham, MA).

3.4.5 Immunocytochemistry

Neurons were grown for 14 days in culture on coverslips coated with poly-D-lysine at which point they were treated with 20μM NMDA for 5 minutes. Cultures were fixed at 15 days in culture in 4% paraformaldehyde in PBS for 10 min, permeabilized with 0.1% Triton X-100 in PBS + 5% normal goat serum, and immunostained with mouse anti-MAP2 (1:500) from Rockland, followed by secondary antibodies conjugated to Alexa-Fluor® 488 (Invitrogen, 1:250). Nuclei were stained with Hoechst dye (1:1000). Coverslips were mounted on glass slides with Fluoromount G and then imaged. Neurons were visualized by immunofluorescence under a 10X objective on an EVOS FL microscope. Only neurons positive for MAP2 immunostaining and Hoechst staining were counted and used for statistical analysis.[89,148,149]

3.4.6 Semi-Automated Sholl analysis

Hippocampal neurons were grown for 14 days in culture on coverslips coated with poly-D-lysine and transfected with pEGFP using Effectene (Qiagen) following the manufacturer's instructions. Neurons were then fixed in 4% paraformaldehyde in PBS for 10 min, permeabilized with 0.1% Triton X-100 in PBS + 5% normal goat serum, and immunostained with rabbit anti-MAP2 (1:500) and mouse anti-GFP (1:500) followed by secondary antibodies conjugated to Alexa-Fluor® 555 or Alexa-Fluor® 488 (all antibodies from Rockland). Coverslips were mounted on glass slides with Fluoromount G and then imaged. Neurons were visualized by immunofluorescence under a 20X objective on an Olympus IX50 microscope with a Cooke Sensicam CCD-cooled camera, fluorescence, imaging system, and Image Pro software. The experimenter was blinded to the condition when taking images and analyzing dendrite morphology. Only GFP-positive neurons with clear neuronal morphology were examined. Next, 8-bit images were used to trace neurons using the NeuronJ plugin for ImageJ (NIH, Bethesda, MD). Tracing files were generated, and using MATLAB (Mathworks), these tracing files were subsequently converted to SWC files, and connectivity was assessed using NeuronStudio software. Sholl analysis was performed using a 6 μm ring interval starting at 9.3 μm from the soma.[104] Raw data were then exported to Excel using MATLAB and subjected to statistical analysis. Sholl analysis was performed using our Bonfire software[104,150], which is freely available to the scientific community.

3.4.7 Synaptic Cluster analysis

Cortical neurons (47,244 cells/cm^2) grown on glass coverslips (12mm) for 14 days in culture were fixed in 4% paraformaldehyde in phosphate-buffered saline (PBS) for 10 min, permeabilized with 0.1% Triton X-100 in PBS + 5% normal goat serum, and immunostained with rabbit anti-synaptophysin (Zymed Laboratories; 1:500) and mouse anti-PSD-95 (Antibodies Inc; 1:500) followed by secondary antibodies conjugated with Alexa-Fluor® 488 or Alexa-Fluor® 647 (Invitrogen; 1:250). Images of dendritic segments were taken with a 60X Plan Apo oil-immersion objective (NA 1.4) using a Yokogawa CSU-10 spinning disk confocal head attached to an inverted fluorescence microscope (Olympus IX50). X-Y and Z-resolution were set as 0.067 μm-0.067 μm and 0.2 μm, respectively, to count synaptic puncta. Puncta along dendritic segments were counted from 20 μm to 80 μm from the soma for 15-30 μm of secondary or tertiary dendrite segment length. Puncta were counted for at least 20 neurons for each experimental condition, and analysis was performed with the experimenter blinded to the condition. Synapse Counter (ImageJ plug in) was used to analyze 21 apposition of synaptophysin and PSD-95 puncta.[151] Statistical analysis was performed using One-way ANOVA followed Tukey's multiple comparisons test in Instat (Graphpad).

3.4.8 Western Blot analysis

On DIV 10, neuronal cultures plated in Falcon tissue culture plates were lysed in RIPA lysis buffer (50 mM Tris (pH 7.4), 1% NP40, 0.25% sodium deoxycholate, 150 mM NaCl, 1μM EDTA supplemented with protease and phosphatase inhibitors), and extracts were spun at 4^{0}C at 3000 x *g* for 5-7 minutes to remove debris. Protein concentration was

measured by a standard Bradford assay. Proteins (15 µg per sample) were resolved by SDS-polyacrylamide electrophoresis using 8.0% gels and transferred onto 0.2 µm nitrocellulose membrane (Bio-Rad, Hercules, CA) at 4^0C in 20% methanol Tris-Glycine buffer (25 mM Tris, 192 mM glycine, 20% v/v methanol) for 2.5 hours at a constant current (0.5 Amp). Membranes were blocked in 3% milk in TBS-T (50 mM Tris, 150 mM NaCl, pH 7.6) for 1 hour and incubated in primary antibodies overnight at 4^0C. Membranes were then incubated for 1 hour in secondary HRP-conjugated antibodies and subjected to ECL-Plus Western Blotting Detection System (Pierce/Thermo Fisher, Rockland, IL). All phosphorylated protein levels were normalized to the total amount of each protein. Quantification was performed using the band analysis function of Alpha Imager software (Protein Simple).

3.4.9 Electrophysiology

Whole cell patch-clamp recordings were performed on the soma of cortical neurons. For recordings, cells were bathed in artificial cerebrospinal fluid containing (in mM): 140 NaCl, 5 KCl, 2 $CaCl_2$, 2 $MgCl_2$, 10 HEPES, and 10 glucose (pH 7.4 adjusted with NaOH; 290-310 mOsmol). Recording electrodes (3 –5 MΩ) contained a K^+-based internal solution composed of (in mM): 126 K-gluconate, 4 KCl, 10 HEPES, 4 ATP-Mg, 0.3 GTP-Na_2, and 10 phosphocreatine (pH 7.2; 280 –300 mOsmol). To record spontaneous excitatory postsynaptic currents (sEPSCs), $GABA_A$-mediated neurotransmission was blocked with 50 µM picrotoxin (Tocris, R & D Systems; Minneapolis, MN). Miniature excitatory postsynaptic currents (mEPSCs) were recorded in the presence of 1 µM tetrodotoxin (to block the action potentials) and 50 µM picrotoxin to block inhibitory neurotransmission

(Tocris, R & D Systems; Minneapolis, MN) in the external solution, and 10 µM QX-314 (Tocris, R & D Systems; Minneapolis, MN) in the internal solution, as previously described.[85,86] The membrane potential was held at -70mV throughout all experiments. Data were amplified and filtered at 2 kHz by a patch-clamp amplifier (Multiclamp 700B), digitalized (DIGIDATA 1440A), stored, and analyzed by pCLAMP (Molecular Devices; Union City, CA). Data were discarded when the input resistance changed >20% during recording.

3.4.10 Statistics

Immunofluorescence and electrophysiological data were analyzed for changes in treatment conditions when compared to control cells treated with vehicle. Data were analyzed with ANOVA followed by Tukey-Kramer's multiple comparisons test using InStat and Prism software (GraphPad). Electrophysiology data were analyzed by calculating the frequency of events from at least 5 neurons per treatment condition per neuronal culture, from at least 3 cultures. p values <0.05 were considered significant.

3.5 Acknowledgments

This work was supported by New Jersey Commission on Brain Injury Research grant # CBIR12MIG011 (to BLF and GD). PS was supported in part by National Institutes of Health Biotechnology Training Grant T32 GM008339-20 and by New Jersey Commission on Brain Injury Research predoctoral fellowship #CBIR16FEL013. GK received funding

from the Aresty Undergraduate Research Fellowship. MVP was supported in part by New Jersey Commission on Brain Injury Research predoctoral fellowship #CBIR15FEL009.

Chapter 4: Activation of microglial P2Y12 receptor is required for outward potassium currents in response to neuronal injury

The work in this chapter has been previously published in the following article: Swiatkowski P, Murugan M, Eyo UB, Rangaraju S, Oh SB, Wu LJ (2016). Activation of microglial P2Y12 receptor is required for outward potassium currents in response to neuronal injury. *Neuroscience* 318:22-33

4.1 Introduction

Microglia, the resident immune cells in the central nervous system (CNS), plays an important role in healthy and disease brain. The microglial processes are highly motile, constantly surveying the surrounding neural parenchyma and promptly respond to brain injury.[154,155] Evidence indicates that the microglial processes are preferentially directed towards synapses, where they may be involved in monitoring and regulating neuronal activity.[156,157] However, in response to injury, the microglial process motility becomes targeted towards the site of insult. This site-directed movement or chemotaxis of microglial processes was shown to be in response to ATP released by damaged neurons and astrocytes.[155,158]

Accumulating body of literature implicates ATP-induced activation of purinergic receptors in microglial chemotaxis towards the injury site. Among the purinergic receptors, P2Y12 receptor (P2Y12R) subtype is exclusively expressed in microglia in the CNS and is essential for microglial chemotactic response to injury.[159] Unlike the other metabotropic

P2Y receptors which transduce their signals through Gq-phospholipase C pathways[160], the P2Y12R couples to Gi-adenylyl cyclase pathways through which it mediates the morphological and dynamic responses of microglia to extracellular nucleotides.[161,162] ATP/ADP-induced activation of P2Y12R through its signaling elicits an outward potassium current in microglia. Blocking this current with quinine, a nonselective potassium channel antagonist, abolished chemotaxis to ATP, implying that this current is important for ATP/ADP-mediated microglia motility.[163] In spite of the advances mentioned above, the purinergic signaling pathway coupled to the potassium channel is poorly documented[164,165] and the potassium channel associated with P2Y12-mediated microglial chemotaxis remains unidentified.

Microglial P2Y12R plays a pivotal role in neuropathological conditions. Our recent study showed that mice deficient in P2Y12R experienced worsened seizure outcome after kainic acid injections, suggesting a neuroprotective role for microglial P2Y12R in epilepsy.[166] P2Y12R in spinal microglia was also shown to be involved in the pathogenesis of neuropathic pain after peripheral nerve injury[167] and ischemic stroke.[168] Therefore, understanding microglial P2Y12R signaling will provide novel candidates for therapeutic interventions in pathologies implicating microglia P2Y12R. In this study, we investigate the identity of the K^+ channel coupled to P2Y12R signaling, as well as the intracellular pathway mediating the response. We found the ATP-induced outward current to be largely dependent on P2Y12R activation and mediated by G-proteins. In addition, P2Y12R-coupled outward potassium current was also activated in response to laser-induced single neuron injury.

4.2 Results

4.2.1 Characterization of microglial response to ATP, ADP and UDP

Using electrophysiological and imaging tools, we first characterized the microglial response to local application of ATP (non-selective P2X/P2Y agonist, 1mM), ADP (potent agonist of P2Y12, 1mM), and UDP (potent agonist of P2Y6, 1mM) in acute cortical slices of wild type mice. The application of all three nucleotides induced process extension (Figure 4.1A-C) and a rapid inward current followed by small outward potassium current (Figure 4.1D-F) in cortical microglia. However, puff application of ACSF did not induce an outward current or microglial chemotaxis (data not shown). ATP-induced inward currents are mediated by P2X receptors and outward currents are mediated by P2Y receptors in microglia.[170,171] Since the reversal potential for non-selective cation channels associated with P2X receptors (inward current) is close to 0mV, a holding potential of -10mV invokes both an inward and outward current following ATP puff application.[163] Analysis of the chemotactic response showed that there was no significant difference in the number of responding microglial processes, average process velocity or the peak response velocity (ATP 2.02 ± 0.109 μm/min, ADP 1.96 ± 0.111 μm/min, UDP 2.26 ± 0.127 μm/min) towards ATP, ADP or UDP puff application (Figure 4.1H-I). It is important to note that the chemotactic response to UDP was not noted in all instances (3 out of 5 experiments showed positive response). In the experiments with negative response, microglial processes were found crawling within the UDP filled pipette and blocking the puff application. A previous report stated that UDP does not evoke chemotaxis but only induces phagocytosis.[172,173] It is important to note that the earlier studies were performed in microglia cultures and hence the dynamic properties of the cultured microglia may not

fully represent the *in vivo* conditions. The chemotactic response to UDP is a novel finding and needs to be further investigated.

The voltage ramp test was performed before and following the puff application of ATP, ADP and UDP; the difference in the ramp was then used to calculate the reverse potential for the respective nucleotides (Figure 4.1J). The reversal potential for ATP, ADP and UDP were found to be -66.06 ± 0.431 mV, -67.64 ± 0.310 mV and -60.36 ± 0.360 mV, respectively (n=5 for each group). Here, in addition to the chemotaxis, we found that there were no significant differences in intensity or kinetics of the outward currents in response to the nucleotides (Figure 4.1K-L). Moreover, the current-voltage relationship for the outward current in response to the nucleotides was similar, suggesting that the same potassium channel might mediate the ATP/ADP/UDP-induced outward current.

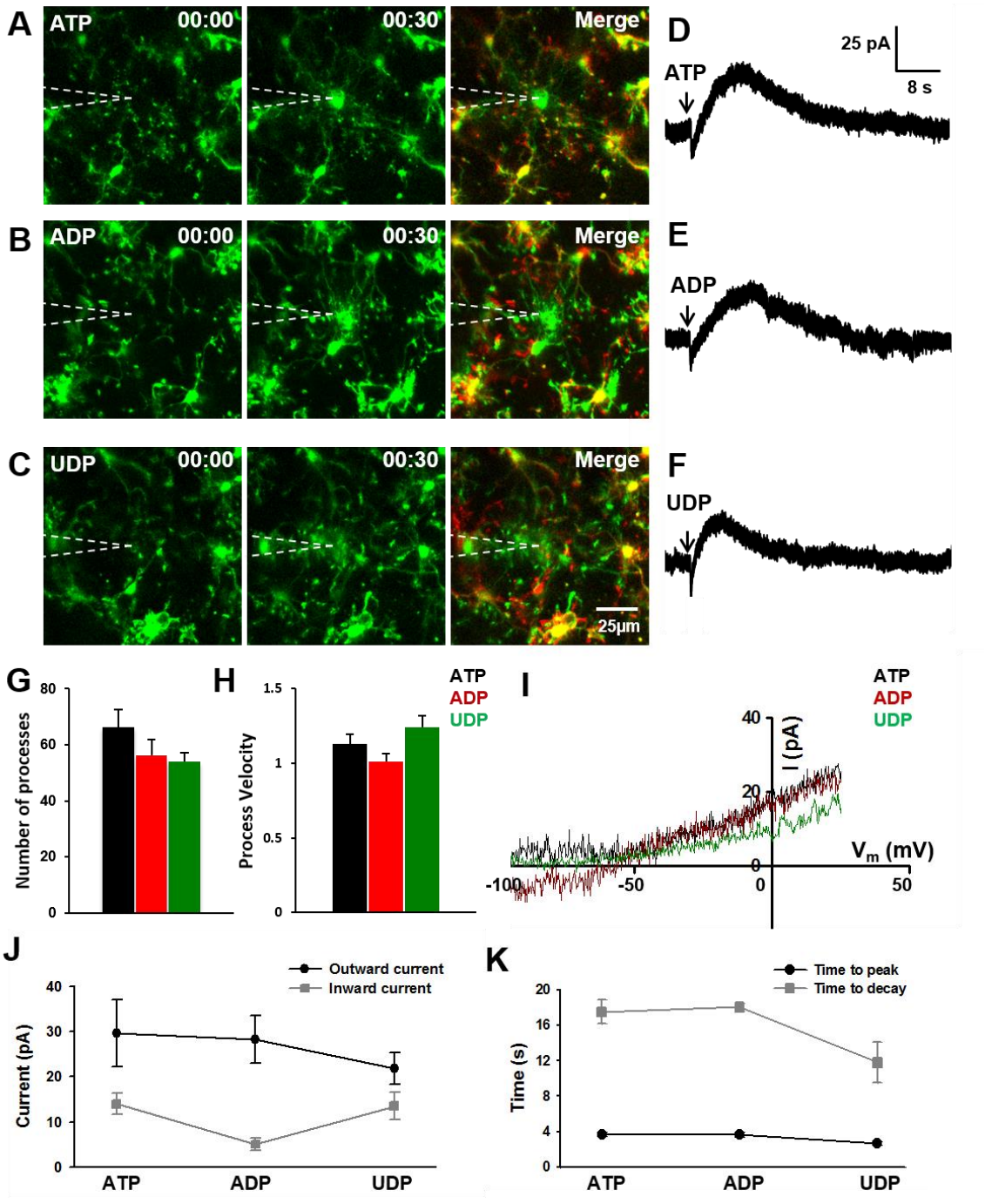

Figure 4.1. Dynamic and electrophysiological characteristics of microglial response to ATP, ADP and UDP. Two-photon images showing local application of 1mM of ATP (*A),* ADP (*B)* and UDP *(C)* induced rapid extension of microglial processes toward the tip of puff pipette in acute cortical slices of wild type (WT) mice (A: n =5, B: n=5, C: n= 4) .

Two time points (0 and 30 min) are shown here. The merged image is an overlay of imaging at 0 min (red) and 30 min (green). Scale bar: 25 μm. Unless otherwise stated, merged pictures are the overlay of imaging at 0 min (red) and 30 min (green) in the following figures. Whole cell patch clamp recordings of microglia using K^+ intracellular solution (IS) showed that local application of 1mM of ATP *(D)*, ADP *(E)* and UDP *(F)* induced a rapid small inward current followed by an outward current (D-F: n=5). Holding potential is -20mV. The number of responding microglial processes *(G)* and the process velocity *(H)* in response to ATP, ADP and UDP was analyzed. *(I)* A representative IV trace obtained from the difference in ramp test (from -100 to +20 mV, 500 ms) performed before and during the ATP/ADP/UDP-induced outward current. From the IV curve, the reversal potential for ATP, ADP and UDP were found to be -66.06 ± 0.431 mV (n=5), -67.64 ± 0.310 mV (n=5) and -60.36 ± 0.360 mV (n=5), respectively. The intensity of inward / outward microglia currents *(J)* and the kinetics of the outward current *(K)* in response to the nucleotides are summarized. Error bars represent SEM.

4.2.2 ATP/ ADP/ UDP-induced microglial chemotactic response and outward currents require P2Y12 receptor activation

In order to test whether P2Y12R signaling was required for the process extension and outward potassium currents in microglial response to the nucleotides, we applied ATP, ADP and UDP (1mM) to acute cortical slices derived from P2Y12 KO mice. Both nucleotide-induced process extension (Figure 4.2A-C) and outward currents (Figure 4.2D-F) were abolished in P2Y12R deficient microglia. Surprisingly, even the application of

UDP, a P2Y6 agonist, did not produce process extension or outward current in P2Y12 KO microglia. Since, it is known that ATP/ADP cannot activate P2Y6 receptors and neither can UDP act on P2Y12/13 receptors[172], we hypothesize that the decrease in UDP-evoked outward current in P2Y12KO may be due to the indirect effect of P2Y12 mediated signaling in P2Y6 receptor activation. Hence, a synergistic effect between the different purinergic channels cannot be excluded. Based on our results, we hypothesize that UDP could induce ATP release and hence the chemotactic response could be indirect. Firstly, in addition to the outward current, UDP also-induced an inward current which is likely mediated by P2X receptors (P2X7). This inward current remained unaffected in P2Y12 -/- mice. Since UDP is not known to activate P2X receptor, the results may further support the hypothesis that UDP act on microglia through indirect release of ATP. Secondly, we show that quinine blocks also blocks the UDP-induced outward current further supporting our hypothesis. Thirdly, the absence of chemotactic response towards UDP in P2Y12 -/- mice confirmed our hypothesis that UDP indirectly caused the release of ATP, and the outward current is predominantly mediated by P2Y12 receptors. Our results confirm that P2Y12R signaling is essential for ATP/ADP/UDP-mediated microglial chemotactic response and outward potassium currents (Figure 4.2G). This led us to further investigate the identity of the potassium channel coupled to P2Y12 receptor and investigate the underlying signaling pathway.

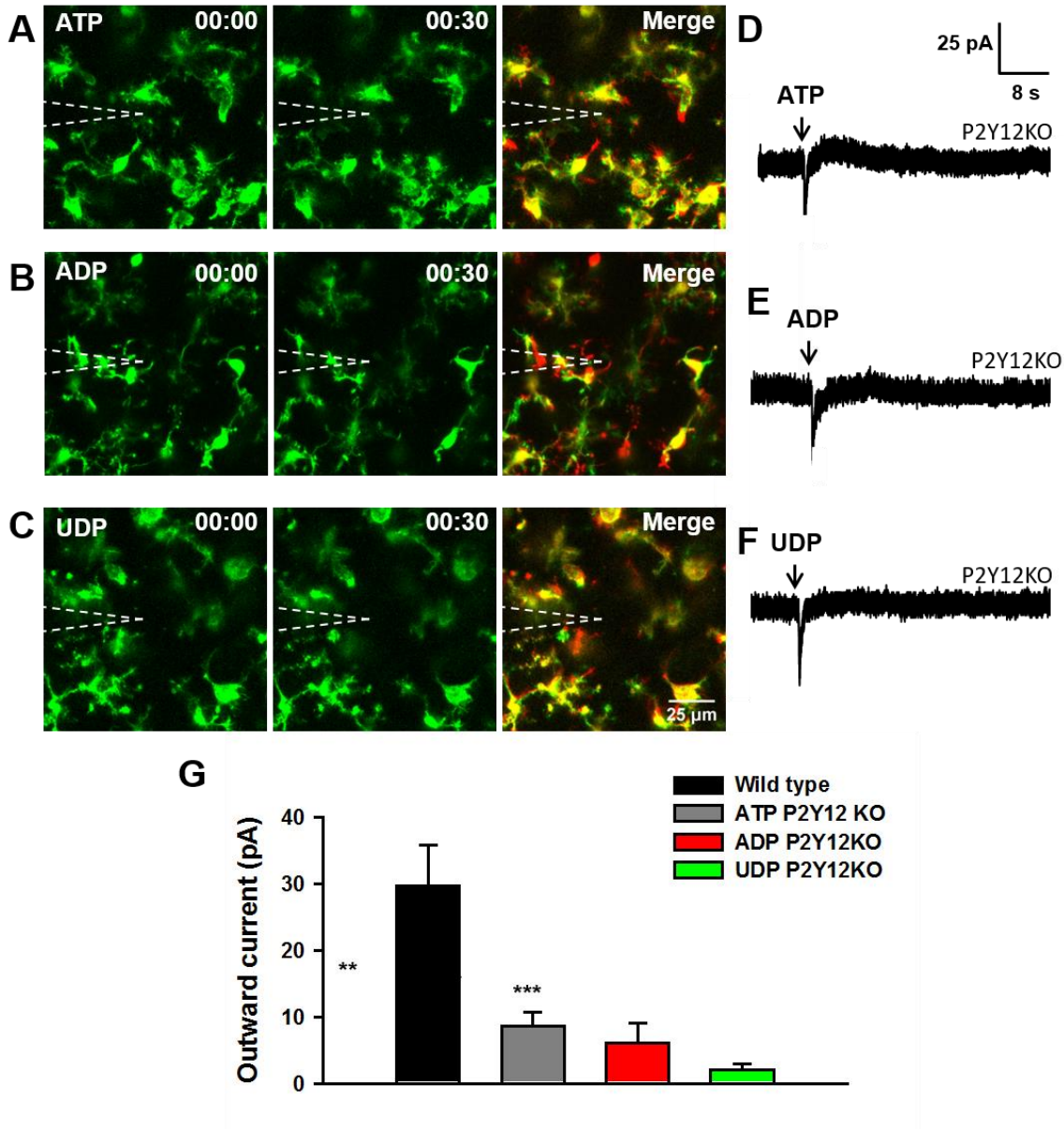

Figure 4.2. Microglial chemotactic response to ATP, ADP and UDP requires purinergic signaling and P2Y12 receptor. Two photon images showing local application of 1mM of ATP *(A)*, ADP *(B)* and UDP *(C)* failed to induce robust microlgial process extension toward the puff pipette in acute brain slices obtained from P2Y12 KO mice (A-C: n =3). Scale: 25 µm. In the P2Y12 KO mice, abolition in outward currents in response to 1mM of ATP *(D)*, ADP *(E)* and UDP *(F)* was noted (D-F: n=5), suggesting an

association between P2Y12 receptor mediated outward current and microglial chemotactic response. *(G)* The intensity of outward microglia currents in response to the nucleotides is summarized and was found to be significantly reduced in P2Y12 KO compared to WT mice. Error bars represent SEM. **P<0.01, ***P<0.001(ANOVA Tukey-Kramer multiple comparisons test).

4.2.3 Potassium channels are coupled to P2Y12 receptor signaling

We applied two approaches to investigate the identity of the ion channel coupled to microglial P2Y12R activation. In our first approach, whole cell patch recordings of microglia with internal solution containing cesium ions, which is known to block potassium currents[21], were performed. Predictably, the application of ATP, ADP, and UDP did not induce an outward current in the presence of cesium (Figure 4.3A). In our second approach, we recorded microglial currents following ATP application in the presence of broad potassium channel blockers: TEA (10 mM), quinine (1 mM), or 4-AP (5 mM) (Figure 4.3B). Both TEA and 4-AP were unsuccessful at blocking the outward current, while quinine effectively abolished any ATP mediated potassium outward current. Quinine also blocked the ATP-induced chemotactic response towards the puff pipette (data not shown[163]). Outwardly rectifying currents of two-pore domain potassium (K2P) channels have been shown to possess similar characteristics with weak sensitivity to classical blockers of K channels, such as TEA and 4-AP, but are sensitive to quinine and bupivacaine[175,176]. In line with this, low concentrations of bupivacaine (400 μM) partially blocked the ATP-induced outward current in microglia (Figure 4.3C). These results suggest

that a K2P channel may be coupled to P2Y12 receptor and that the current mediated by this channel is quinine/ bupivacaine-sensitive (Figure 4.3D).

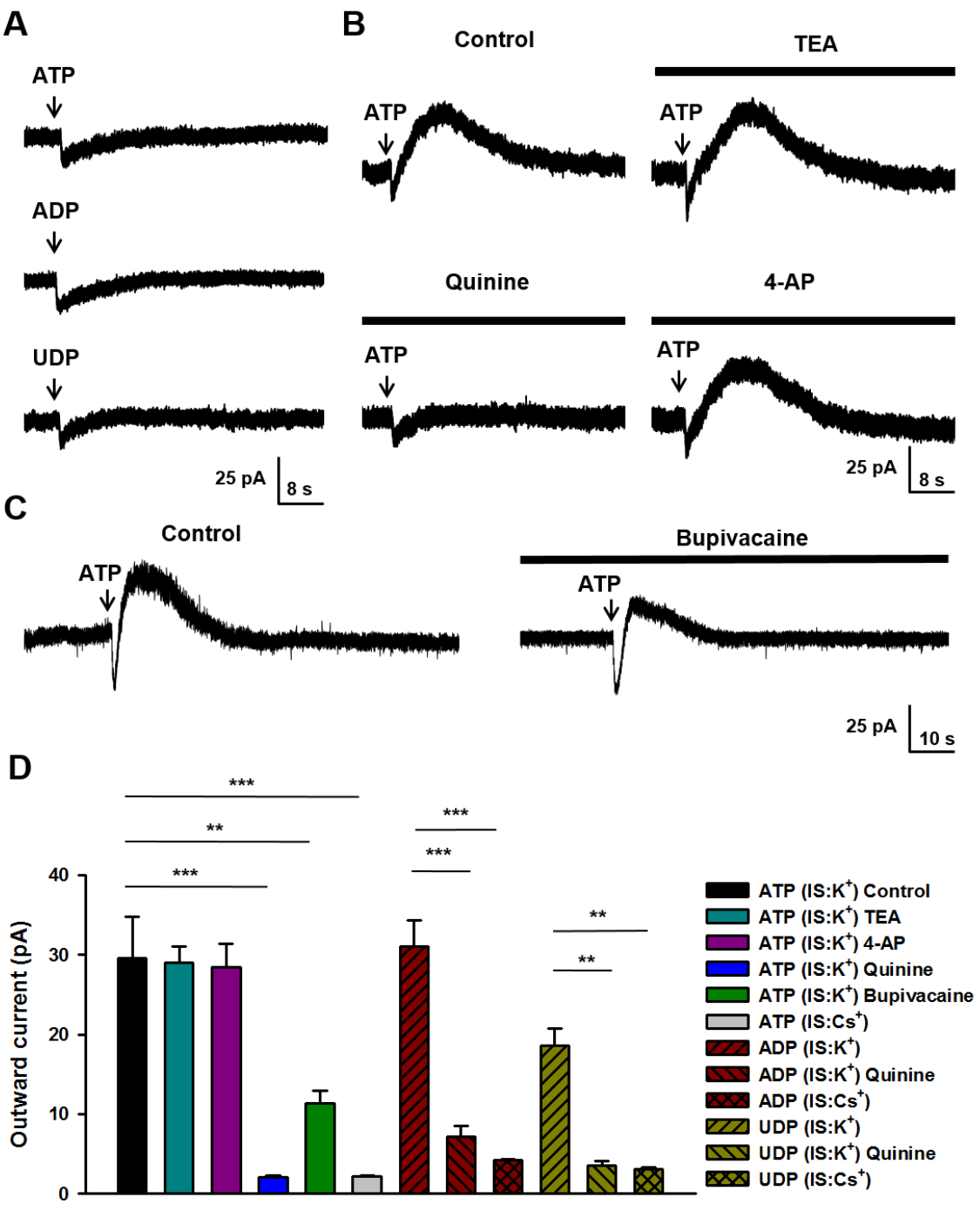

Figure 4.3. Potassium channels are coupled to P2Y12 receptor signaling. *(A)* In whole cell recordings made from microglia, ATP, ADP and UDP induced outward currents were abolished when cesium chloride was used as internal solution, suggesting that ATP/ADP/UDP-induced outward currents are mediated by potassium channels (n=5). *(B)*

Broad spectrum potassium channel blockers such as TEA (10mM) and 4-AP (5mM) were unsuccessful at blocking the outward current, while quinine (1mM) effectively abolished any ATP-mediated potassium current (n=5 for each treatment group). *(C)* Low concentration of Bupivacaine (400 μM) was able to partially block the ATP-induced outward current. *(D)* Summarized results showing outward currents induced by ATP/ADP/UDP with K^+ or Cs^+ internal solution (IS) in the presence of broad-spectrum potassium channel blockers (such as TEA, 4-AP or quinine) or bupivacaine. (***$p<0.001$) (ANOVA Tukey-Kramer multiple comparisons test).

4.2.4 Intracellular pathways coupling P2Y12 receptor to the potassium channel

We then went on to elucidate the intracellular pathway coupling ATP-induced activation of microglial P2Y12R using a pharmacological approach. P2Y12R has been found to have a direct effect on adenylyl cyclase, causing its inhibition and reduced production of cAMP.[177-179] To this end, we recorded ATP induced currents in the presence of forskolin (10 μM), a drug known to increase the intracellular levels of cAMP (Figure 4.4A). Interestingly, we observed no apparent changes in the ATP-induced microglial outward current, suggesting that cAMP levels are not responsible for direct or indirect activation of the P2Y12R-associated K^+ channel (Figure 4.4A, B). A number of downstream targets of G-protein signaling such as protein kinase A, phospholipase C, protein kinase C and intracellular calcium, have been implicated as most crucial elements of purinergic signaling and potassium channel activation.[180-184] Hence, to test whether the P2Y12R-K^+ channel was coupled by G-protein signaling, we included GDPβS (1 μM), in the internal solution

and recorded microglia current responses to puff application of ATP (Figure 4.4A). Indeed, GDPβS effectively blocked the outward current (Figure 4.4A, B). We further tested pertussis toxin (PTX, 4 μM), which is known to inactivate G_i/G_o G proteins, on ATP-induced outward currents in microglia. Consistently, PTX inhibited microglial ATP-activated outward K currents (Figure 4.4A, B).

We also tested whether the microglial P2Y12R-mediated outward current is linked to the store operated Ca^{2+} channel (SOC).[185] Microglia in acute slices were patched with internal solution containing EGTA (5 mM) and current responses to local application of ATP were recorded (Figure 4.4C). We detected no significant inhibition of the outward current (Figure 4.4D), implying that microglia P2Y12R-mediated outward current is not dependent on intracellular calcium. Together, these results suggest that P2Y12R is coupled to G_i/G_o G-proteins and their downstream targets independent of cAMP pathway or Ca^{2+} to activate the P2Y12R-associated outward potassium currents in microglia.

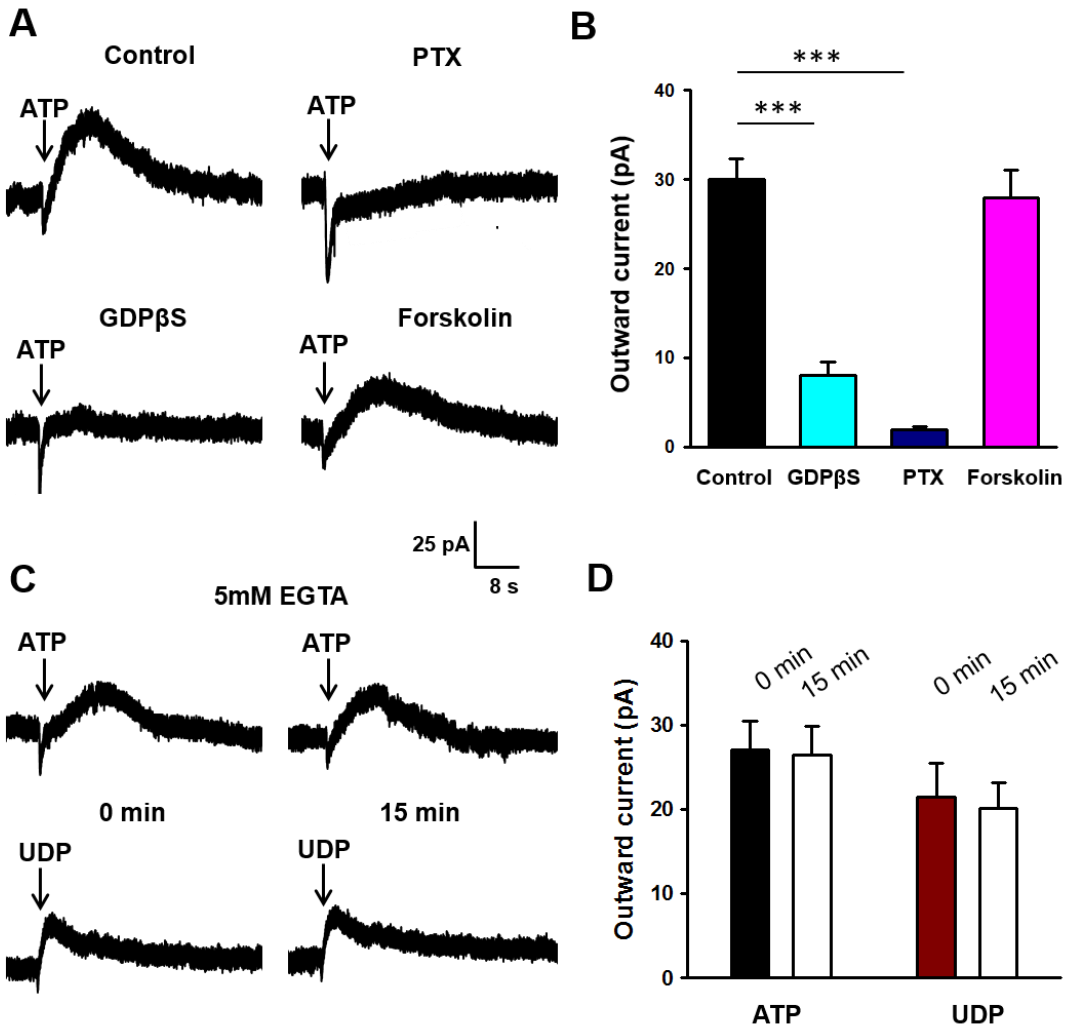

Figure 4.4. Analysis of the intracellular pathways coupling P2Y12 receptor to the potassium channel. *(A)* Perfusion of Forskolin did not alter the ATP-induced outward currents, whereas inclusion of G-protein inhibitors, PTX or GDPβS in the internal solution abolished ATP-induced outward currents in microglia, suggesting that G-proteins are involved in the coupling of P2Y12 receptor and the potassium channel (n=5). *(B)* Summarized results showing the effect of PTX or GDPβS in significantly reducing ATP-induced outward currents. ***p< 0.001. *(C)* Microglia in acute cortical slices were patched with internal solution containing EGTA (5mM) and responses to local application of ATP

and UDP showed no inhibition of the outward current, implying that it is not dependent on intracellular Ca^{2+} (ATP: n=5; UDP: n=3). *(D)* Summarized data depicting outward currents in response to ATP/UDP in the presence of EGTA (5mM) in the internal solution is shown. No significant differences between groups. All error bars represent SEM; ANOVA Tukey-Kramer multiple comparisons test.

4.2.5 Neuronal injury induced P2Y12R-mediated outward currents in microglia

We then pursued to address the physiological relevance of ATP-induced microglial outward current after brain injury. We were able to induce single neuron injury associated with microglial process chemotaxis in the brain slices using two photon laser beam.[166] Interestingly, we found that the outward current response was recorded from a microglia when the neighboring neuron was damaged with a laser (Figure 4.5A). The injury-induced outward microglial current was similar to the one induced by ATP was recorded in WT mice, which was absent in P2Y12 KO mice (Figure 4.5B). A recent study showed that laser irradiation mediated increase in extracellular ATP was is in the nanomolar range[186] suggesting that the lack of inward current by laser burn could be due to the insufficient ATP released following laser-induced nerve injury. Next, we recorded laser burn induced currents in the presence of previously described K^+ channel blockers: TEA, 4-AP, quinine or bupivacaine (Figure 4.5C). Again, only quinine and bupivacaine were successful at inhibiting the outward current (Figure 4.5D). Similar to the ATP-induced current, the laser burn-induced current was also sensitive to GDPβS (data not shown). Also, we found that quinine could block the laser burn induced chemotactic response (data not shown). Our

data also shows that the amplitude of the outward current diminishes with increasing distance from the laser burn (Figure 4.5E). This is in line with a previous report in which the amplitude of current decreased with ATP concentration.[163] Since the ATP concentration gradient reduces with distance, the amplitude of outward current reduces as the distance from the ATP source/ injury site increases. Collectively, these data suggests that laser damage to a single neuron is sufficient to produce outward potassium currents in microglia, most likely due to release of ATP from injured neuron and activation of microglial P2Y12R-associated K^+ channel.

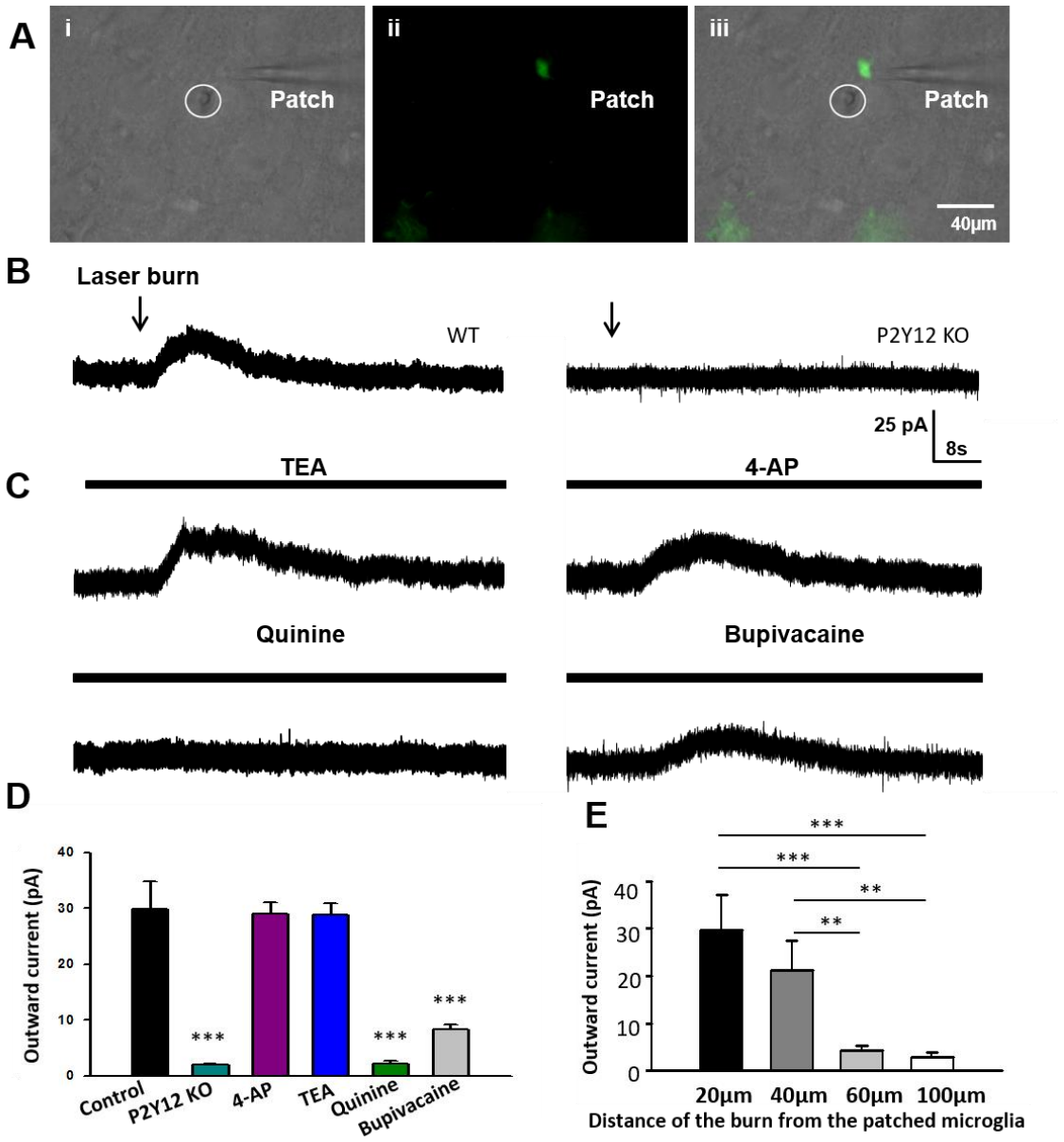

Figure 4.5. Laser burn injury induced ATP-like outward currents in microglia. *(A)* Whole-cell patch clamp recordings of microglia identified by GFP labeling. Patch refers to the patch pipette and the white circle encloses the laser burn site where a single neuron is damaged. Scale bar: 40 μm *(B)* Laser burn induced outward currents in microglia resembled the ATP-induced outward currents in WT mice. However, laser-burn induced outward current was absent in P2Y12 KO (n=8 for each group). *(C)* Like the ATP-induced

outward current, the laser burn-induced current was sensitive to quinine and bupivacaine, but not TEA and 4-AP (n=5 for each group). *(D)* Summarized data represents the laser burn induced outward current in the presence of broad spectrum potassium blockers or bupivacaine. *(E)* Data shows that the amplitude of the outward current diminishes with increasing distance between the burn site and patched microglia. * $p<0.05$, ** $p<0.01$, *** $p<0.001$. (n=3 for each group). All error bars represent SEM. ANOVA Tukey-Kramer multiple comparisons test.

4.3 Discussion

Our current findings indicate that ATP-induced microglial P2Y12R activation elicits outward potassium currents via the opening of potassium channels. In this study, we investigate the identity of the potassium channel coupled to P2Y12R and the intracellular signaling pathway linking the receptor to the channel. Additionally, the properties of microglial outward current in response to neuronal injury was found to be similar to the one induced by ATP/ ADP. Also we show that this injury-induced microglial current was mediated by P2Y12R.

4.3.1 K^+ channel coupled to microglial P2Y12R

P2Y12R were initially identified on platelets and are responsible for platelet activation and aggregation during the blood clotting process.[161] The expression of P2Y12R in microglia was first described by Sasaki et al[187] and has been implicated in microglia activation,

migration, chemotaxis and phagocytic ability.[159,163,188-190] P2Y12R plays a vital role in microglia activation, as they act as the primary site at which nucleotides act to induce microglial chemotaxis in response to local CNS injury.[159,189] P2Y12R activation has also been shown to mediate microglial process extension and convergence towards dendrites following neuronal hyperactivity.[166,191] Apart from chemotaxis, P2Y12-dependent purinergic signaling regulates the phagocytic ability of microglia.[190,192,193] In platelets, G-protein gated inwardly rectifying potassium (GIRK) channels was identified to be the functional effectors downstream of P2Y12 receptor activation.[194] Although the P2Y12R has been shown to be important for a myriad of microglial functions, the effectors mediating its effects in microglia have not been identified.

Coupling to ion channels is an important component of P2Y12R signal transduction, but one that has remained unknown. In studies of channel coupling by P2YR, heterologous expression in commonly transfected host cell lines such as CHO or HEK293, or in the Xenopus oocyte is done. However, usually both the P2Y receptor and the identified ion channel under study are introduced into the cells, and even then, the final interaction and protein environment of those components may be far from that in native cell.[195] In this study, we used an electrophysiological approach to reveal the identity of the channel coupled to microglia P2Y12R. The results of our study show that ATP/ADP/UDP-induced chemotaxis and outward currents were abolished in P2Y12 KO mice, indicating that they are mediated by microglial P2Y12R signaling. In addition, we showed that the ATP-induced currents were potassium currents sensitive to quinine and bupivacaine, but insensitive to TEA and AP-4. Similarly, outwardly rectifying currents of the K2P channels show similar characteristics with weak sensitivity to classical blockers of K channels, such

as TEA and 4-AP, but are sensitive to quinine or quinidine[175] and low concentrations of bupivacaine.[176] Therefore, leak K2P channels may be the functional effectors of the P2Y12R–mediated signaling in microglia activation. The exact subtype of K2P channel linked to P2Y12R still remains unknown and warrants further investigation.

4.3.2 Intracellular signaling pathway associated with P2Y12R activation

P2Y receptors, unlike P2X receptors, are metabotropic in nature and act via G protein signaling. In platelets, P2Y12R was shown to be coupled to Gαi2, by photolabeling with radiolabeled GTP[196] and was confirmed in Gαi2-deficient mouse platelets.[197] Consistent with these studies, our results show that P2Y12R is coupled to potassium channels via a G_i/G_o-protein signaling pathway.

A majority of the P2Y receptors are linked to phospholipase C and mediate increases in inositol phosphates. However, P2Y12R are associated with reduced cyclic AMP[198], and this pathway has been extensively characterized in human platelets and in rat glioma cells.[161,199,200] Another study showed that similar reduction in cyclic AMP in rat endothelial cells was mediated by P2Y12R.[201] In our study, addition of forskolin to enhance the levels of cyclic AMP did not have any effect on ATP-induced P2Y12R-mediated outward current. This suggests that cAMP levels are not responsible for direct or indirect activation of the P2Y12R-associated K^+ channel. This however does not rule out the possibility that reduction in cAMP levels and coupling to potassium channels may be two independent downstream signaling pathways following microglia P2Y12R activation.

4.3.3 Microglial P2Y12R signaling in injury

Microglial P2Y12R has been implicated in a number of neuropathological conditions such as epilepsy[166], neuropathic pain[167,202] and ischemic stroke.[168] Microglial P2YR activation is associated with neuroinflammation[203] and is a hallmark response to brain injury.[204] Following injury, neurons and astrocytes release nucleotides such as ATP/ADP and UDP, which act on purinergic receptors in microglia.[172,205] ATP/ADP is a chemoattractant, while UDP elicits a phagocytic response in microglia.[172,173] Hence, it is suggested that the adenosine and uridene nucleotides may act on the microglial purinergic receptors in a coordinated fashion aiding in chemotaxis and phagocytosis, respectively, following injury. Two photon *in vivo* imaging studies show that optically injured site is rapidly sealed by microglia cell processes and this process extension is mediated by P2Y12R.[159,163,166] In this study we show that focal laser burn injury of a neighboring neuron resulted in outward potassium current in microglia similar the ATP-induced microglial current. Like the ATP-induced outward current, the focal burn-induced current was inhibited by quinine but not TEA and 4-AP and was abolished in P2Y12R deficiency. Taken together our study suggests that ATP/injury-induced P2Y12R activation results in initiation of G-protein coupled cascade of events involving opening of potassium channels in microglia.

In addition to the animal models that implicate microglia P2Y12R in pathological scenarios, a recent study showed that alternatively activated human microglia expresses P2Y12R.[206] In humans, molecular defects in P2Y12R have been identified in four families of patients with hemorrhagic syndromes.[207] The significance of a defect in microglial P2Y12R has not been studied in humans, but would be a worthy investigation. Given the physiological and pathological relevance of microglia P2Y12R activation, understanding

the underlying signaling pathway will provide novel insights for developing therapies for the treatment of clinical conditions that implicate microglial P2Y12R.

4.4 Methods

4.4.1 Animals

Both male and female C57BL/6N mice were used in accordance with the institutional guidelines, as approved by the Animal Care and Use Committee at Rutgers University. Heterozygous GFP reporter mice ($CX3CR1^{GFP/GFP}$) expressing GFP under the control of the fractalkine receptor (CX3CR1) promoter[169] were obtained from Jackson Laboratory. The $CX3CR1^{GFP/-}$ mice were used as wild-type mice in this study. P2Y12 knockout (P2Y12 KO) mice were obtained from Dr. Michael Dailey at the University of Iowa. The $CX3CR1^{GFP/-}$ P2Y12 KO was obtained by mating the above-mentioned mouse lines.

4.4.2 Slice Preparation

Freshly isolated cortical slices were prepared from 3-6-week-old mice. Briefly, mice were anesthetized and swiftly decapitated. Brains from decapitated mice were carefully removed and placed in ice-cold oxygenated (95% O_2 and 5% CO_2) artificial cerebrospinal fluid (ACSF) with the following composition (in mM): NaCl, 124; $NaHCO_3$, 25; KCl, 2.5; KH_2PO_4, 1; $CaCl_2$, 2; $MgSO_4$, 2; glucose, 10 and sucrose added to make 300-320mOsmol. Coronal slices (300 µm) were prepared and transferred to a recovery chamber for 30 m

with oxygenated ACSF with the same composition as above at room temperature before imaging or electrophysiological studies.

4.4.3 Two-photon Imaging

Experiments were conducted at room temperature with slices maintained in oxygenated ACSF with the same composition as above in a perfusion chamber at a flow rate of 2mL/min. It is important to note that the dynamic behavior of microglia may differ from the *in vivo* conditions due to variation in parameters such as temperature and changes in extracellular milieu. Microglia were typically imaged using a two-photon microscope (Scientifica Inc, UK) with a Ti:Sapphire laser (Mai Tai; Spectra Physics) tuned to 900nm (for GFP microglia) with a 40X water immersion lens (0.8 NA; Olympus). Fluorescence was detected using two photomultiplier tubes in whole-field detection mode and a 565 nm dichroic mirror with 525/50 nm (green channel) emission filters. The laser power was maintained at 25 mW or below. Typically, 15 consecutive z stack images were collected at 3 µm intervals every minute. To perform a general laser injury, we focused the laser 66X and parked it at ~250 mW at 900 nm for 3 s. The lesion site was induced in a 15 x 15 pixel frame and the size of the resulting laser burn was estimated to vary between 8-15µm (25-50 pixels) in diameter. For imaging experiments, a minimum of three to four slices from different mice from the same litter were randomly selected for imaging per treatment group/ condition. Images were obtained between 50-100µm from the slice surface. 45µm thick sections were made from projection z-stack images taken at 3µm intervals. Pixel size was 1024 x 1024 and field of view was 165µm x 165µm x 45µm. Images were generated

using Image J and Max projection was applied to all images. For responding process velocity and number analysis either directed toward an ATP-containing pipette or a laser-induced injury, time-lapse movies were first registered using the StackReg plugin to eliminate any *x*-*y* drift. For responding process number analysis the number of responding processes at the final frame was manually counted. For process velocity analysis, individual processes were then tracked using the Manual Tracking plugin. Migrating processes were selected at random but only processes that were maintained through at least five frames were used. The average process velocity through the tracked period was determined and averaged from at least eight processes per experiment for three experiments.

4.4.4 Slice Electrophysiology

Whole cell patch-clamp recordings were made on GFP-labeled microglia from cortical slices at ~50 μm from the slice surface. Recording electrodes (4 –5 MΩ) contained a K-based internal solution composed of (in mM): 120 K-gluconate, 5 NaCl, 1 $MgCl_2$, 0.5 EGTA, 10 Na_2Phosphocreatine, and 10 HEPES (pH 7.2; 280 –300 mOsmol). In order to block outward potassium current we used Cs-based internal solution containing (in mM): 115 Cs-$MeSO_3$, 5 NaCl, 10 HEPES, 1 $MgCl_2$, 0.2 EGTA, and 10 Na_2Phosphocreatine (pH 7.2; 280-300 mOsmol). Additionally, to manipulate G proteins, GDPβS (1mM) was included in the internal solution. Unless otherwise stated, the membrane potential was held at -20 mV for microglia throughout all experiments. Data were amplified and filtered at 2 kHz by a patch-clamp amplifier (Multiclamp 700B), digitalized (DIGIDATA 1440A),

stored, and analyzed by pCLAMP (Molecular Devices, Union City, CA). All cells showed small membrane capacitance (24.93 ± 1.2 pF, n =20), high membrane resistance (1.53 ± 0.08 GΩ, n = 20), and a more positive membrane potential (-21.9 ± 1.59 mV, n = 20). Data were discarded when the input resistance changed >20% during recording. The voltage ramp test was performed from -100 to +20 mV in 500 ms. The ramp current/ IV current is linear in resting microglia in brain slices. Rectifying currents were observed in activated microglia and were not chosen in this study. For electrophysiology, a minimum of five cells from at least three different mice from the same litter were randomly selected for recording per condition. Under conventional whole-cell patch clamp recording, the morphology of the patched microglia was not altered much in short time (within 15 min). However, the morphology is difficult to appreciate after GFP is washed out under the whole-cell configuration. In addition, microglia are no longer dynamic and does not extend its processes towards either an ATP puff or laser burn under conventional whole-cell recording while they retain some dynamics under perforated whole-cell recording.[163] For the reason mentioned above, the electrophysiology recordings and imaging were performed in independent experiments.

4.4.5 Drugs

ATP, ADP, UDP, GDPβS and bupivacaine hydrochloride were purchased from Sigma. Pertussis toxin (PTX), forskolin, tetraethylammonium (TEA), quinine, and 4-aminopyridine (4-AP) were purchased from Tocris. Stock solutions of all drugs were made in water and diluted to the appropriate working concentrations in ACSF. Drugs were

applied to the slices either through bath application or using a picopump (WPI pneumatic picopump, Sarasota, FL). The diameter of the drug application pipette tip was ~3–4 μm. The pressure (10 psi) and duration (100 ms) of the puff was controlled and the distance between the patched cell and puff pipette was kept constant (~15 μm). This was achieved by marking the position of the two pipettes (recording and puff) on the display screen and adjusting the distance of the puff pipette until the preferred distance was reached. The holding pressure of the puff pipette was maintained at -2 psi to prevent leakage, but there may still be minimal spontaneous leakage.

4.4.6 Statistical Analysis

For all experiments, the number of mice used for each experimental group is stated in the corresponding figure legend. Data are presented as mean ± SEM. ANOVA with Tukey-Kramer multiple comparisons test was used to establish significance. A p value of <0.05 was considered to be significant.

4.5 Acknowledgments

This work was supported by National Institute of Health (R01NS088627, T32GM8339), New Jersey Commission on Spinal Cord Research (CSCR15ERG015), Michael J. Fox Foundation, and Korean National Research Foundation grant (2012R1A3A2048834). We thank Dr. Michael Dailey (University of Iowa) for providing us with P2Y12 KO mice. We

thank Dr. David Atwell (University College London) for critical reading of the manuscript and his expert comments.

Chapter 5: Conclusions and Future Directions

5.1 Small molecule probes to modulate cypin

The data and conclusions shown in this thesis present good targets for further investigation and development of TBI therapies. In Chapter 2 we describe the role of cypin on neuronal electrophysiology in normal and injured neurons and show its neuroprotective potential attributed to the ability to bind zinc, bind PSD-95, and the guanine deaminase activity of cypin. Due to the ability of cypin to bind PSD-95 it is possible that cypin affects AMPA/NMDA receptor composition at the postsynaptic site, which can affect LTP and LTD, and future efforts should address these questions.

In collaboration with Fox Chase Chemical Diversity Center, Inc., we show that small molecule cypin activators can enhance the neuroprotective capabilities of cypin without its overexpression, presenting an excellent therapeutic approach. Although the data shows great promise, these drugs should be further developed, and any potential studies should investigate the pharmacokinetic and pharmacodynamic properties, as well as metabolism and toxicity *in vivo*.

Additionally, published data from our laboratory show that cypin may play a role in small varicosity formation following NMDA-induced injury.[208] Several reports have shown formation of large varicosities along dendrites and axons in response to injury, and that these varicosities are detrimental to overall health of the neuron.[208,209] Cypin overexpression reduces the size and increases the overall number of varicosities, and effectively leads to neuroprotection.[209] Although the link between small varicosity

formation and neuroprotection is unclear, it should be further explored whether small molecule cypin modulators affect the size or number of varicosities following injury.

Finally, published data from our laboratory shows that uric acid protects spinal cord motor neurons *in vitro* from glutamate induced damage, and data published from another group show that exogenously applied cytosolic PSD-95 interactor (cypin) also displays neuroprotective functions in this paradigm of injury. Therefore, it is possible that activating cypin's enzymatic activity will improve morphology, and electrophysiology of spinal cord motor neurons following SCI leading to recovery of motor functions.

5.2 mTORC1 and GSK3β in brain injury

As seen in Chapter 3, inhibition of mTORC1 or GSK3β following NMDA-induced sublethal injury has beneficial effects on neuronal survival and electrophysiology, which are independent of Akt phosphorylation. LiCl, a potent GSK3β inhibitor used in this study, is an FDA approved drug for a number of psychiatric conditions which makes it an excellent candidate for potential brain injury clinical trials.[210] Although past reports from failed clinical trials employing LiCl are discouraging, new approaches that take into account the type of injury and differences between affected individuals should be considered. We show that early intervention produces the best results, therefore, the use of LiCl for brain injury should be reconsidered for patients with severe damage.

5.3 Microglia in brain injury

Microglia are the resident immune cells of the brain and first responders to brain injury.[211-213] They are highly motile and function as surveying cells by monitoring neuronal behavior as well as responding to damage or pathogens.[211,212,214-216] As shown in Chapter 4, during brain injury, microglia are attracted and recruited to the site of injury by factors released from damaged neurons, such as ATP.[217-220] Additionally, injury induces microglia to become activated and assume either the M1 phenotype, which is pro-inflammatory, or M2, which is anti-inflammatory.[214,215] Multiple reports show that immediately following brain injury microglia exist in the anti-inflammatory M2 state; however, after approximately one week, microglia switch to the pro-inflammatory M1 state, and this phenotype persists for weeks, months, and even years resulting in deleterious effects.[212,215] Therefore, since microglia can exist in either pro- or anti-inflammatory states, the role of microglia in brain injury is controversial.

Although the microglia ablation mouse model has been well characterized, there has been no effort to use this model and elucidate the effect of microglia ablation on traumatic brain injury.[221,222] An elegant study investigating the effects of selective microglia ablation on neuronal survival and function following cerebral ischemia revealed that microglial ablation lead to dysregulated neuronal function and elevated excitotoxicity, an effect reversed by repopulation of microglia.[216] Future studies should, therefore, investigate the effects of global and local microglia ablation immediately or one week following moderate controlled cortical impact (mCCI) in mice, which models TBI. The following aims should be addressed: 1) the effect of global or local microglia ablation on propagation of injury after mCCI; 2) investigation of neuronal survival and physiology following mCCI and

global or local microglia ablation; and 3) elucidate the effect of global or local microglia ablation on cognitive and behavioral recovery following mCCI in mice. By addressing the effects of global or local microglial ablation, any potential future work should provide better understanding of microglia function following brain injury and propose a possible therapeutic approach.

5.4 Conclusions

This body of work focused on a multidimensional approach to investigate TBI and its mechanisms, encompassing responses on molecular and cellular levels. Although these responses are not related, they might be additive and should be investigated as a whole. As shown in Chapter 2, mild CCI, an *in vivo* model of TBI, induces cypin expression at 1 day post injury in ipsilateral and contralateral cortex, but does not alter cypin expression at 2 hours, 7 or 14 days post injury, or in the hippocampus at time points analyzed. On the other hand, moderate CCI, a more severe degree of injury, induced expression of PSD-95 at 1 day post injury in the contralateral hippocampus, but not at 7 or 14 days post injury, or in the cortex. This data suggests that cypin might be involved in early recovery mechanisms following mild injury potentially promoting neurotransmission at the synaptic level, and synchrony of network firing, as our cypin overexpression data suggests. Additionally, in the NMDA-induced injury, an *in vitro* model of secondary injury following TBI, cypin overexpression or activation with H9 or G5 compounds promoted neuronal survival and recovery of mEPSC firing, phenotypes not observed when cypin was knocked down or treated with B9 or G6 compounds.

On the mechanistic level, we investigated the role of the PI3K/Akt/mTORC1 pathway following NMDA-induced injury. Data presented in Chapter 3 show that NMDA-induced injury does not alter phosphorylation of Akt, S6, or GSK3β at 2 and 24 hours following injury. Similarly to the data presented in Chapter 2, NMDA-induced injury lead to a decrease in neuronal survival and mEPSC firing, and these were prevented with the use of RAD001, the mTORC1 inhibitor, or LiCl, the GSK3β inhibitor. These data show potential neuroprotective value of inhibiting these kinases after injury, and present an alternative use for an old drug, LiCl.

Finally, to investigate cellular responses to injury we looked at microglia, the resident immune cells in the central nervous system. Specifically, this work investigated the identity of the potassium channel implicated in microglial P2Y12R-mediated chemotaxis following laser burn neuronal injury and understanding the purinergic signaling pathway coupled to the channel. Data presented in Chapter 4 shows the ATP-induced outward current to be largely dependent on P2Y12R activation and mediated by G-proteins. Knock out of P2Y12R in mice abolished this current. Additionally, the neuronal injury-induced outward current in microglia was sensitive to quinine and low concentrations of bupivacaine but not TEA or 4-AP, indicating that P2Y12R might be associated to a K2P channel. These results suggest that the quinine/bupivacaine-sensitive K2P channels are the functional effectors of the P2Y12-mediated signaling in microglia activation following neuronal injury.

References

1. Cohen, J. S. *et al*. Sports-related concussions in pediatrics. *Curr Opin Pediatr* **21**, 288-293 (2009)
2. Faul, M. *et al*. Traumatic Brain Injury in the United States: Emergency Department Visits, Hospitalizations and Deaths. Atlanta, GA: Centers for Disease Control and Prevention, National Center for Injury Prevention and Control (2010)
3. Elder, G. A. & Cristian, A. Blast-related mild traumatic brain injury: mechanisms of injury and impact on clinical care. *Mt Sinai J Med* **76**, 111-118 (2009)
4. Marshall, L. F. *et al*. Head injury: Recent past, present, and future. *Neurosurgery* **47** (3): 546–61 (2000)
5. Mark, L. P. *et al*. Pictorial review of glutamate excitotoxicity: fundamental concepts for neuroimaging. *AJNR Am J Neuroradiol* **22**, 1813–1824 (2001)
6. Prins, M. *et al*. The pathophysiology of traumatic brain injury at a glance. *Disease Models & Mechanisms* **6** (2013)
7. Ray, S. K. *et al*. Molecular mechanisms in the pathogenesis of traumatic brain injury. *Histol Histopathol* **17**, 1137–1152 (2002)
8. Atkins C.M. Decoding Hippocampal Signaling Deficits after Traumatic Brain Injury. *Transl Stroke Res* **2**(4):546-555 (2011)
9. Shohami, E. & Biegon, A. Novel approach to the role of NMDA receptors in traumatic brain injury. *CNS Neurol Disord Targets* **13**(4):567-573 (2014)
10. Schwarzbach, E. *et al*. Mechanisms Underlying the Inability to Induce Area CA1 LTP in the Mouse After Traumatic Brain Injury. *Hippocampus* **16**(6):541-550 (2006)
11. Santos, A. R. *et al*. Differential Role of the Proteasome in the Early and Late Phases of BDNF-Induced Facilitation of LTP. *J Neurosci* **35**(8):3319-3329 (2015)
12. Morales, D. M. *et al*. Experimental models of traumatic brain injury: do we really need to build a better mousetrap? *Neurosci* **136**:971-989 (2005)
13. Dixon, C. E., Clifton, G. L., Lighthall, J. W., Yaghmai, A. A., & Hayes, R. L. A controlled cortical impact model of traumatic brain injury in the rat. *J Neurosci Methods* **39**:253-262 (1991)
14. Chen, Y. C., Mao, H., Yang, K. H., Abel, T., & Meaney, D. F. A modified controlled cortical impact technique to model mild traumatic brain injury mechanics in mice. *Front Neuro* **5**(100):1-14 (2014)
15. Akum, B. F. *et al*. Cypin regulates dendrite patterning in hippocampal neurons by promoting microtubule assembly. *Nat Neurosci* **7**:145–152 (2004)
16. Firestein, B. L. *et al*. Cypin: a cytosolic regulator of PSD-95 postsynaptic targeting. *Neuron* **24**(3): p. 659-72 (1999)
17. Tseng, C. Y. & Firestein, B. L. The role of PSD-95 and cypin in morphological changes in dendrites following sublethal NMDA exposure. *J Neurosci* **31**(43):15468-15480 (2011)
18. Fernandez, J. R., Welsh, W. J. & Firestein, B. L. Structural characterization of the zinc binding domain in cytosolic PSD-95 interactor (cypin): Role of zinc binding in guanine deamination and dendrite branching. *Proteins* **70**, 873-881, doi:10.1002/prot.21683 (2008).

19. Page, T. & Coleman, M. Purine metabolism abnormalities in a hyperuricosuric subclass of autism. *Biochimica et Biophysica Acta* **1500**:291-296 (2000)
20. Chen, X. *et al*. PSD-95 family MAGUKs are essential for anchoring AMPA and NMDA receptor complexes at the postsynaptic density. *PNAS* E6983-6992 (2015)
21. Chen, X. *et al*. PSD-95 is required to sustain the molecular organization of the postsynaptic density. *J Neurosci* **31**(17):6329-6338 (2011)
22. Wakade, C. *et al*. Delayed reduction in hippocampal post-synaptic density protein-95 expression temporally correlates with cognitive dysfunction following controlled cortical impact in mice. *J Neurosurg* **113**(6):1195-1201
23. Hu, S. Q. *et al*. Overexpression of the PDZ1 Domain of PSD-95 Diminishes Ischemic Brain Injury Via Inhibition of the GluR6.PSD-95.MLK3 Pathway. *J Neurosci Research* **87**:3626-3638 (2009)
24. Sen, T. *et al*. Activation of PERK Elicits Memory Impairment through Inactivation of CREB and Downregulation of PSD95 After Traumatic Brain Injury. *J Neurosci* **37**(24):5900-5911 (2017)
25. Davalos, D. *et al*. ATP mediates rapid microglial response to local brain injury *in vivo*. *Nature Neurosci* **8**(6):752-758 (2005)
26. Haynes, S. E. *et al*. The P2Y12 receptor regulates microglial activation by extracellular nucleotides. *Nature Neurosci* **9**(12):1512-1519 (2006)
27. Ohsawa, K. *et al*. Involvement of P2X4 and P2Y12 receptors in ATP-induced microglial chemotaxis. *Glia* 55:604-616 (2007)
28. Boucsein, C. *et al*. Purinergic receptors on microglial cells: functional expression in acute brain slices and modulation of microglial activation *in vitro*. *European J Neurosci* 17:2267-2276 (2003)
29. Dou, T. *et al*. Microglial migration mediated by ATP-induced ATP release from lysosomes. *Cell Research* **22**:1022-1033 (2012)
30. Eder, C. Ion channels in microglia (brain macrophages). *American J Physio* **275**:C327-C342 (1998)
31. Ilschner, S. *et al*. Modulation of potassium currents in cultured murine microglial cells by receptor activation and intracellular pathways. *Neuroscience* **66**(4):983-1000 (1995)
32. Schilling, T. *et al*. Functional importance of Ca^{2+}-activated K^{+} channels for lysophosphatidic acid-induced microglial migration. *European J Neurosci* **19**:1469-1474 (2004)
33. Wu, L. J., Vadakkan, K. I. & Zhuo, M. ATP-induced chemotaxis of microglial processes requires P2Y receptor-activated initiation of outward potassium currents. *Glia* **55**:810-821 (2007)
34. Schilling, T. & Eder, C. Ion channel expression in resting and activated microglia of hippocampal slices from juvenile mice. *Brain Research* **1186**:21-28 (2007)
35. Webster, C. M. *et al*. Microglial P2Y12 deficiency/inhibition protects against brain ischemia. *PLoS One* **8**(8):e70927 (2013)
36. Kataoka, A. *et al*. Involvement of vasodilator-stimulated phosphoprotein in UDP-induced microglial actin aggregation via PKC- and Rho-dependent pathways. *Purinergic Signaling* **7**:403-411 (2011)
37. Nakamura, T. *et al*. UDP induces intestial epithelial migration via the P2Y6 receptor. *British J Pharm* **170**:883-892 (2013)

38. Chen, M. *et al*. A novel role for snapin in dendrite patterning: interaction with cypin. *Mol Biol Cell* **16**(11):5103-5114 (2005)
39. Vites, O., Rhee, J. S., Schwarz, M., Rosenmund, C. & Jahn, R. Reinvestigation of the role of snapin in neurotransmitter release. *J Biol Chem* **279**:26251-26256 (2004)
40. Nolan, S. Traumatic Brain Injury A Review. *Critical Care Nursing Quarterly* **28**, 188-194 (2005).
41. Pearn, M. L. *et al.* Pathophysiology Associated with Traumatic Brain Injury: Current Treatments and Potential Novel Therapeutics. *Cell Mol Neurobiol* **37**, 571-585, doi:10.1007/s10571-016-0400-1 (2017).
42. Prins, M., Greco, T., Alexander, D. & Giza, C. C. The pathophysiology of traumatic brain injury at a glance. *Dis Model Mech* **6**, 1307-1315, doi:10.1242/dmm.011585 (2013).
43. Tseng, C. Y. & Firestein, B. L. The role of PSD-95 and cypin in morphological changes in dendrites following sublethal NMDA exposure. *J Neurosci* **31**, 15468-15480, doi:10.1523/JNEUROSCI.2442-11.2011 (2011).
44. Kapucu, F. E. *et al.* Burst analysis tool for developing neuronal networks exhibiting highly varying action potential dynamics. *Front Comput Neurosci* **6**, 38, doi:10.3389/fncom.2012.00038 (2012).
45. Persi, E., Horn, D., Volman, V., Segev, R., Ben-Jacob, E. Modeling of Synchronized Bursting Events: The Importance of Inhomogeneity. *Neural Computation* **16**, 2577-2595 (2004).
46. Chen, Y., Mao, H., Yang, K. H., Abel, T. & Meaney, D. F. A modified controlled cortical impact technique to model mild traumatic brain injury mechanics in mice. *Front Neurol* **5**, 100, doi:10.3389/fneur.2014.00100 (2014).
47. Hall, E. D. *et al.* Spatial and temporal characteristics of neurodegeneration after controlled cortical impact in mice: more than a focal brain injury. *J Neurotrauma* **22**, 252-265, doi:10.1089/neu.2005.22.252 (2005).
48. Osier, N. D. & Dixon, C. E. The Controlled Cortical Impact Model: Applications, Considerations for Researchers, and Future Directions. *Front Neurol* **7**, 134, doi:10.3389/fneur.2016.00134 (2016).
49. Vakil, E. The effect of moderate to severe traumatic brain injury (TBI) on different aspects of memory: a selective review. *J Clin Exp Neuropsychol* **27**, 977-1021, doi:10.1080/13803390490919245 (2005).
50. Bliss, T. V. P., Collingridge, G.L. A synaptic model of memory: long-term potentiaion in the hippocampus. *Nature* **361** (1993).
51. Malenka, R. C. & Bear, M. F. LTP and LTD: an embarrassment of riches. *Neuron* **44**, 5-21, doi:10.1016/j.neuron.2004.09.012 (2004).
52. Luscher, C. & Malenka, R. C. NMDA receptor-dependent long-term potentiation and long-term depression (LTP/LTD). *Cold Spring Harb Perspect Biol* **4**, doi:10.1101/cshperspect.a005710 (2012).
53. Hegde, A. N. The ubiquitin-proteasome pathway and synaptic plasticity. *Learn Mem* **17**, 314-327, doi:10.1101/lm.1504010 (2010).
54. Ben-Ari, Y., Aniksztejn, L. & Bregestovski, P. Protein kinase C modulation of NMDA currents: an important link for LTP induction. *Trends in Neurosciences* **15**, 333-339, doi:10.1016/0166-2236(92)90049-e (1992).

55. Sen, T., Gupta, R., Kaiser, H. & Sen, N. Activation of PERK Elicits Memory Impairment through Inactivation of CREB and Downregulation of PSD95 After Traumatic Brain Injury. *J Neurosci* **37**, 5900-5911, doi:10.1523/JNEUROSCI.2343-16.2017 (2017).
56. Akum, B. F. *et al.* Cypin regulates dendrite patterning in hippocampal neurons by promoting microtubule assembly. *Nat Neurosci* **7**, 145-152, doi:10.1038/nn1179 (2004).
57. Firestein, B. L., Brenman, J.E., Aoki, C., Sanchez-Perez, A.M., El-Husseini, A. ED., Bredt, D.S. Cypin: A Cytosolic Regulator of PSD-95 Postsynaptic Targeting. *Neuron* **24**, 659-672 (1999).
58. Pinheiro, P. S. & Mulle, C. Presynaptic glutamate receptors: physiological functions and mechanisms of action. *Nat Rev Neurosci* **9**, 423-436, doi:10.1038/nrn2379 (2008).
59. Fernandez, J. R., Welsh, W. J. & Firestein, B. L. Structural characterization of the zinc binding domain in cytosolic PSD-95 interactor (cypin): Role of zinc binding in guanine deamination and dendrite branching. *Proteins* **70**, 873-881, doi:10.1002/prot.21683 (2008).
60. Lin, D. D., Cohen, A.S., Coulter, D.A. Zinc-Induced Augmentation of Excitatory Synaptic Currents and Glutamate Receptor Responses in Hippocampal CA3 Neurons. *The American Physiological Society* (2000).
61. Toth, K. Zinc in neurotransmission. *Annu Rev Nutr* **31**, 139-153, doi:10.1146/annurev-nutr-072610-145218 (2011).
62. Zhu, J. *et al.* Chronic zinc exposure decreases the surface expression of NR2A-containing NMDA receptors in cultured hippocampal neurons. *PLoS One* **7**, e46012, doi:10.1371/journal.pone.0046012 (2012).
63. Bakshi, R. *et al.* Neuroprotective effects of urate are mediated by augmenting astrocytic glutathione synthesis and release. *Neurobiol Dis* **82**, 574-579, doi:10.1016/j.nbd.2015.08.022 (2015).
64. Du, Y., Chen, C. P., Tseng, C. Y., Eisenberg, Y. & Firestein, B. L. Astroglia-mediated effects of uric acid to protect spinal cord neurons from glutamate toxicity. *Glia* **55**, 463-472, doi:10.1002/glia.20472 (2007).
65. Hooper, D. C., Spisin, S., Kean, R.B., Champion, J.M., Dickson, G.M., Chaudhry, I., Koprowski, H. Uric acid, a natural scavenger of peroxynitrite, in experimental allergic encephalomyelitis and multiple sclerosis. *PNAS* **95**, 675-680 (1998).
66. Scott, G. S., Cuzzocrea, S., Genovese, T., Koprowski, H., Hooper, D.C. Uric acid protects against secondary damage after spinal cord injury. *PNAS* **102** (2005).
67. Mller BM, et al. SAP102, a novel postsynaptic protein that interacts with NMDA receptor complexes in vivo. *Neuron* **17**(2):255-65 (1996)
68. Cohen, A. S. *et al.* Injury-induced alterations in CNS electrophysiology. *Prog Brain Res* **161**, 143-169, doi:10.1016/S0079-6123(06)61010-8 (2007).
69. Yang, L. *et al.* Spontaneous epileptiform activity in rat neocortex after controlled cortical impact injury. *J Neurotrauma* **27**, 1541-1548, doi:10.1089/neu.2009.1244 (2010).
70. Kang, W. H. *et al.* Alterations in Hippocampal Network Activity after In Vitro Traumatic Brain Injury. *J Neurotrauma* **32**, 1011-1019, doi:10.1089/neu.2014.3667 (2015).
71. Rose, M. E. *et al.* Regulation of interstitial excitatory amino acid concentrations after cortical contusion injury. *Brain Res* **935**, 40-46 (2002).

72. Kramer, D. R., Fujii, T., Ohiorhenuan, I. & Liu, C. Y. Cortical spreading depolarization: Pathophysiology, implications, and future directions. *J Clin Neurosci* **24**, 22-27, doi:10.1016/j.jocn.2015.08.004 (2016).
73. Lynch, D. R. & Dawson, T. M. Secondary mechanisms in neuronal trauma. *Curr Opin Neurol* **7**, 510-516 (1994).
74. Kostandy, B. B. The role of glutamate in neuronal ischemic injury: the role of spark in fire. *Neurol Sci* **33**, 223-237, doi:10.1007/s10072-011-0828-5 (2012).
75. Coyle, J. T., Murphy, T. H., Puttfarcken, P. S., Lyons, E. W. & Vornov, J. J. The non-excitatory mechanisms of glutamate induced neurotoxicity. *Epilepsy Res* **10**, 41-48 (1991).
76. Mattson, M. P., Guthrie, P. B. & Kater, S. B. Intrinsic factors in the selective vulnerability of hippocampal pyramidal neurons. *Prog Clin Biol Res* **317**, 333-351 (1989).
77. Chen, S. *et al.* Alterations in mammalian target of rapamycin signaling pathways after traumatic brain injury. *J Cereb Blood Flow Metab* **27**, 939-949, doi:10.1038/sj.jcbfm.9600393 (2007).
78. Park, J. *et al.* Combination therapy targeting Akt and mammalian target of rapamycin improves functional outcome after controlled cortical impact in mice. *J Cereb Blood Flow Metab* **32**, 330-340, doi:10.1038/jcbfm.2011.131 (2012).
79. Nikolaeva, I., Crowell, B., Valenziano, J., Meaney, D. & D'Arcangelo, G. Beneficial Effects of Early mTORC1 Inhibition after Traumatic Brain Injury. *J Neurotrauma* **33**, 183-193, doi:10.1089/neu.2015.3899 (2016).
80. Don, A. S. *et al.* Targeting mTOR as a novel therapeutic strategy for traumatic CNS injuries. *Drug Discov Today* **17**, 861-868, doi:10.1016/j.drudis.2012.04.010 (2012).
81. Gong, R., Park, C. S., Abbassi, N. R. & Tang, S. J. Roles of glutamate receptors and the mammalian target of rapamycin (mTOR) signaling pathway in activity-dependent dendritic protein synthesis in hippocampal neurons. *J Biol Chem* **281**, 18802-18815, doi:10.1074/jbc.M512524200 (2006).
82. Lenz, G. & Avruch, J. Glutamatergic regulation of the p70S6 kinase in primary mouse neurons. *J Biol Chem* **280**, 38121-38124, doi:10.1074/jbc.C500363200 (2005).
83. Fingar, D. C., Salama, S., Tsou, C., Harlow, E. & Blenis, J. Mammalian cell size is controlled by mTOR and its downstream targets S6K1 and 4EBP1/eIF4E. *Genes Dev* **16**, 1472-1487, doi:10.1101/gad.995802 (2002).
84. Erlich, S., Alexandrovich, A., Shohami, E. & Pinkas-Kramarski, R. Rapamycin is a neuroprotective treatment for traumatic brain injury. *Neurobiol Dis* **26**, 86-93, doi:10.1016/j.nbd.2006.12.003 (2007).
85. Wu, H. *et al.* Simvastatin-mediated upregulation of VEGF and BDNF, activation of the PI3K/Akt pathway, and increase of neurogenesis are associated with therapeutic improvement after traumatic brain injury. *J Neurotrauma* **25**, 130-139, doi:10.1089/neu.2007.0369 (2008).
86. Hasbani, M. J., Hyrc, K. L., Faddis, B. T., Romano, C. & Goldberg, M. P. Distinct roles for sodium, chloride, and calcium in excitotoxic dendritic injury and recovery. *Exp Neurol* **154**, 241-258, doi:10.1006/exnr.1998.6929 (1998).
87. Hasbani, M. J., Viquez, N. M. & Goldberg, M. P. NMDA receptors mediate hypoxic spine loss in cultured neurons. *Neuroreport* **12**, 2731-2735 (2001).

88. Inoue, H. & Okada, Y. Roles of volume-sensitive chloride channel in excitotoxic neuronal injury. *J Neurosci* **27**, 1445-1455, doi:10.1523/JNEUROSCI.4694-06.2007 (2007).
89. Tseng, C. Y. & Firestein, B. L. The role of PSD-95 and cypin in morphological changes in dendrites following sublethal NMDA exposure. *J Neurosci* **31**, 15468-15480, doi:10.1523/JNEUROSCI.2442-11.2011 (2011).
90. Durukan, A. & Tatlisumak, T. Acute ischemic stroke: overview of major experimental rodent models, pathophysiology, and therapy of focal cerebral ischemia. *Pharmacol Biochem Behav* **87**, 179-197, doi:10.1016/j.pbb.2007.04.015 (2007).
91. Emery, D. G. & Lucas, J. H. Ultrastructural damage and neuritic beading in cold-stressed spinal neurons with comparisons to NMDA and A23187 toxicity. *Brain Res* **692**, 161-173 (1995).
92. Zhao, L. R. *et al.* Synthetic fibronectin peptide exerts neuroprotective effects on transient focal brain ischemia in rats. *Brain Res* **1054**, 1-8, doi:10.1016/j.brainres.2005.04.056 (2005).
93. Li, P. & Murphy, T. H. Two-photon imaging during prolonged middle cerebral artery occlusion in mice reveals recovery of dendritic structure after reperfusion. *J Neurosci* **28**, 11970-11979, doi:10.1523/JNEUROSCI.3724-08.2008 (2008).
94. Brown, C. E. & Murphy, T. H. Livin' on the edge: imaging dendritic spine turnover in the peri-infarct zone during ischemic stroke and recovery. *Neuroscientist* **14**, 139-146, doi:10.1177/1073858407309854 (2008).
95. Brown, C. E., Li, P., Boyd, J. D., Delaney, K. R. & Murphy, T. H. Extensive turnover of dendritic spines and vascular remodeling in cortical tissues recovering from stroke. *J Neurosci* **27**, 4101-4109, doi:10.1523/JNEUROSCI.4295-06.2007 (2007).
96. Gisselsson, L., Toresson, H., Ruscher, K. & Wieloch, T. Rho kinase inhibition protects CA1 cells in organotypic hippocampal slices during in vitro ischemia. *Brain Res* **1316**, 92-100, doi:10.1016/j.brainres.2009.11.087 (2010).
97. Meller, R. *et al.* Ubiquitin proteasome-mediated synaptic reorganization: a novel mechanism underlying rapid ischemic tolerance. *J Neurosci* **28**, 50-59, doi:10.1523/JNEUROSCI.3474-07.2008 (2008).
98. Hasbani, M. J., Schlief, M. L., Fisher, D. A. & Goldberg, M. P. Dendritic spines lost during glutamate receptor activation reemerge at original sites of synaptic contact. *J Neurosci* **21**, 2393-2403 (2001).
99. Piper, M. *et al.* Differential requirement of F-actin and microtubule cytoskeleton in cue-induced local protein synthesis in axonal growth cones. *Neural Dev* **10**, 3, doi:10.1186/s13064-015-0031-0 (2015).
100. Mego, M. *et al.* Phase II study of everolimus in refractory testicular germ cell tumors. *Urol Oncol* **34**, 122 e117-122, doi:10.1016/j.urolonc.2015.10.010 (2016).
101. Oki, Y. *et al.* Phase II study of an AKT inhibitor MK2206 in patients with relapsed or refractory lymphoma. *Br J Haematol* **171**, 463-470, doi:10.1111/bjh.13603 (2015).
102. Rugo, H. S. *et al.* Meta-analysis of stomatitis in clinical studies of everolimus: incidence and relationship with efficacy. *Ann Oncol* **27**, 519-525, doi:10.1093/annonc/mdv595 (2016).

103. Hernandez, K. *et al.* Overexpression of Isoforms of Nitric Oxide Synthase 1 Adaptor Protein, Encoded by a Risk Gene for Schizophrenia, Alters Actin Dynamics and Synaptic Function. *Front Cell Neurosci* **10**, 6, doi:10.3389/fncel.2016.00006 (2016).
104. Kutzing, M. K., Langhammer, C. G., Luo, V., Lakdawala, H. & Firestein, B. L. Automated Sholl analysis of digitized neuronal morphology at multiple scales. *J Vis Exp*, doi:10.3791/23542354 (2010).
105. Kutzing, M. K., Luo, V. & Firestein, B. L. Protection from glutamate-induced excitotoxicity by memantine. *Ann Biomed Eng* **40**, 1170-1181, doi:10.1007/s10439-011-0494-z (2012).
106. Liu, L. *et al*. Role of NMDA Receptor Subtypes in Governing the Direction of Hippocampal Synaptic Plasticity. *Science* **304**, 1021-1024 (2004).
107. Cummings, J. A., Mulkey, R. M., Nicoll, R. A. & Malenka, R. C. Ca2+ Signaling Requirements for Long-Term Depression in the Hippocampus. *Neuron* **16**, 825-833 (1996).
108. Wu, H. *et al.* Increase in phosphorylation of Akt and its downstream signaling targets and suppression of apoptosis by simvastatin after traumatic brain injury. *Journal of neurosurgery* **109**, 691-698, doi:10.3171/JNS/2008/109/10/0691 (2008).
109. Chen, X. *et al.* GSK-3beta downregulates Nrf2 in cultured cortical neurons and in a rat model of cerebral ischemia-reperfusion. *Scientific reports* **6**, 20196, doi:10.1038/srep20196 (2016).
110. Szydlowski, M., Jablonska, E. & Juszczynski, P. FOXO1 transcription factor: a critical effector of the PI3K-AKT axis in B-cell development. *Int Rev Immunol* **33**, 146-157, doi:10.3109/08830185.2014.885022 (2014).
111. Hay, N. Interplay between FOXO, TOR, and Akt. *Biochim Biophys Acta* **1813**, 1965-1970, doi:10.1016/j.bbamcr.2011.03.013 (2011).
112. Dharaneeswaran, H. *et al.* FOXO1-mediated activation of Akt plays a critical role in vascular homeostasis. *Circ Res* **115**, 238-251, doi:10.1161/CIRCRESAHA.115.303227 (2014).
113. Zhu, D., Lipsky, R. H. & Marini, A. M. Co-activation of the phosphatidylinositol-3-kinase/Akt signaling pathway by N-methyl-D-aspartate and TrkB receptors in cerebellar granule cell neurons. *Amino Acids* **23**, 11-17, doi:10.1007/s00726-001-0103-9 (2002).
114. Sanchez-Perez, A. M., Llansola, M. & Felipo, V. Modulation of NMDA receptors by AKT kinase. *Neurochem Int* **49**, 351-358, doi:10.1016/j.neuint.2006.02.005 (2006).
115. Prins, M., Greco, T., Alexander, D. & Giza, C. C. The pathophysiology of traumatic brain injury at a glance. *Disease models & mechanisms* **6**, 1307-1315, doi:10.1242/dmm.011585 (2013).
116. Ray, S. K., Dixon, C. E. & Banik, N. L. Molecular mechanisms in the pathogenesis of traumatic brain injury. *Histol Histopathol* **17**, 1137-1152 (2002).
117. Mark, L. P. *et al*. Pictorial Review of Glutamate Excitotoxicity: Fundamental Concepts for Neuroimaging. *AJNR Am J Neuroradiol* **22**, 1813–1824 (2001).
118. Shohami, E. & Biegon, A. Novel approach to the role of NMDA receptors in traumatic brain injury. *CNS Neurol Disord Drug Targets* **13**, 567-573 (2014).
119. Ding, K. *et al.* Rapamycin protects against apoptotic neuronal death and improves neurologic function after traumatic brain injury in mice via modulation of the mTOR-

p53-Bax axis. *The Journal of surgical research* **194**, 239-247, doi:10.1016/j.jss.2014.09.026 (2015).
120. Ge, X. T. *et al.* miR-21 improves the neurological outcome after traumatic brain injury in rats. *Scientific reports* **4**, 6718, doi:10.1038/srep06718 (2014).
121. Jourdain, P. *et al.* L-Lactate protects neurons against excitotoxicity: implication of an ATP-mediated signaling cascade. *Scientific reports* **6**, 21250, doi:10.1038/srep21250 (2016).
122. Liu, Q. *et al.* Akt and mTOR mediate programmed necrosis in neurons. *Cell death & disease* **5**, e1084, doi:10.1038/cddis.2014.69 (2014).
123. Zhang, L., Ding, K., Wang, H., Wu, Y. & Xu, J. Traumatic Brain Injury-Induced Neuronal Apoptosis is Reduced Through Modulation of PI3K and Autophagy Pathways in Mouse by FTY720. *Cellular and molecular neurobiology* **36**, 131-142, doi:10.1007/s10571-015-0227-1 (2016).
124. Otmakhov, N. *et al.* Excitotoxic insult results in a long-lasting activation of CaMKIIalpha and mitochondrial damage in living hippocampal neurons. *PloS one* **10**, e0120881, doi:10.1371/journal.pone.0120881 (2015).
125. Zhu, X. *et al.* Role of Akt and mammalian target of rapamycin in functional outcome after concussive brain injury in mice. *J Cereb Blood Flow Metab* **34**, 1531-1539, doi:10.1038/jcbfm.2014.113 (2014).
126. Logue, O. C., Cramer, N. P., Xu, X., Perl, D. P. & Galdzicki, Z. Alterations of functional properties of hippocampal networks following repetitive closed-head injury. *Exp Neurol* **277**, 227-243, doi:10.1016/j.expneurol.2015.12.019 (2016).
127. Peineau, S. *et al.* The role of GSK-3 in synaptic plasticity. *British journal of pharmacology* **153 Suppl 1**, S428-437, doi:10.1038/bjp.2008.2 (2008).
128. Dash, P. K. *et al.* Involvement of the glycogen synthase kinase-3 signaling pathway in TBI pathology and neurocognitive outcome. *PloS one* **6**, e24648, doi:10.1371/journal.pone.0024648 (2011).
129. Wei, J., Liu, W. & Yan, Z. Regulation of AMPA receptor trafficking and function by glycogen synthase kinase 3. *J Biol Chem* **285**, 26369-26376, doi:10.1074/jbc.M110.121376 (2010).
130. Chen, P., Gu, Z., Liu, W. & Yan, Z. Glycogen synthase kinase 3 regulates N-methyl-D-aspartate receptor channel trafficking and function in cortical neurons. *Molecular pharmacology* **72**, 40-51, doi:10.1124/mol.107.034942 (2007).
131. Kumar, V., Zhang, M. X., Swank, M. W., Kunz, J. & Wu, G. Y. Regulation of dendritic morphogenesis by Ras-PI3K-Akt-mTOR and Ras-MAPK signaling pathways. *J Neurosci* **25**, 11288-11299, doi:10.1523/JNEUROSCI.2284-05.2005 (2005).
132. Han, S. Phosphorylation of Tuberin as a Novel Mechanism for Somatic Inactivation of the Tuberous Sclerosis Complex Proteins in Brain Lesions. *Cancer Research* **64**, 812-816, doi:10.1158/0008-5472.can-03-3277 (2004).
133. Ma, L., Chen, Z., Erdjument-Bromage, H., Tempst, P. & Pandolfi, P. P. Phosphorylation and functional inactivation of TSC2 by Erk implications for tuberous sclerosis and cancer pathogenesis. *Cell* **121**, 179-193, doi:10.1016/j.cell.2005.02.031 (2005).
134. Chen, Y., Zheng, Y. & Foster, D. A. Phospholipase D confers rapamycin resistance in human breast cancer cells. *Oncogene* **22**, 3937-3942, doi:10.1038/sj.onc.1206565 (2003).

135. Hornberger, T. A. *et al.* The role of phospholipase D and phosphatidic acid in the mechanical activation of mTOR signaling in skeletal muscle. *Proceedings of the National Academy of Sciences of the United States of America* **103**, 4741-4746, doi:10.1073/pnas.0600678103 (2006).
136. Hawley, S. A. *et al.* Complexes between the LKB1 tumor suppressor, STRAD / and MO25 / are upstream kinases in the AMP-activated protein kinase cascade. *Journal of Biology* **2**, 28 (2003).
137. Shaw, R. J. *et al.* The tumor suppressor LKB1 kinase directly activates AMP-activated kinase and regulates apoptosis in response to energy stress. *Proceedings of the National Academy of Sciences of the United States of America* **101**, 3329-3335, doi:10.1073/pnas.0308061100 (2004).
138. Woods, A. *et al.* LKB1 Is the Upstream Kinase in the AMP-Activated Protein Kinase Cascade. *Current Biology* **13**, 2004-2008, doi:10.1016/j.cub.2003.10.031 (2003).
139. Arsham, A. M., Howell, J. J. & Simon, M. C. A novel hypoxia-inducible factor-independent hypoxic response regulating mammalian target of rapamycin and its targets. *J Biol Chem* **278**, 29655-29660, doi:10.1074/jbc.M212770200 (2003).
140. Brugarolas, J. *et al.* Regulation of mTOR function in response to hypoxia by REDD1 and the TSC1/TSC2 tumor suppressor complex. *Genes Dev* **18**, 2893-2904, doi:10.1101/gad.1256804 (2004).
141. Sofer, A., Lei, K., Johannessen, C. M. & Ellisen, L. W. Regulation of mTOR and cell growth in response to energy stress by REDD1. *Molecular and cellular biology* **25**, 5834-5845, doi:10.1128/MCB.25.14.5834-5845.2005 (2005).
142. DeYoung, M. P., Horak, P., Sofer, A., Sgroi, D. & Ellisen, L. W. Hypoxia regulates TSC1/2-mTOR signaling and tumor suppression through REDD1-mediated 14-3-3 shuttling. *Genes Dev* **22**, 239-251, doi:10.1101/gad.1617608 (2008).
143. Findlay, G. M., Yan, L., Procter, J., Mieulet, V. & Lamb, R. F. A MAP4 kinase related to Ste20 is a nutrient-sensitive regulator of mTOR signalling. *The Biochemical journal* **403**, 13-20, doi:10.1042/BJ20061881 (2007).
144. Zhang, B. Y. *et al.* Akt-independent GSK3 inactivation downstream of PI3K signaling regulates mammalian axon regeneration. *Biochemical and biophysical research communications* **443**, 743-748, doi:10.1016/j.bbrc.2013.12.037 (2014).
145. Chen, S. *et al.* Celecoxib promotes c-FLIP degradation through Akt-independent inhibition of GSK3. *Cancer Res* **71**, 6270-6281, doi:10.1158/0008-5472.CAN-11-0838 (2011).
146. Hai-Rong Shi, L.-Q. Z., Shao-Hui Wang, Xin-An Liu, Qing Tian, Qi Zhang, Qun Wang, Jian-Zhi Wang. 17β-estradiol attenuates glycogen synthase kinase-3β activation and tau hyperphosphorylation in Akt-independent manner. *Journal of Neural Transmission* **115**, 879-888 (2008).
147. McCubrey, J. A. *et al.* GSK-3 as potential target for therapeutic intervention in cancer. *Oncotarget* **5**, 30 (2014).
148. Mizuno, T. *et al.* Interleukin-34 selectively enhances the neuroprotective effects of microglia to attenuate oligomeric amyloid-beta neurotoxicity. *Am J Pathol* **179**, 2016-2027, doi:10.1016/j.ajpath.2011.06.011 (2011).
149. Mizuno, T. *et al.* Interferon-gamma directly induces neurotoxicity through a neuron specific, calcium-permeable complex of IFN-gamma receptor and AMPA GluR1 receptor. *FASEB J* **22**, 1797-1806, doi:10.1096/fj.07-099499 (2008).

150. Langhammer, C. G. *et al.* Automated Sholl analysis of digitized neuronal morphology at multiple scales: Whole cell Sholl analysis versus Sholl analysis of arbor subregions. *Cytometry A* **77**, 1160-1168, doi:10.1002/cyto.a.20954 (2010).
151. Dzyubenko, E., Rozenberg, A., Hermann, D. M. & Faissner, A. Colocalization of synapse marker proteins evaluated by STED-microscopy reveals patterns of neuronal synapse distribution in vitro. *J Neurosci Methods* **273**, 149-159, doi:10.1016/j.jneumeth.2016.09.001 (2016).
152. Pang, Z. P., Cao, P., Xu, W. & Sudhof, T. C. Calmodulin controls synaptic strength via presynaptic activation of calmodulin kinase II. *J Neurosci* **30**, 4132-4142, doi:10.1523/JNEUROSCI.3129-09.2010 (2010).
153. Eyo, U. B. *et al.* Neuronal hyperactivity recruits microglial processes via neuronal NMDA receptors and microglial P2Y12 receptors after status epilepticus. *J Neurosci* **34**, 10528-10540, doi:10.1523/JNEUROSCI.0416-14.2014 (2014).
154. Nimmerjahn, F. Kirchhoff, F. Helmchen, Resting microglial cells are highly dynamic surveillants of brain parenchyma in vivo. *Science* **308**, 1314-1318 (2005).
155. Davalos, D. *et al.* ATP mediates rapid microglial response to local brain injury in vivo. *Nat Neurosci* **8**, 752-758 (2005).
156. Wake, H., Moorhouse, A. J., Jinno, S., Kohsaka, S. & Nabekura, J. Resting microglia directly monitor the functional state of synapses in vivo and determine the fate of ischemic terminals. *J Neurosci* **29**, 3974-3980 (2009).
157. Tremblay, M., Lowery, R. L. & Majewska, A. K. Microglial interactions with synapses are modulated by visual experience. *PLoS Biol* **8**, e1000527 (2010).
158. Pascual, O., Achour, S. B., Rostaing, P., Triller, A. & Bessis, A. Microglia activation triggers astrocyte-mediated modulation of excitatory neurotransmission. *Proc Natl Acad Sci U S A* **109**, E197-205 (2012).
159. Haynes, S. E. *et al.* The P2Y12 receptor regulates microglial activation by extracellular nucleotides. *Nat Neurosci* **9**, 1512-1519 (2006).
160. Burnstock, G. in *P2 Purinoceptors: Localization, Function and Transduction Mechanisms*, D. G. Chadwick, J, Ed. (Wiley, New York, 2008), vol. 198, pp. 346.
161. Hollopeter, G. *et al.* Identification of the platelet ADP receptor targeted by antithrombotic drugs. *Nature* **409**, 202-207 (2001).
162. Zhang, F. L. *et al.* ADP is the cognate ligand for the orphan G protein-coupled receptor SP1999. *J Biol Chem* **276**, 8608-8615 (2001).
163. Wu, L. J., Vadakkan, K. I. & Zhuo, M. ATP-induced chemotaxis of microglial processes requires P2Y receptor-activated initiation of outward potassium currents. *Glia* **55**, 810-821 (2007).
164. Schilling, T. & Eder, C. Ion channel expression in resting and activated microglia of hippocampal slices from juvenile mice. *Brain Res* **1186**, 21-28 (2007).
165. Schwab. Ion channels and transporters on the move. *News Physiol Sci* **16**, 29-33 (2001).
166. Eyo, U. B. *et al.* Neuronal hyperactivity recruits microglial processes via neuronal NMDA receptors and microglial P2Y12 receptors after status epilepticus. *J Neurosci* **34**, 10528-10540 (2014).
167. Tozaki-Saitoh, H. *et al.* P2Y12 receptors in spinal microglia are required for neuropathic pain after peripheral nerve injury. *J Neurosci* **28**, 4949-4956 (2008).

168. Webster, C. M. *et al.* Microglial P2Y12 deficiency/inhibition protects against brain ischemia. *PLoS One* **8**, e70927 (2013).
169. Jung, S. *et al.* Analysis of fractalkine receptor CX(3)CR1 function by targeted deletion and green fluorescent protein reporter gene insertion. *Molecular and cellular biology* **20**, 4106-4114 (2000).
170. Boucsein, C. *et al.* Purinergic receptors on microglial cells: functional expression in acute brain slices and modulation of microglial activation in vitro. *Eur J Neurosci* **17**, 2267-2276 (2003).
171. Haas, S., Brockhaus, J., Verkhratsky, A. & Kettenmann, H. ATP-induced membrane currents in ameboid microglia acutely isolated from mouse brain slices. *Neuroscience* **75**, 257-261 (1996).
172. Koizumi, S. *et al.* UDP acting at P2Y6 receptors is a mediator of microglial phagocytosis. *Nature* **446**, 1091-1095 (2007).
173. Neher, J. J., Neniskyte, U., Hornik, Y. & Brown, G. C. Inhibition of UDP/P2Y6 purinergic signaling prevents phagocytosis of viable neurons by activated microglia in vitro and in vivo. *Glia* **62**, 1463-1475 (2014).
174. Hagiwara, S., Miyazaki, S. & Rosenthal, N. P. Potassium current and the effect of cesium on this current during anomalous rectification of the egg cell membrane of a starfish. *J Gen Physiol* **67**, 621-638 (1976).
175. Girard, C. *et al.* Genomic and functional characteristics of novel human pancreatic 2P domain K(+) channels. *Biochem Biophys Res Commun* **282**, 249-256 (2001).
176. Shin, H. W. *et al.* The inhibitory effects of bupivacaine, levobupivacaine, and ropivacaine on K2P (two-pore domain potassium) channel TREK-1. *J Anesth* **28**, 81-86 (2014).
177. Unterberger, U., Moskvina, E., Scholze, T., Freissmuth, M. & Boehm, S. Inhibition of adenylyl cyclase by neuronal P2Y receptors. *Br J Pharmacol* **135**, 673-684 (2002).
178. Witkowski, G., Rola, R. & Szulczyk, P. Effect of cyclic adenosine monophosphate on the G protein-dependent inward rectifier K(+)-like channel current in medial prefrontal cortex pyramidal neurons. *J Physiol Pharmacol* **63**, 457-462 (2012).
179. Yang, J. *et al.* Signaling through Gi family members in platelets. Redundancy and specificity in the regulation of adenylyl cyclase and other effectors. *J Biol Chem* **277**, 46035-46042 (2002).
180. Eichhoff, G., Brawek, B. & Garaschuk, O. Microglial calcium signal acts as a rapid sensor of single neuron damage in vivo. *Biochim Biophys Acta* **1813**, 1014-1024 (2011).
181. Honda, S. *et al.* Extracellular ATP or ADP induce chemotaxis of cultured microglia through Gi/o-coupled P2Y receptors. *J Neurosci* **21**, 1975-1982 (2001).
182. Illes, P., Nörenberg, W. & Gebicke-Haerter, P. J. Molecular mechanisms of microglial activation. B. Voltage- and purinoceptor-operated channels in microglia. *Neurochem Int* **29**, 13-24 (1996).
183. Kataoka *et al.*, Involvement of vasodilator-stimulated phosphoprotein in UDP-induced microglial actin aggregation via PKC- and Rho-dependent pathways. *Purinergic Signal* **7**, 403-411 (2011).

184. Nasu-Tada, K., Koizumi, S. & Inoue, K. Involvement of beta1 integrin in microglial chemotaxis and proliferation on fibronectin: different regulations by ADP through PKA. *Glia* **52**, 98-107 (2005).
185. Jantaratnotai, N., Choi, H. B. & McLarnon, J. G. ATP stimulates chemokine production via a store-operated calcium entry pathway in C6 glioma cells. *BMC Cancer* **9**, 442 (2009).
186. Xu, P. *et al.* Extracellular ATP enhances radiation-induced brain injury through microglial activation and paracrine signaling via P2X7 receptor. *Brain Behav Immun*, (2015).
187. Sasaki, Y. *et al.* Selective expression of Gi/o-coupled ATP receptor P2Y12 in microglia in rat brain. *Glia* **44**, 242-250 (2003).
188. Orr, G., Orr, A. L., Li, X. J., Gross, R. E. & Traynelis, S. F. Adenosine A(2A) receptor mediates microglial process retraction. *Nat Neurosci* **12**, 872-878 (2009).
189. De Simone, R. *et al.* TGF-β and LPS modulate ADP-induced migration of microglial cells through P2Y1 and P2Y12 receptor expression. *J Neurochem* **115**, 450-459 (2010).
190. Sunkaria, Bhardwaj, S., Halder, A., Yadav, A. & Sandhir, R. Migration and Phagocytic Ability of Activated Microglia During Post-natal Development is Mediated by Calcium-Dependent Purinergic Signalling. *Mol Neurobiol*, (2015).
191. Eyo, U. B. *et al.* Modulation of microglial process convergence toward neuronal dendrites by extracellular calcium. *J Neurosci* **35**, 2417-2422 (2015).
192. Preissler, J. *et al.* Altered microglial phagocytosis in GPR34-deficient mice. *Glia* **63**, 206-215 (2015).
193. Michaelis, M., Nieswandt, B., Stegner, D., Eilers, J. & Kraft, R. STIM1, STIM2, and Orai1 regulate store-operated calcium entry and purinergic activation of microglia. *Glia* **63**, 652-663 (2015).
194. Shankar, H. *et al.* Role of G protein-gated inwardly rectifying potassium channels in P2Y12 receptor-mediated platelet functional responses. *Blood* **104**, 1335-1343 (2004).
195. Marcet, B., Chappe, V., Delmas, P. & Verrier, B. Pharmacological and signaling properties of endogenous P2Y1 receptors in cystic fibrosis transmembrane conductance regulator-expressing Chinese hamster ovary cells. *J Pharmacol Exp Ther* **309**, 533-539 (2004).
196. Ohlmann, P. *et al.* The human platelet ADP receptor activates Gi2 proteins. *Biochem J* **312**, 775-779 (1995).
197. Jantzen, H. M., Milstone, D. S., Gousset, L., Conley, P. B. & Mortensen, R. M. Impaired activation of murine platelets lacking G alpha(i2). *J Clin Invest* **108**, 477-483 (2001).
198. Harden, T. K., Boyer, J. L. & Nicholas, R. A. P2-purinergic receptors: subtype-associated signaling responses and structure. *Annu Rev Pharmacol Toxicol* **35**, 541-579 (1995).
199. Boyer, J. L., Lazarowski, E. R., Chen, X. H. & Harden, T. K. Identification of a P2Y-purinergic receptor that inhibits adenylyl cyclase. *J Pharmacol Exp Ther* **267**, 1140-1146 (1993).
200. Jin, J. *et al.* The C6-2B glioma cell P2Y(AC) receptor is pharmacologically and molecularly identical to the platelet P2Y(12) receptor. *Br J Pharmacol* **133**, 521-528 (2001).

201. Simon, J. *et al.* Activity of adenosine diphosphates and triphosphates on a P2Y(T) -type receptor in brain capillary endothelial cells. *Br J Pharmacol* **132**, 173-182 (2001).
202. Kobayashi, K. *et al.* P2Y12 receptor upregulation in activated microglia is a gateway of p38 signaling and neuropathic pain. *J Neurosci* **28**, 2892-2902 (2008).
203. Gyoneva, S. *et al.* Adenosine A2A receptor antagonism reverses inflammation-induced impairment of microglial process extension in a model of Parkinson's disease. *Neurobiol Dis* **67**, 191-202 (2014).
204. Hernandez-Ontiveros, D. G. *et al.* Microglia activation as a biomarker for traumatic brain injury. *Front Neurol* **4**, 30 (2013).
205. Lazarowski, E. R., Homolya, L., Boucher, R. C. & Harden, T. K. Direct demonstration of mechanically induced release of cellular UTP and its implication for uridine nucleotide receptor activation. *J Biol Chem* **272**, 24348-24354 (1997).
206. Moore, C. S. *et al.* P2Y12 expression and function in alternatively activated human microglia. *Neurol Neuroimmunol Neuroinflamm* **2**, e80 (2015).
207. Cattaneo, M. The P2 receptors and congenital platelet function defects. *Semin Thromb Hemost* **31**, 168-173 (2005).
208. Tang-Schomer, M. D., Johnson, V. E., Baas, P. W., Stewart, W. & Smith, D. H. Partial interruption of axonal transport due to microtubule breakage accounts for the formation of periodic varicosities after traumatic axonal injury. *Exp Neurol* **233**, 364-372, doi:10.1016/j.expneurol.2011.10.030 (2012).
209. Tseng, C. Y. & Firestein, B. L. The role of PSD-95 and cypin in morphological changes in dendrites following sublethal NMDA exposure. *J Neurosci* **31**, 15468-15480, doi:10.1523/JNEUROSCI.2442-11.2011 (2011).
210. Leeds, P. R. *et al.* A new avenue for lithium: intervention in traumatic brain injury. *ACS Chem Neurosci* **5**, 422-433, doi:10.1021/cn500040g (2014).
211. Axel Nimmerjahn, F. K. & Fritjof Helmchen. Resting Microglial Cells Are Highly Dynamic Surveillants of Brain Parenchyma in Vivo. *Science* **308** (2005).
212. Loane, D. J. & Kumar, A. Microglia in the TBI brain: The good, the bad, and the dysregulated. *Exp Neurol* **275 Pt 3**, 316-327, doi:10.1016/j.expneurol.2015.08.018 (2016).
213. Rosa, C. *et al*. Synaptic Pruning by Microglia Is Necessary for Normal Brain Development. *Science* **333** (2011).
214. Corps, K. N., Roth, T. L. & McGavern, D. B. Inflammation and neuroprotection in traumatic brain injury. *JAMA Neurol* **72**, 355-362, doi:10.1001/jamaneurol.2014.3558 (2015).
215. Kumar, A. & Loane, D. J. Neuroinflammation after traumatic brain injury: opportunities for therapeutic intervention. *Brain Behav Immun* **26**, 1191-1201, doi:10.1016/j.bbi.2012.06.008 (2012).
216. Szalay, G. *et al.* Microglia protect against brain injury and their selective elimination dysregulates neuronal network activity after stroke. *Nat Commun* **7**, 11499, doi:10.1038/ncomms11499 (2016).
217. Davalos, D. *et al.* ATP mediates rapid microglial response to local brain injury in vivo. *Nat Neurosci* **8**, 752-758, doi:10.1038/nn1472 (2005).
218. Haynes, S. E. *et al.* The P2Y12 receptor regulates microglial activation by extracellular nucleotides. *Nat Neurosci* **9**, 1512-1519, doi:10.1038/nn1805 (2006).

219. Swiatkowski, P. *et al.* Activation of microglial P2Y12 receptor is required for outward potassium currents in response to neuronal injury. *Neuroscience* **318**, 22-33, doi:10.1016/j.neuroscience.2016.01.008 (2016).
220. Roth, T. L. *et al.* Transcranial amelioration of inflammation and cell death after brain injury. *Nature* **505**, 223-228, doi:10.1038/nature12808 (2014).
221. Parkhurst, C. N. *et al.* Microglia promote learning-dependent synapse formation through brain-derived neurotrophic factor. *Cell* **155**, 1596-1609, doi:10.1016/j.cell.2013.11.030 (2013).
222. Peng, J. *et al.* Microglia and monocytes synergistically promote the transition from acute to chronic pain after nerve injury. *Nat Commun* **7**, 12029, doi:10.1038/ncomms12029 (2016).
223. Hedlund, E., Karlsson, M., Osborn, T., Ludwig, W. & Isacson, O. Global gene expression profiling of somatic motor neuron populations with different vulnerability identify molecules and pathways of degeneration and protection. *Brain* **133** (2010)